POLYTECHNIQUE MONTRÉAL

affiliée à l'Université de Montréal

Clustering of the White Matter Tracts in the Rat Spinal Cord Based on Quantitative Histology

HARRIS NAMI

Institut de génie biomédical

Mémoire présenté en vue de l'obtention du diplôme de *Maitrise ès sciences appliquées*

Génie biomédical

Août 2019

POLYTECHNIQUE MONTRÉAL

affiliée à l'Université de Montréal

Ce mémoire intitulé :

Clustering of the White Matter Tracts in the Rat Spinal Cord Based on Quantitative Histology

présenté par **Harris NAMI**

en vue de l'obtention du diplôme de *Maitrise ès sciences appliquées*

a été dûment accepté par le jury d'examen constitué de :

Jean PROVOST, président

Julien COHEN-ADAD, membre et directeur de recherche

Nikola STIKOV, membre et codirecteur de recherche

Samuel KADOURY, membre

DEDICATION

I would like to dedicate this thesis to my family, whom without their unwavering support I would not be where I am today.

ACKNOWLEDGEMENTS

I would like to acknowledge all my fellow colleagues at the NeuroPoly lab that have helped me throughout my 2 years in the lab. In particular, I would like to thank Agah, Aldo, Alexandru, Ariane, Atef, Charley, Christian, Gabriel, Maxime, Nibardo, Ryan, Tanguy, and Tommy for all of their help, interactions and useful discussions the past 2 years. I would like to thank my supervisor and co-supervisor Julien and Nikola for being very supportive and insightful with every project I worked on. They are amongst the most intelligent people I have had the pleasure of working under and truly learnt a lot from them.

RÉSUMÉ

La matière blanche de la moelle épinière est vraiment importante pour la transmission de l'information entre le corps et le cerveau et vice-versa. La matière blanche est divisée entre différents faisceaux (tracts) dépendamment de la fonctionnalité de chaque faisceau. Dans les pathologies qui affectent la moelle épinière, c'est normalement les faisceaux de la matière blanche qui sont les plus affectées. Comprendre comment les faisceaux sont divisés est donc important pour mettre en place une méthodologie qui peut facilement identifier les faisceaux sains et les comparer avec ceux qui sont pathologiques. Présentement, les techniques utilisées pour déterminer les faisceaux de la matière blanche sont des techniques relativement anciennes qui utilisent différents types des colorants pour identifier différents types de cellules. Les atlas de matière blanche étaient créés par la suite visuellement en se basant sur ces colorants. En plus, l'atlas était souvent créé sur un seul échantillon (e.g. un rat), ainsi, même avec plusieurs colorants, il n'était pas possible de visualiser tous les faisceaux. Le but de ce projet était justement de créer une méthodologie qui permet de visualiser tous les faisceaux de la matière blanche en combinant une haute résolution en histologie quantitative et un algorithme de regroupement. On a appliqué trois types d'algorithmes de regroupement: l'agglomerative clustering, le k-means clustering et le spectral clustering. On a aussi validé les trois algorithmes visuellement en comparant la position des faisceaux avec les anciens atlas et aussi quantitativement avec la silhouette score et le davies-bouldin score. L'algorithme de l'agglomerative clustering a permis d'identifier des faisceaux similaires à ceux de l'ancien atlas de Paxinos pour le rat que les deux autres algorithmes de regroupement. Par contre, en utilisant les méthodes de validation quantitative, on a constaté que le spectral clustering a un meilleur score (0.43 silhouette et 0.85 davies-bouldin) que les deux autres algorithmes. On peut voir cependant que les clusters de l'agglomerative clustering semble donner de meilleur résultat et plus stable que les deux autres algorithmes. En particulier, on a pu identifier des faisceaux que le paxinos atlas de rat ne comprend pas. En conclusion, on a vu que le fait d'appliquer un algorithme de regroupement sur des données quantitatives d'histologie a donné des résultats comparables avec ce qui est déjà dans la littérature. On pouvait alors essayer d'implémenter ça sur d'autres espèces et sur des données pathologiques pour voir comment les pathologies affectent les faisceauxs de la matière blanche.

ABSTRACT

The white matter tracts in the spinal cord make up the entire cytoarchitecture of how information travels from the body to the brain and vice-versa. It is usually the white matter tracts that are the target of pathologies and thus would impact all the various functions of the body from motor control to loss of organ function. It is therefore quite important to understand how the tracts are grouped and to develop more easily available and simple to use techniques to do so. The methods at this point in time that have been used to characterize the white matter tracts have all been done using manual staining techniques and visual delineation of the tracts based off of these stains. Furthermore, specifically for the rat atlas, the gold standard was done using only a single specimen. Moreover, they were still unable to visualize all of the tracts that based off of the literature are supposed to be there. Therefore, we have developed a pipeline to be able to visualize the tracts of the white matter based solely on high resolution quantitative histology using only one stain to visualize the myelin sheath from which then we can obtain various metric maps such as the axon diameter and density as well as myelin thickness. We applied three clustering algorithms on the averaged metric maps of the 5 rats to visualize the best results for the clustering and then validated them quantitatively. The algorithms we tested were agglomerative clustering, k-means clustering and spectral clustering along with the validation methods of silhouette score and davies-bouldin score. Based on the visual comparison between the results and the gold standard atlases currently in use, agglomerative clustering seemed to have a more representative output in comparison. The clusters also seemed more stable for agglomerative clustering compared to the other two techniques. However, based on the quantitative validation, the silhouette score was higher for spectral clustering (0.43) versus 0.38 and 0.37 for agglomerative clustering and k-means clustering respectively. The davies-bouldin score was better for spectral and k-means clustering (0.85 and 0.87) whereas for agglomerative clustering a score of 2.68 was obtained. All things taken into account however, it would seem that agglomerative clustering with the use of a connectivity matrix gives the most stable and comparable results. Thus, we were able to implement a pipeline using quantitative metrics as the sole inputs to obtain very similar results to the gold standard atlases with an applied clustering algorithm. We can therefore apply this pipeline on other species to investigate the placement of the white matter tracts as well as implement it on pathological data to see how pathologies would affect the white matter tracts.

TABLE OF CONTENTS

LIST OF TABLES

LIST OF FIGURES

LIST OF SYMBOLS AND ABBREVIATIONS

SEM Scanning Electron Microscope

DDSA Dodecenyl succinic anhydride

DMP 2,4,6-{tri(dimehtylaminoethyl)phenol}

NMA Nadic methyl anhydride

LIST OF APPENDICES

CHAPTER 1 INTRODUCTION

1.1 Research Context and Objectives

Understanding the neuroanatomy and structural organization of the spinal cord is important to ascertain the underlying pathophysiology of neurodegenerative diseases. The spinal cord is one of two main organs comprising the central nervous system (the other being the brain). It is the organ responsible for transmitting information from the body to the brain and vice-versa. The spinal cord is segmented into 31 different levels, and the levels are grouped into 4 different categories. The first 8 levels are categorized as the Cervical (C1 to C8), the next 13 are the Thoracic (T1 to T13), the 6 after that are the Lumbar (L1 to L6) and the last 4 are the sacral (S1 to S4). Each level has a specific responsibility in charge of controlling and transmitting information from various parts of the body as summarized in figure 1.1 below.

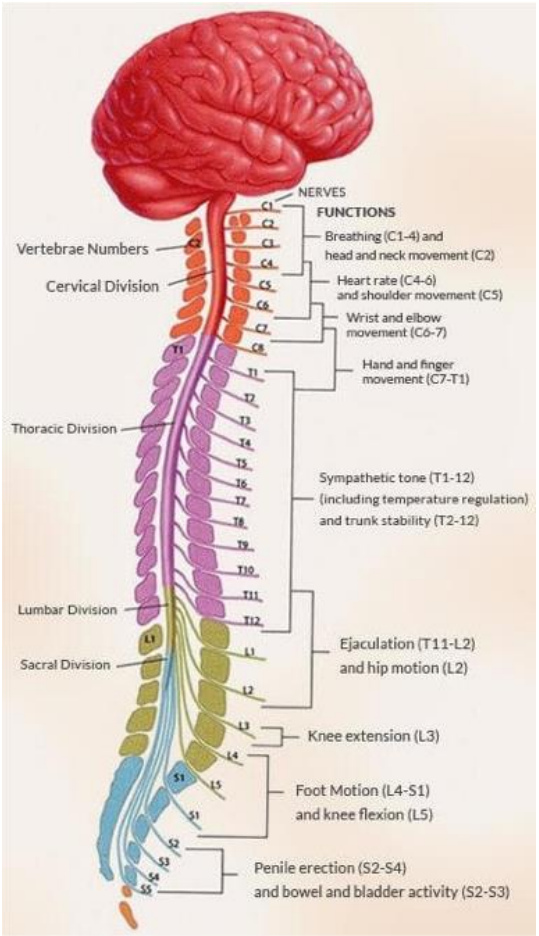

Figure 1.1: Outline of the spinal cord and the functions related to each level [1].

The spinal cord is composed of nerve cells that are wrapped around by a lipid layer known as the myelin sheath. These nerve cells; also known as neurons, have nerve fibers (axons) that are responsible for the transmission of the electrical impulses that carries the information. Specifically, it is the myelin sheath's conductivity that allows for the signals to propagate through the axons to reach their destination.

Furthermore, the spinal cord is visually and functionally divided into two distinct areas, there is the grey matter (which can be recognized by its butterfly like structure) and the white matter. The grey matter is composed of a whole host of different cell bodies, including a majority of unmyelinated axons (though there are a few myelinated axons as well). This is what distinguishes the grey matter from the white matter and where the colour difference arises from, as the white matter contains mostly myelinated axons and fewer cell bodies. One of the main reasons to want to characterize the white matter of the spinal cord is due to the myelinated axons. As mentioned, the myelin sheath is responsible for the conduction of the electrical signals for the axon. However, in central nervous system pathologies or even any form of spinal cord injury or trauma, it is the myelin sheath that ends up degrading or being damaged and it is due to this that information is halted and bodily functions cease. And as diseases progress, eventually even the axons end up dying. Therefore, in order to better understand the pathophysiology of these disease, it is first important to truly gain a grasp of the underlying structures and functions of the spinal cord white matter.

One of the lesser understood aspects of the spinal cord is the organization of the white matter tracts. The white matter tracts in the spinal cord are organized into bundles of myelinated axons where each bundle represents a specific function. The tracts can further be distinguished between ascending and descending, where the ascending tracts are the nerves that relay sensory information from the body to the brain and the descending tracts relay motor control information from the brain to the body. To make matters more complicated, these tracts also end up varying from species to species and therefore trying to understand the groupings of the tracts in one species may not necessarily apply to another species. Understanding the positioning and groupings of these tracts to better understand their functionality would better help to understand how pathologies would affect the body. For example, in multiple sclerosis, lesions form at various positions on the spinal cord (and throughout) and so if we know that the lesion is located on one tract or even on multiple

tracts, we would be able to know the functions of the body affected and thus be able to better mitigate the symptoms.

An underutilized tool for studies in the spinal cord is the use of a clustering algorithm. Clustering is the notion of trying to group and classify patterns within the data to give you more information about what is going on. Though some studies have attempted to use it, it has never been the main focus of their study and has never been done on high resolution, quantitative images. For instance, in the context of the brain, clustering is used as a means of categorizing the various sections of the brain, known as brain parcellation. There are a plethora of clustering algorithms available, each with their own unique way of parsing the data. In the spinal cord, this could be a useful tool to help better group the cytoarchitecture of the white matter tracts and gain a more quantitative basis for these groupings if we were to use quantitative inputs.

Thus, the objective of this study is to create a pipeline and methodology that could outline the white matter tracts based solely on the inherent quantitative information of the spinal cord using a clustering algorithm to do so. The quantitative information would be obtained from high resolution scanning electron microscopy images that would be segmented with AxonSeg; a software developed in the lab to obtain various metrics [2]. This would involve using metrics like the axon density, axon diameter, axon volume fraction, g-ratio, myelin volume fraction, and myelin thickness. These metrics would then be used as inputs into a clustering algorithm so as to gain a sense of how the spinal cord white matter is parcellated based on this information.

1.2 Thesis Organization

The thesis is organized as follows. Chapter 2 will discuss the background and literature review of the past work and current work being done on the tract delineation of the spinal cord. This will discuss the anatomy of the spinal cord along with the various studies looking at clustering of the spinal cord in comparison to those studies that have been done on the brain. Chapter 3 will discuss the methodologies used to achieve our goals. This includes from obtaining the tissue and preparing it, to obtaining the images and processing them as well as clustering them. The 4th chapter will discuss the results obtained from the image treatment and clustering, and the 5th chapter will discuss these results in the context of how good the results are comparatively to past studies and what

limitations were encountered. Lastly, chapter 6 will conclude with a summary of the study and what the results were, along with recommendations for improvements on the study and what can be done in the future with the implemented pipeline.

CHAPTER 2 BACKGROUND AND LITERATURE REVIEW

2.1 Anatomy of the Spinal Cord

2.1.1 Nerve Cells (Neurons) and the nervous system

The spinal cord is used as a primary means for the transmission of signals, however it is also responsible for processing reflexes as it would take too long for the signal to travel all the way to the brain and back down to the limbs for initiating movements in response to some sort of pain or stimuli. It is, as mentioned earlier, composed of neurons which are the main cells found in the brain and spinal cord that are responsible for the transmission of information via electrical signals. They are composed of a cell body that contains the nucleus with branching dendrites that receive the electrical signals (also known as action potentials) from other neurons as well as the axon which is the main source of transmission of information [3]. Axons transmit the information through conduction of signals via the encompassing myelin sheath. The myelin sheath is a lipid bilayer wrapped around the axon and is the one responsible for the propagation of the action potential. Once the signal reaches the end of the axon, there are synaptic terminals that release neurotransmitters that cause the release of certain ions that will then trigger a new action potential to begin to the neighbouring neuron receiving the action potential (known as the postsynaptic action potential) [4]. The myelin sheath and the axon are the focus for a lot of neurodegenerative pathologies as these tend to degrade for diseases. There are three main types of neurons that are found in the body. The first is the sensory neuron that sends signals based on stimuli from the five senses which are received and to be interpreted by the brain. The second are the motor neurons which send signals from the brain to the body through the spinal cord for locomotion. And the last types of neurons are the interneurons that connect two other sets of neurons together [3].

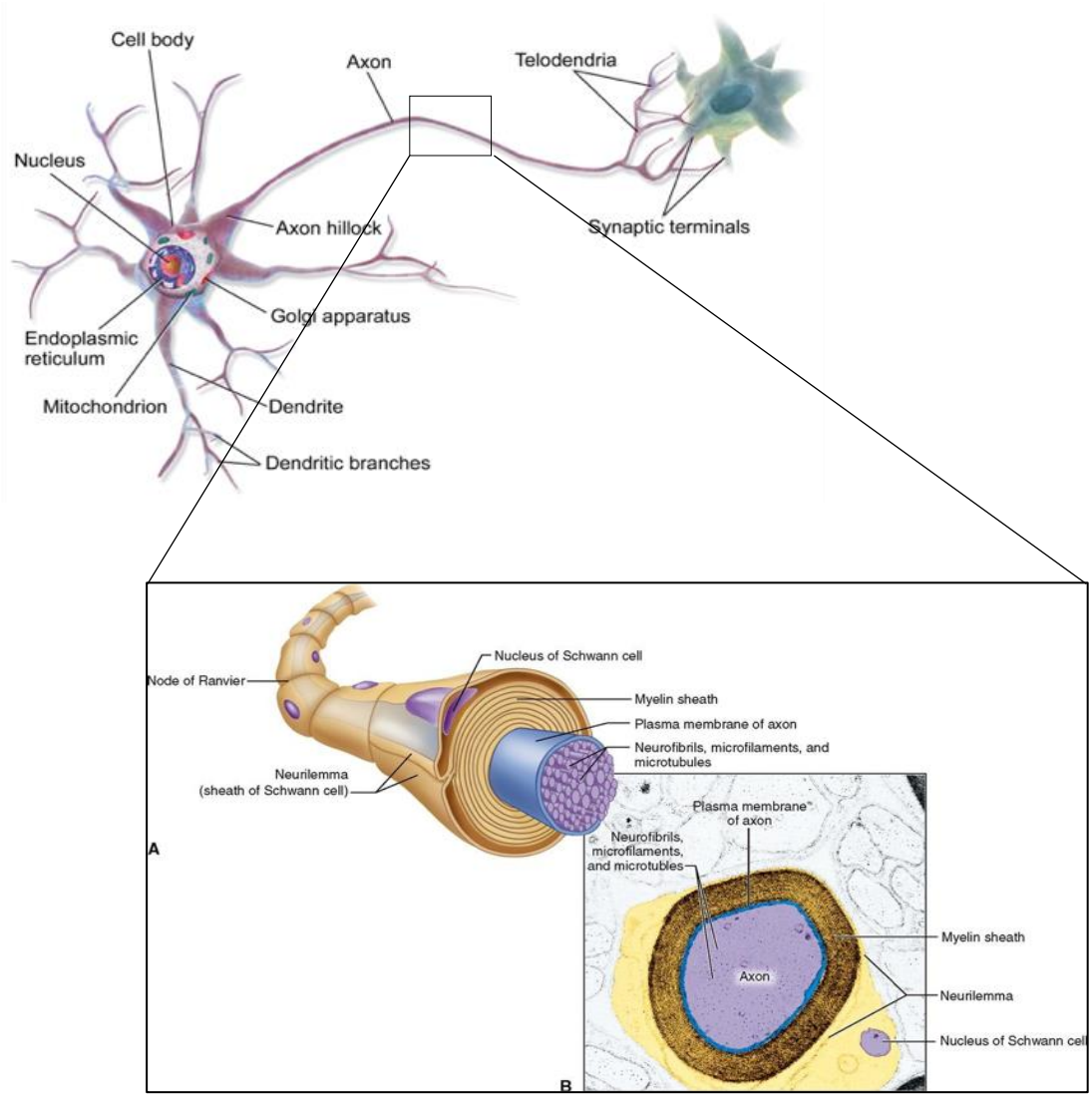

Figure 2.1: a) Close up of a full neuron with the various components labelled. b) Zoom in on the axon that shows the cross-section view of an axon including the myelin sheath wrapped around it. [5, 6].

2.1.2 Grey Matter

The grey matter of the spinal cord is the butterfly structure in the middle and contains a variety of different cells. It is broken down into three main sections: the anterior column, the posterior column and the lateral column [7]. Each column has a specific functionality and specific characteristics that aid with their functions. The columns can be further broken down based on this functionality into what are called the rexed laminae. There are 10 total laminae spread out across the columns, the first 6 (I-VI) being in the posterior column, laminae 7 and 10 (VII and X) in the lateral column and laminae 8 and 9 (VIII-IX) in the anterior grey column. The anterior column is responsible for the innervation of the muscles for motor functionality [7]. There are three main types of neurons found in the anterior gray column, the first is the alpha motor neuron which are responsible for the contraction of the skeletal muscles (extrafusal muscles) [8]. These are characterized by larger cell bodies. The second type of neuron found in the anterior column is the gamma neuron. The gamma neuron is smaller than the alpha neuron and is responsible for the innervation of the intrafusal muscles which are responsible for measuring the length of the contractions of the muscles and thus regulates the stretching of the muscles [8]. The last type of neurons found in the gray matter is the "small" neuron which are believed to be interneurons, but there is not enough information on them to validate this. If they are in fact interneurons, then they would be there to just create the circuits between the motor neurons and the receptor neurons [7]. The posterior column is responsible for the reception of sensory information from the body [7]. It is the subdivisions of the laminae that are responsible for the reception of the different types of sensory inputs. Laminae I and II receive pain, temperature and itching inputs, laminae III and IV receive mechanical pressure information and laminae V and VI receive proprioceptive information [8]. The lateral grey column receives inputs as a part of the sympathetic nervous system responsible for the "fight or flight" response [7]. This means it helps mediate the signals concerned with all the functions when going into a situation that a person may deem dangerous.

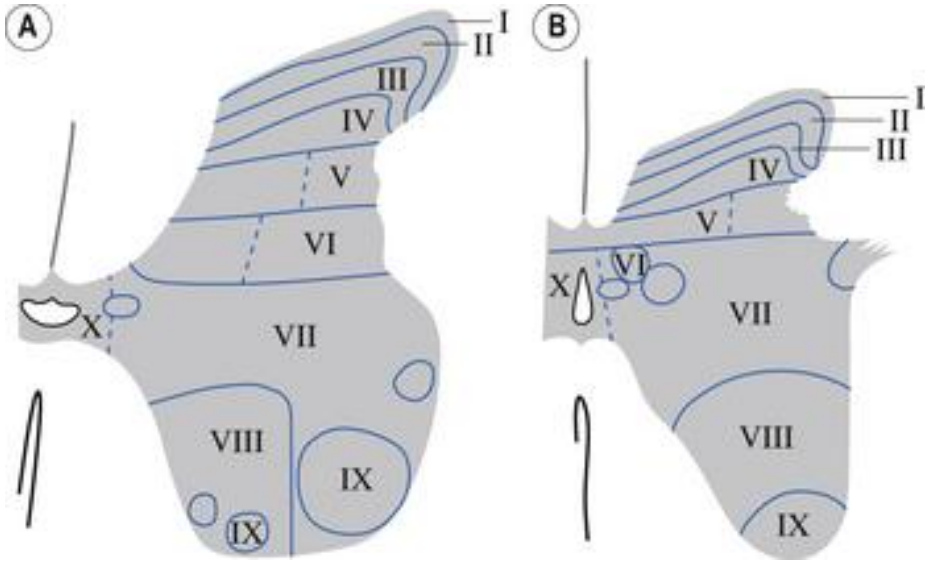

Figure 2.2: The 10 rexed laminae of the grey matter that separates it based on functionality (A) for Cervical and (B) for Lumbar [9].

2.1.3 White Matter

The white matter of the spinal cord is the area that surrounds the grey matter. As mentioned earlier, it is composed of mostly myelinated axons and is a main focus in a lot of studies as it is where a lot of pathologies target. The organization of the white matter consists of different tracts based on functionality. For instance, in the human spinal cord, there are 14 (or 13 depending on which references you are looking at) major ascending and descending tracts (as shown in Figure 2.3) [3]. Figure 2.3 shows a reference from Gray's anatomy that lists all the white matter tracts in 2 spinal cord levels (as some tracts become non-existent as you go lower down the spinal cord) whereas figure 2.3b shows a different source with less tracts and different positioning and sizes of the tracts.

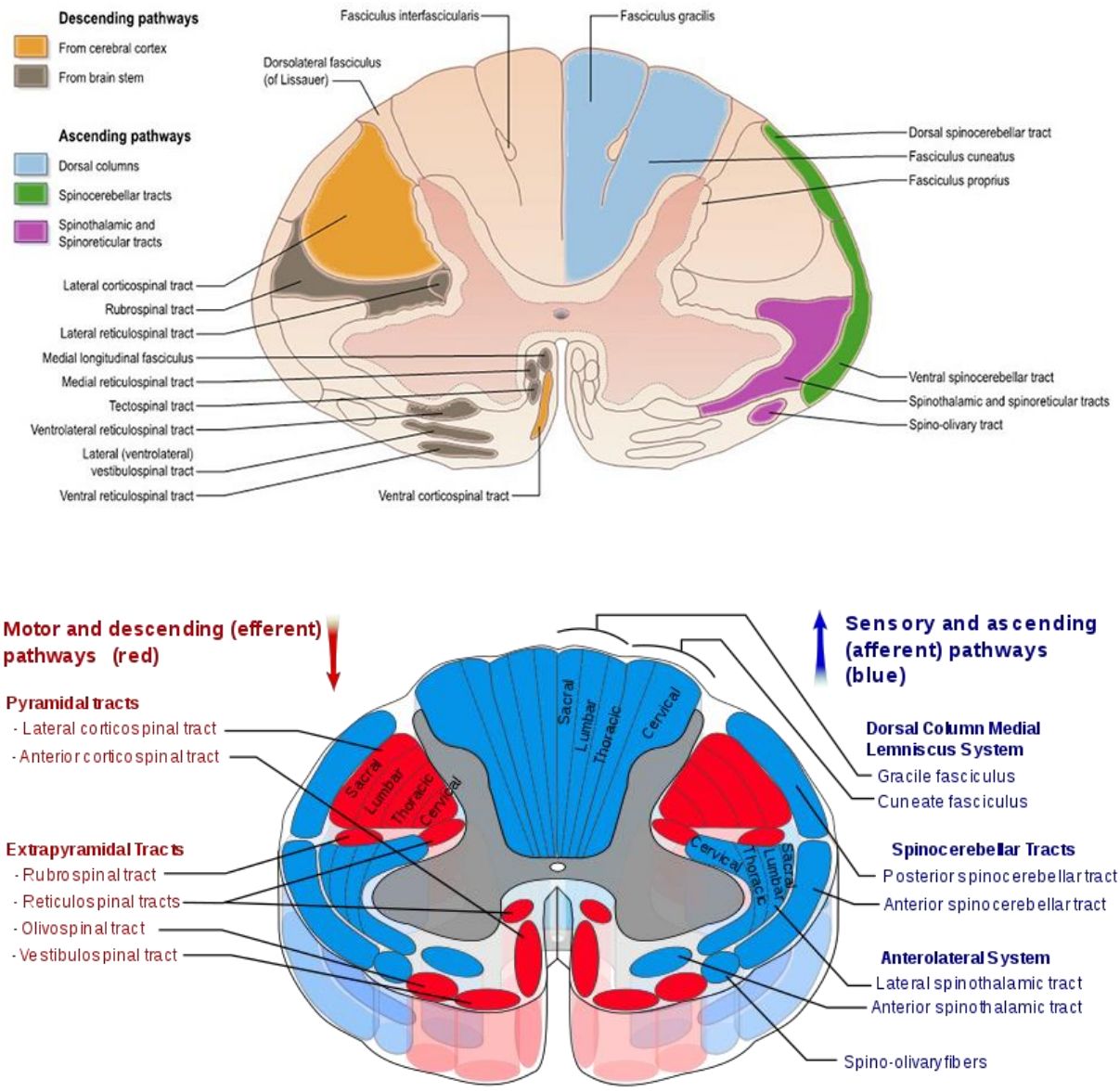

Figure 2.3: a) Ascending and descending white matter tracts of the human spinal cord at the cervical level [3] b) Tracts of the human spinal cord from another source. A comparison of the two figures from different sources showing the different positioning and sizing of the tracts. (image done by Polarlys and Mikael Häggström, used with permission).

And even moreso, if we were to compare these tract configurations with the Human Paxinos atlas (figure 2.4), we would see that a majority of the tracts are not even present or outlined in this one [10]. This would mean that with their staining techniques they were unable to establish all the

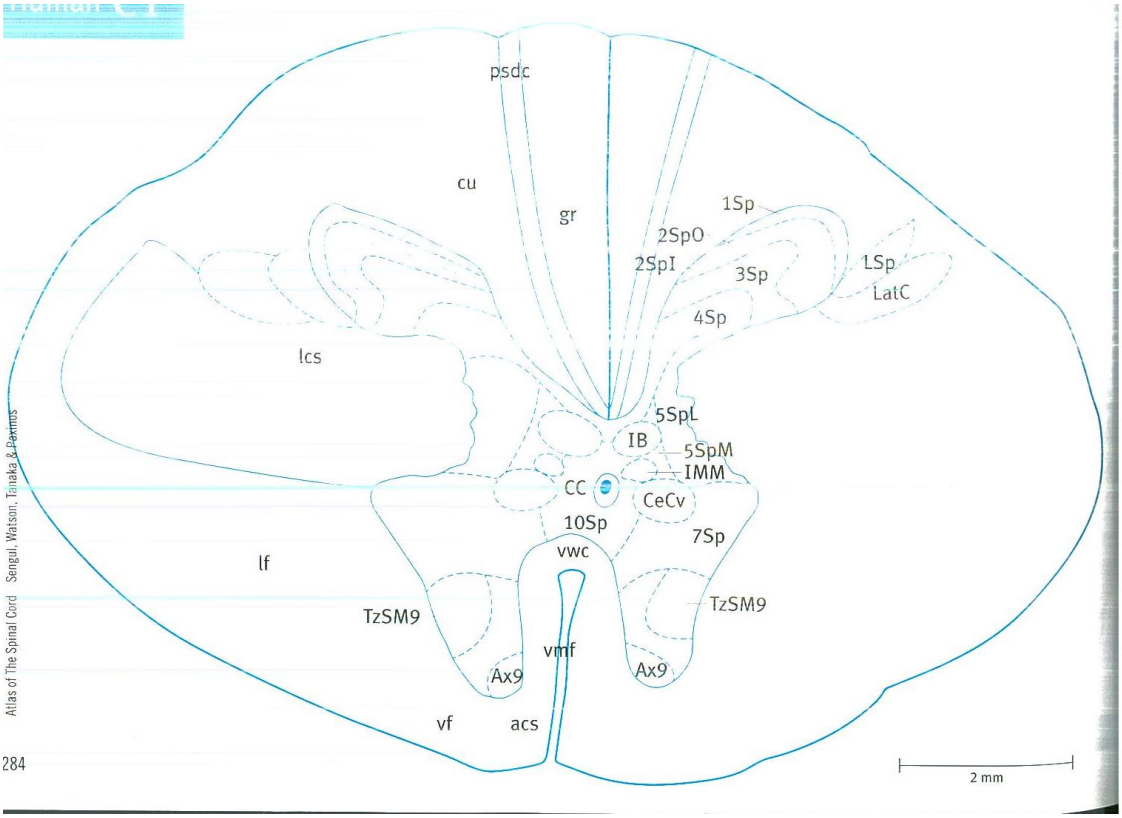

Figure 2.4: Paxinos Atlas figure of the white matter tracts for the human at level C1[10]

The rat spinal cord on the other hand has not been investigated quite as thoroughly as the human, with only one major study having been conducted on the entire cytoarchitecture of the white matter [10]. This is from the Paxinos group as well, that was only able to distinguish 7 major pathways in the white matter (as shown in Figure 2.5) [10]. They state that with their staining they were unable to identify all the tracts (just like in the Human) but to assume the positions of the tracts based off of what they have seen across species as well as what has been shown in the literature [11-18]. One has to also take into account the fact that these studies were done on single specimen samples, with older, manual staining techniques and through visual identification of the tracts, as well as being done almost 40 years ago. Something to note however is that dependent on the species, though most of the tracts remain in the same position, the corticospinal tract between rodents and human are not in the same spot [10]. In the human it is located in the ventral side of the spinal cord, whereas for the rat it is located dorsally [10].

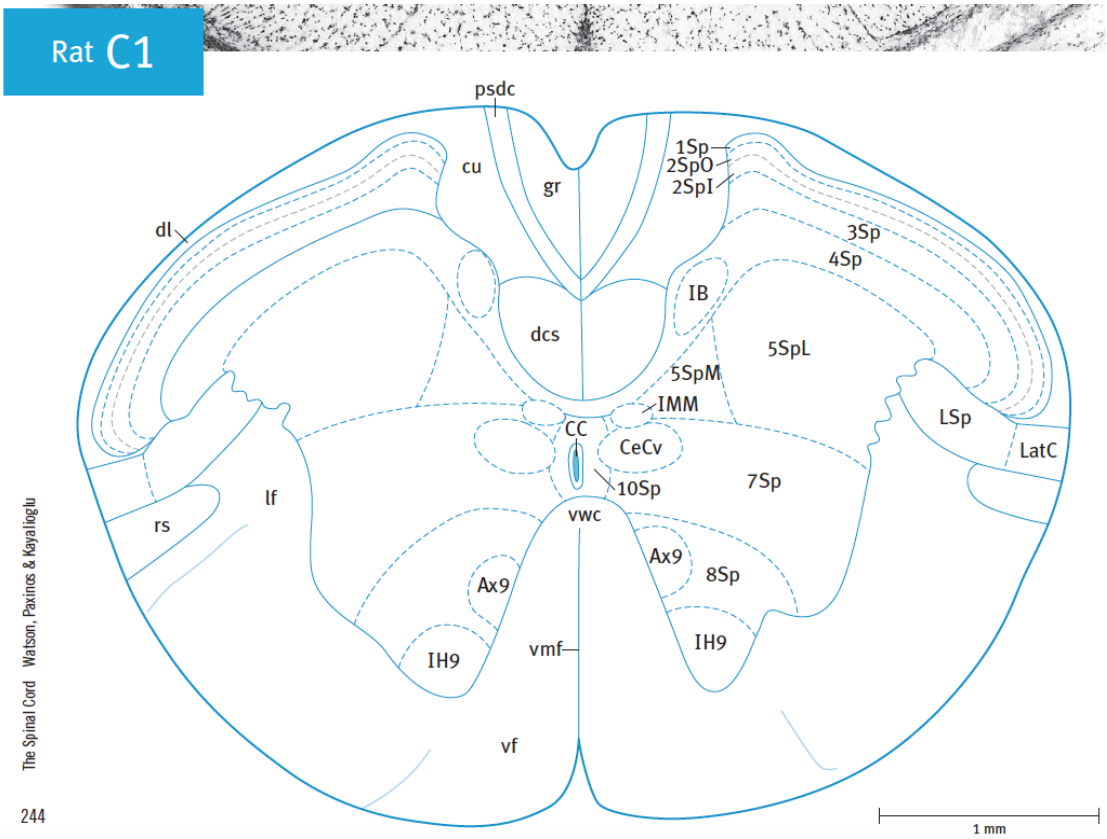

Figure 2.5: White matter tracts of the rat spinal cord of C1 from the Paxinos atlas[10]

To compare this to a similar species, the mouse spinal cord is observed to have 14 major tracts (as shown in Figure 2.6) [19]. This study came from the same Paxinos group but also extrapolated data from a variety of other sources to come up with this atlas. It would seem more plausible that the rat atlas would be comparable to the mouse atlas seeing that they share many similar anatomical features and traits and both come from the rodent family.

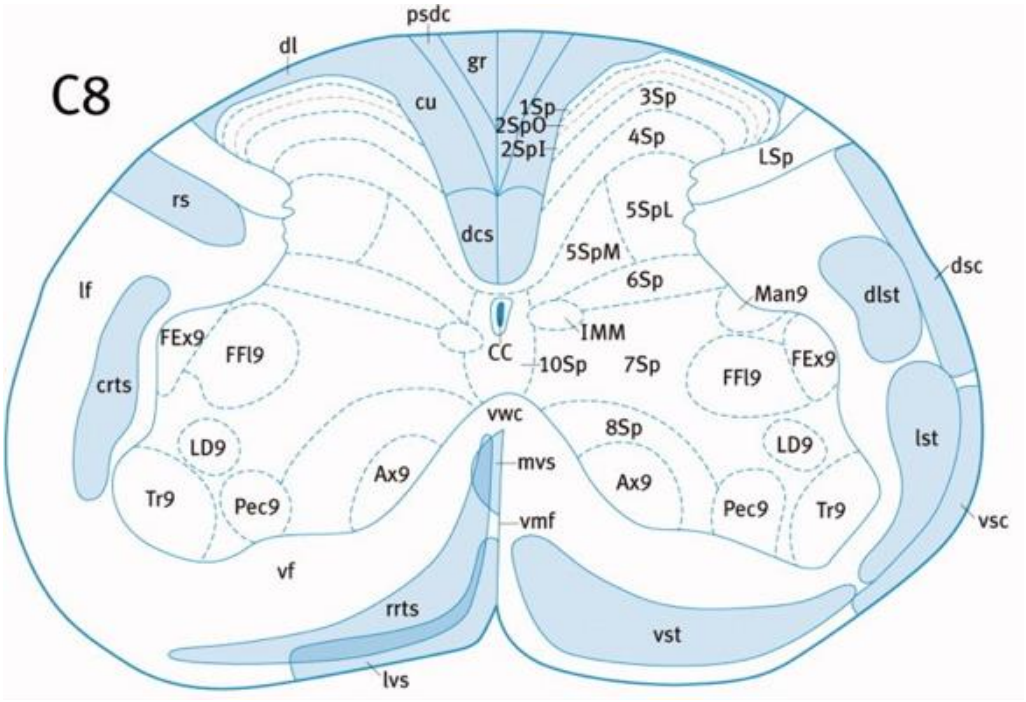

Figure 2.6: White matter tracts of the spinal cord of a mouse from the paxinos atlas [19]

Therefore, we can already see the differences that arise from species to species with regards to the white matter tracts. More so, depending on where one looks, the white matter tracts tend to vary from study to study as well. Not only this, but the zones and the sizes of some of the tracts also end up varying depending on the source. The studies are also very painstaking to do and quite tedious, and even when they are done there is no guarantee that all the tracts will be observed and thus they would need to extrapolate information from other species to complete the missing information. This reinforces the fact that there is a need to study the white matter tracts of the spinal cord in a more robust manner to obtain a consensus on the number of tracts as well as their positions and sizes.

As mentioned in the previous paragraphs, there are roughly 14 major pathways in the white matter. There are 8 ascending tracts found within the spinal cord of the rat. They consist of the gracile fasciculus, cuneate fasciculus, lateral spinothalamic tract, ventral spinothalamic tract, dorsal spinocerebellar tract, ventral spinocerebellar tract and the fasciculus proprius as highlighted in Figure 2.7 below [20]. Furthermore, other studies have shown that the gracile and cuneate fasciculus actually contain another tract that is present between both tracts called the postsynaptic

dorsal column (which can be seen in both of the figures for the mouse and rat spinal cord above) [21].

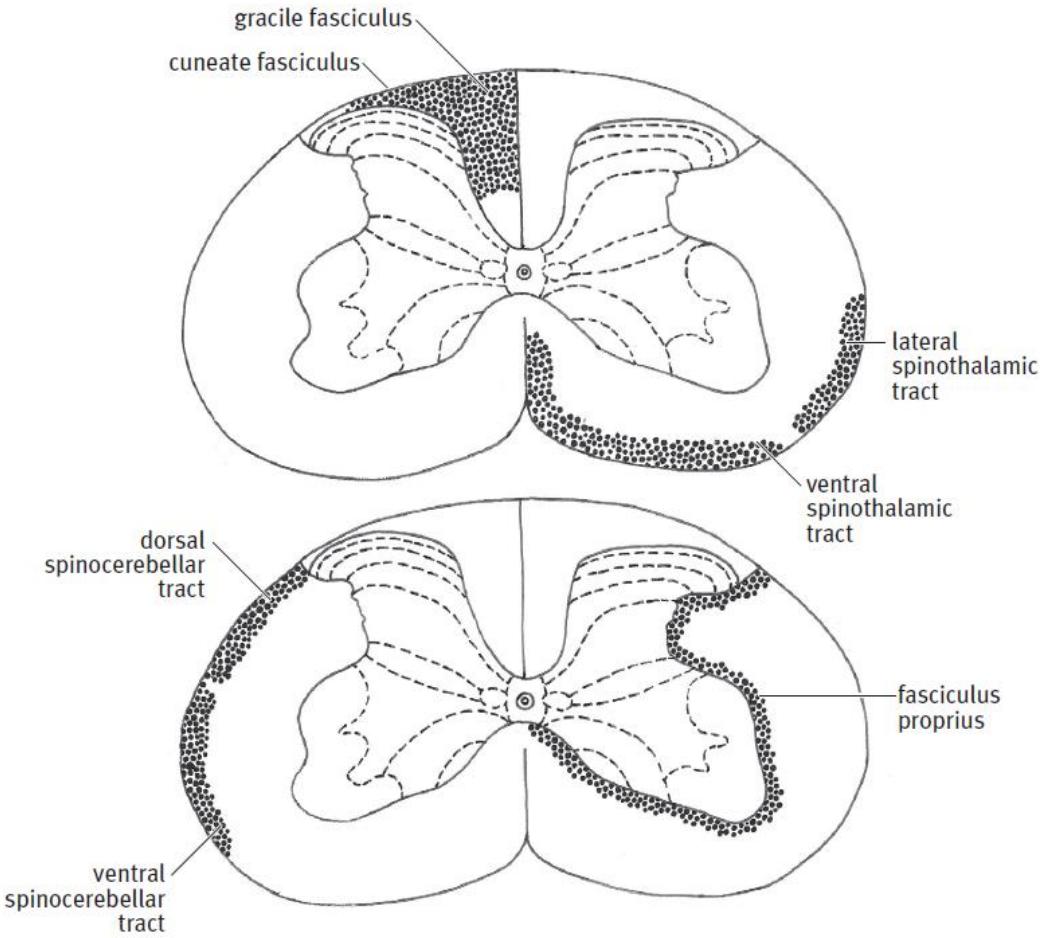

Figure 2.7: Overall major ascending white matter tracts found in the spinal cord [20]

The gracile fasciculus, cuneate fasciculus and postsynaptic dorsal column are part of the dorsal column pathway that is present throughout the entirety of the spinal cord. The gracile funiculus is responsible for the transmission of proprioception signals coming from the lower body (legs and trunk) whereas the cuneate fasciculus is responsible for those signals originating from the upper body and trunk [22-25]. The postsynaptic dorsal column has been shown to be a major tract for the signalling of visceral pain [26, 27]. The afferent nerve fibres of the cuneate funiculus are located from C1 until and including T6, and those from the gracile funiculus are in T7 and onwards [20, 25]. Both tracts also provide deep touch, vibrational and visceral pain sensation information.

The spinothalamic tract is split up into two parts, the first is the lateral spinothalamic tract and the second is the ventral spinothalamic tract. The lateral spinothalamic tract is responsible for conveying pain and temperature sensations, whereas the ventral spinothalamic tract is responsible for the general (or crude) touch and pressure sensations (meaning non-localized) [28, 29]. Both of these tracts are located across the entirety of the spinal cord, meaning that they are responsible for conveying this information from the entire body [30, 31].

The next two tracts are the spinocerebellar tracts which are also separated into two tracts as well, split between the ventral and the dorsal sides of the spinal cord. Both tracts are responsible for the transmission of information of the coordination of movement as well as posture for the lower limbs, however the differences arise in the fact that for the ventral tract the information is more general from larger receptive fields whereas for the dorsal tract the information transmitted is fine coordination of individual muscles [32-34].

The last tract to note in the diagram but is not entirely an ascending nor descending tract is the fasciculus proprius. This tract is simply the cumuluation of tract fibers that arise in the spinal cord but also terminate in the spinal cord and therefore do not reach or transmit information to the brain. They are categorized as short fibers and both ascend and descend but strictly remain within the spinal cord [20].

There are 6 main descending tracts in the rat spinal cord. They consist of the corticospinal tract, rubrospinal tract, medial vestibulospinal tract, lateral vestibulospinal tract, medullary reticulospinal tract and the pontine reticulospinal tract (Figure 2.8) [35].

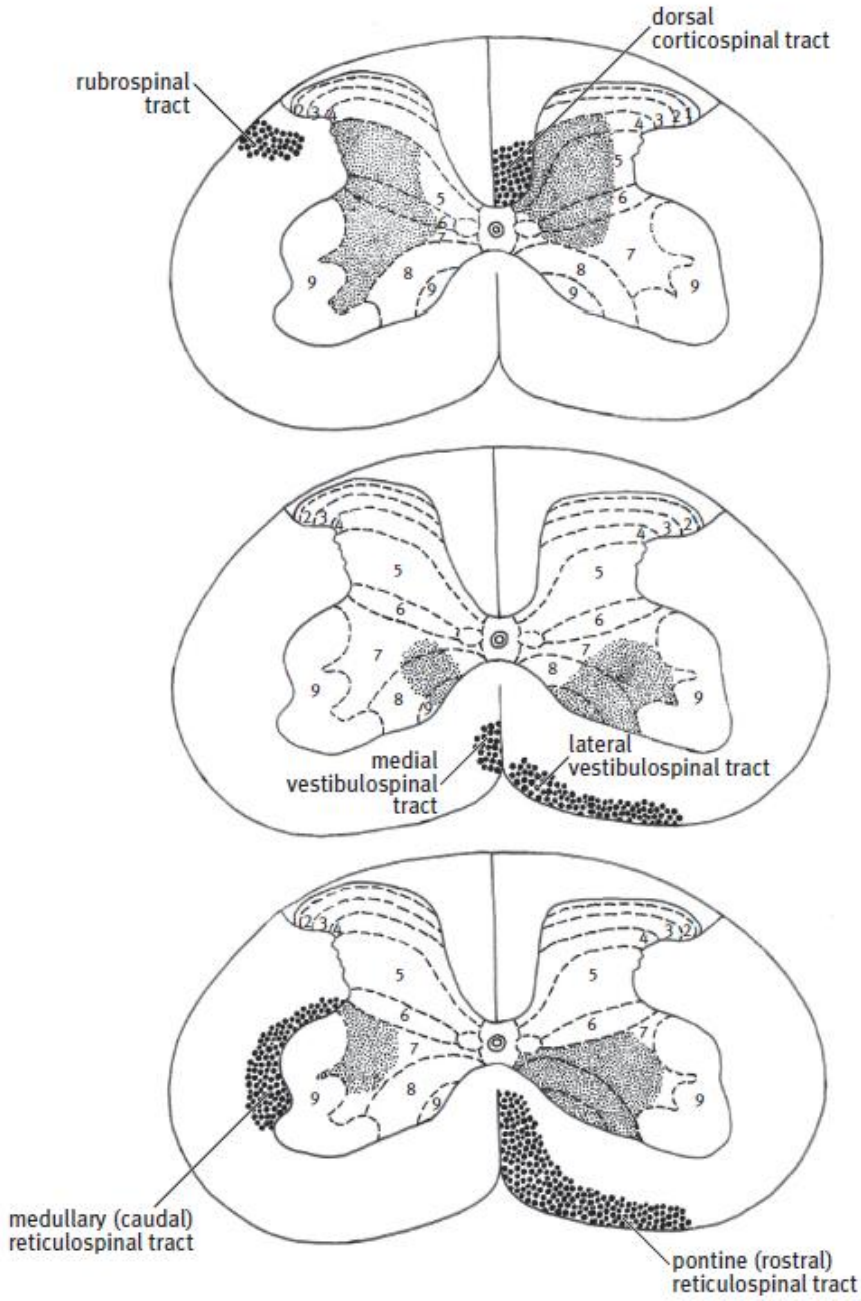

Figure 2.8: Overall major descending white matter tracts found in the spinal cord [35]

The dorsal corticospinal tract is one of the more important and major tracts of the spinal cord. It is present in all mammals, the difference being in where the tract is found between species. In the rat, as mentioned through the name, it is found in the dorsal column area. This tract is one of the main tracts for motor control, where damage to this tract ends up resulting in paralysis [36].

The next descending tract is the rubrospinal tract which is responsible for some locomotion functions, especially seen in vertebrates with fins or limbs that are used for movement. It has also been observed to play a role in skilled motor functions [37].

The next tract is the vestibulospinal tract that is divided into two parts; the medial vestibulospinal tract and the lateral vestibulospinal tract. The medial vestibulospinal tract controls the positioning of the head with respect to the positioning of the body as well as the stabilization of the head which is known as the vestibulocollic reflex [38, 39]

The last two tracts are the reticulospinal tracts which are also divided into two segments: the medullary (caudal) reticulospinal tract and the pontine (rostral) reticulospinal tract. These tracts are responsible for movement, preparatory and posture control as well as involvement in sensory and autonomic functions [12, 13, 17].

One of the difficulties facing the delineation of the white matter tracts from the previous atlases is that many stains need to be used in unison to be able to determine the variations in all the different types of cells which would be used as a the principle method of outlining the tracts. Furthermore, since this is the case, the determination of the tracts would then have to be done visually to try and locate the boundaries of the tracts when the composition of cells and their morphometrics change. This can be observed in the figure below taken from the Paxinos atlas showing the variety of stains used and trying to observe the tracts based on these stains.

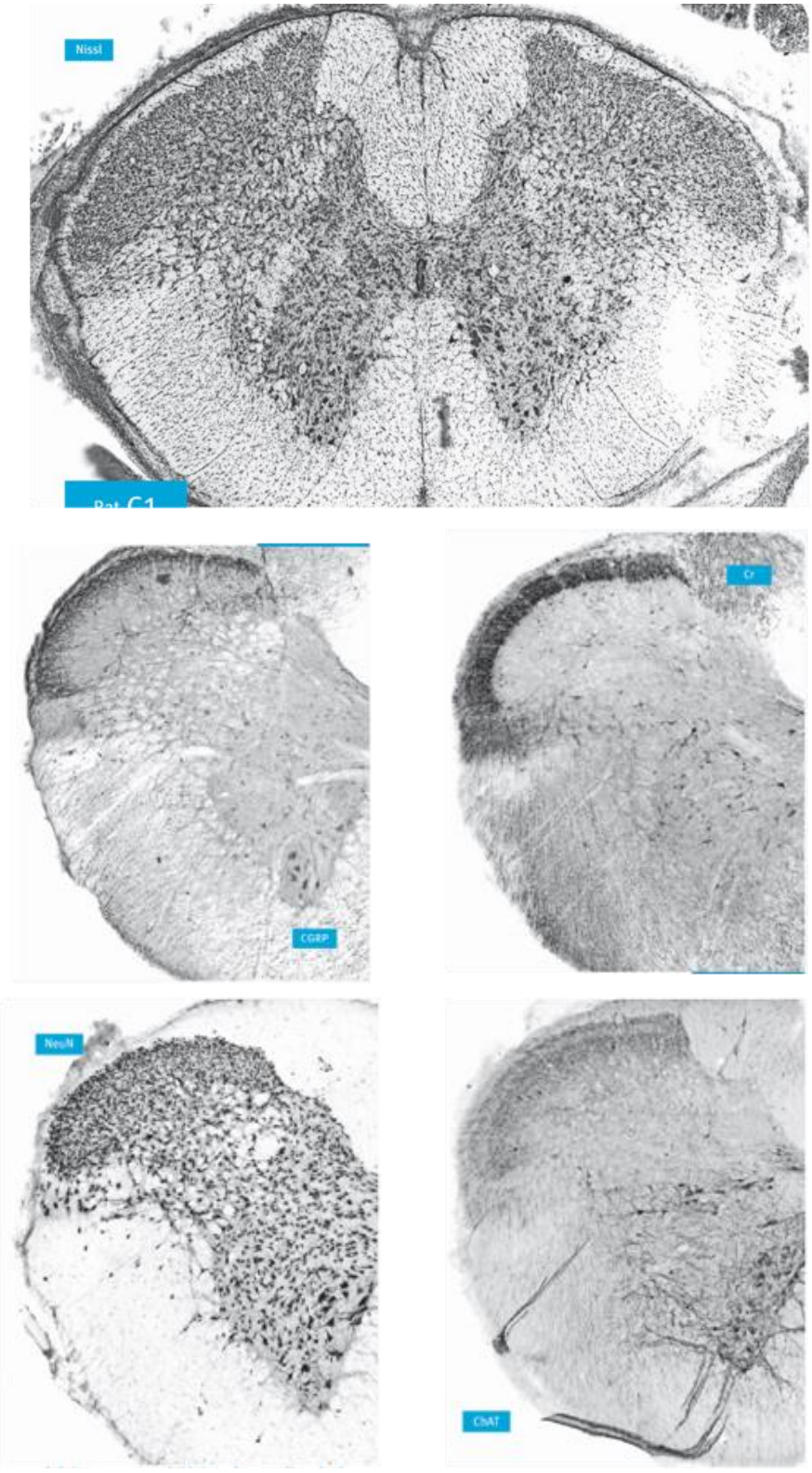

Figure 2.9: Various stains on C1 level of rat spinal cord showing the delineation of the white matter tracts [10]

2.2 Scanning Electron Microscopy

Microscopy is one of the most standard methods to obtain high resolution images of tissue samples. In general, one of the more commonly used forms of microscopy is optical microscopy due to its relative ease of use and inexpensive systems. Optical microscopy operates by simply using a light to shine on the sample with a system of lenses to enhance and magnify the object. However, there are limits to the resolution and capabilities of optical microscopy [40, 41]. Therefore, one of the options used at this moment for a lot of high resolution histology is scanning electron microscopy (SEM). Electron microscopy uses an accelerated electron beam to produce the light, and due to this, electron microscopy can yield higher resolution images [42]. It works by having an electron source (usually a tungsten filament) that fires a concentrated electron beam at the sample such that the electrons released from the sample are then scattered and detected to obtain the image [42]. There are various detection methods that can be used to detect the different types of electrons that are scattered from the samples. The most common is the detection of the secondary electrons (SE) which are the electrons released from the valence shells of the atoms from the sample [42]. Since these electrons more commonly occur from the surface of the image, it often yields higher resolution of the surfaces of the samples. The second detection method is for the backscattered electrons (BSE) that occur as a result of the electron beam being elastically scattered after coming in contact with the sample (comparison between SE and BSE shown in Figure 2.9) [43].

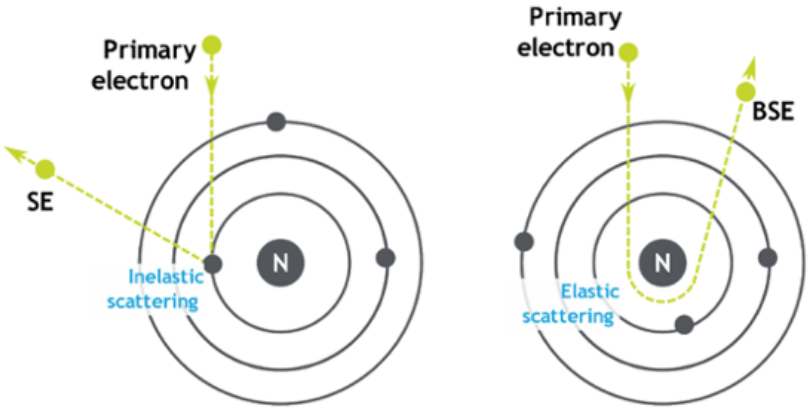

Figure 2.10: A comparison between how secondary electrons vs. back scattered electrons are formed [44]

These electrons can be scattered back at different angles and therefore can be detected to obtain different types of information (shown in Figure 2.10). The first is high-angle BSEs which as the name implies are scattered back at a higher angle and therefore can yield information such as z-contrast and compositional differences in the sample [45]. However it also does not have very high spatial resolution. The second type is the low-angle BSEs which yield more surface and topographical information with a much higher spatial resolution [45]. This does not yield much on the compositional differences however. Therefore in order to detect surface tissue structure where only the axon and myelin are of concern, the low-angle BSE detection method would be the most appropriate. However, if one wanted to look at more internal structures, high-angle BSE detection might be more useful.

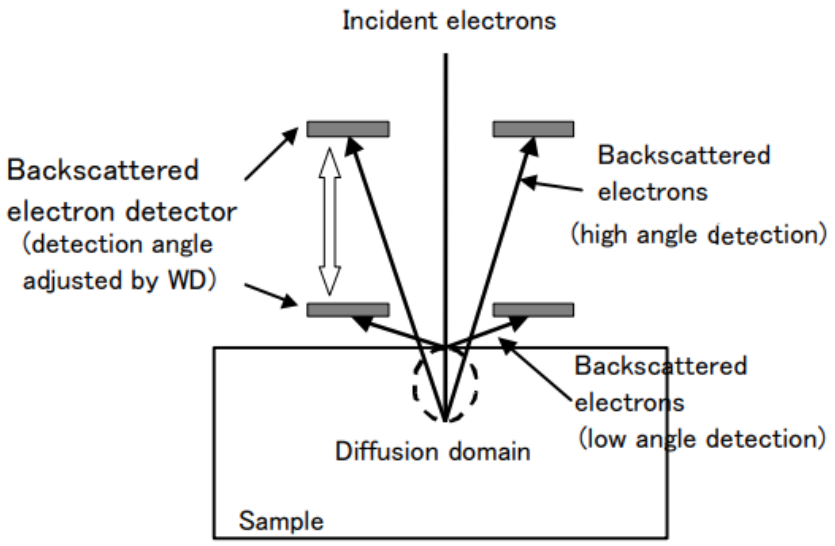

Figure 2.11: The different angles that backscattered electrons are released and at what positions they can be captured by the detectors in the SEM [46]

The trade off with using SEM however is that it is a much more expensive system and it requires extensive sample preparation in order to obtain the appropriate images, especially when dealing with biological samples [47]. The sample preparation usually requires the samples to be embedded in a resin, finely polished to ensure a smooth and flat surface and also coated in gold to ensure appropriate conductivity. Furthermore, the samples also need to be fixed and dehydrated so that the samples are dry since they will be placed into a high vacuum chamber.

Despite these stringent preparation requirements, SEM can still yield very high resolution, high contrast and detailed images that can aid in the investigation of tissue microstructure. An example of this would be from Mikula et al, that were able to obtain ultra-high resolution images of the brain tissue microstructure as shown in Figure 2.11 below [48].

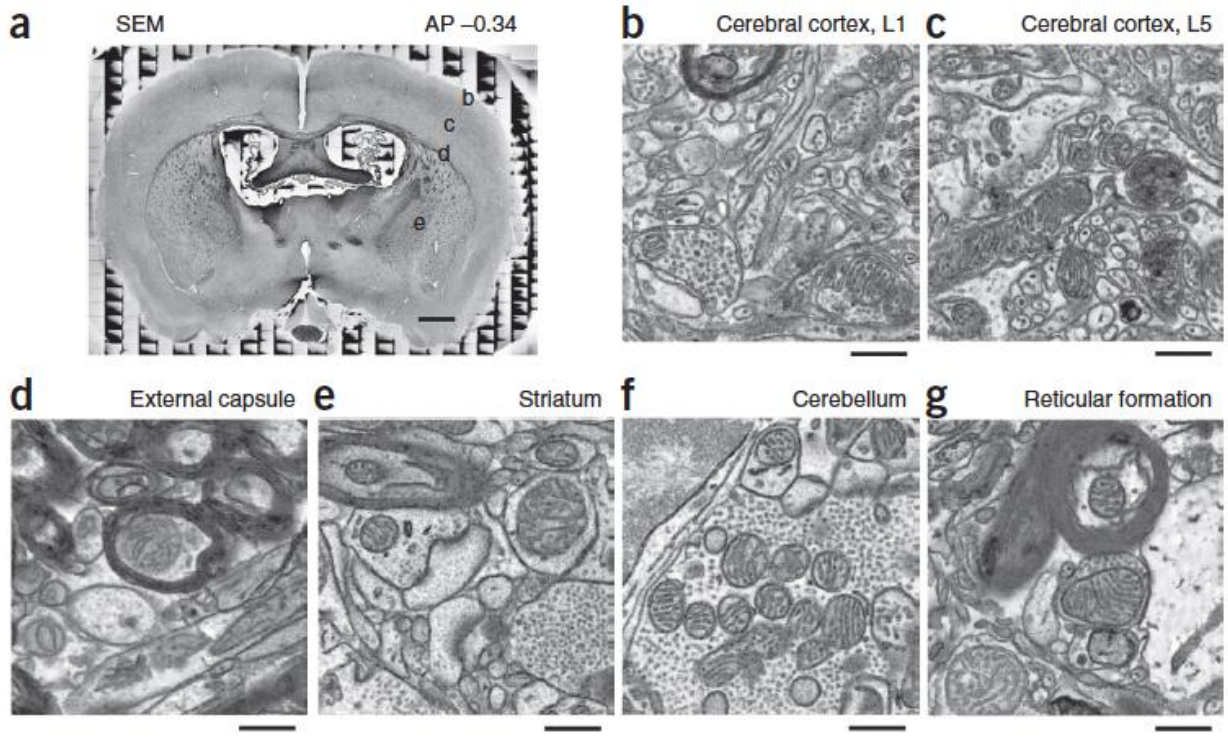

Figure 2.12: Various sections of a rat brain from Miklua et al. showing the in-depth and high quality images obtained by SEM [48]

The higher the resolution of the images, the more accurate representation of the investigation of the tissue microstructure. This would allow one to obtain quantifiable metrics more precisely to be then used for further analysis. Therefore, there is quite an importance placed on the quality of the images obtained.

2.3 Clustering

The concept of clustering is to find and group patterns within the data. These patterns tend to be points within the data that have similar properties (i.e. similar values in pixel intensity). It is a form of unsupervised learning as once the input parameters are set it starts to group and re-group the data based on the specified distance metrics and measurements. A summary of clustering algorithms and their main parameters is shown below (Figure 2.12).

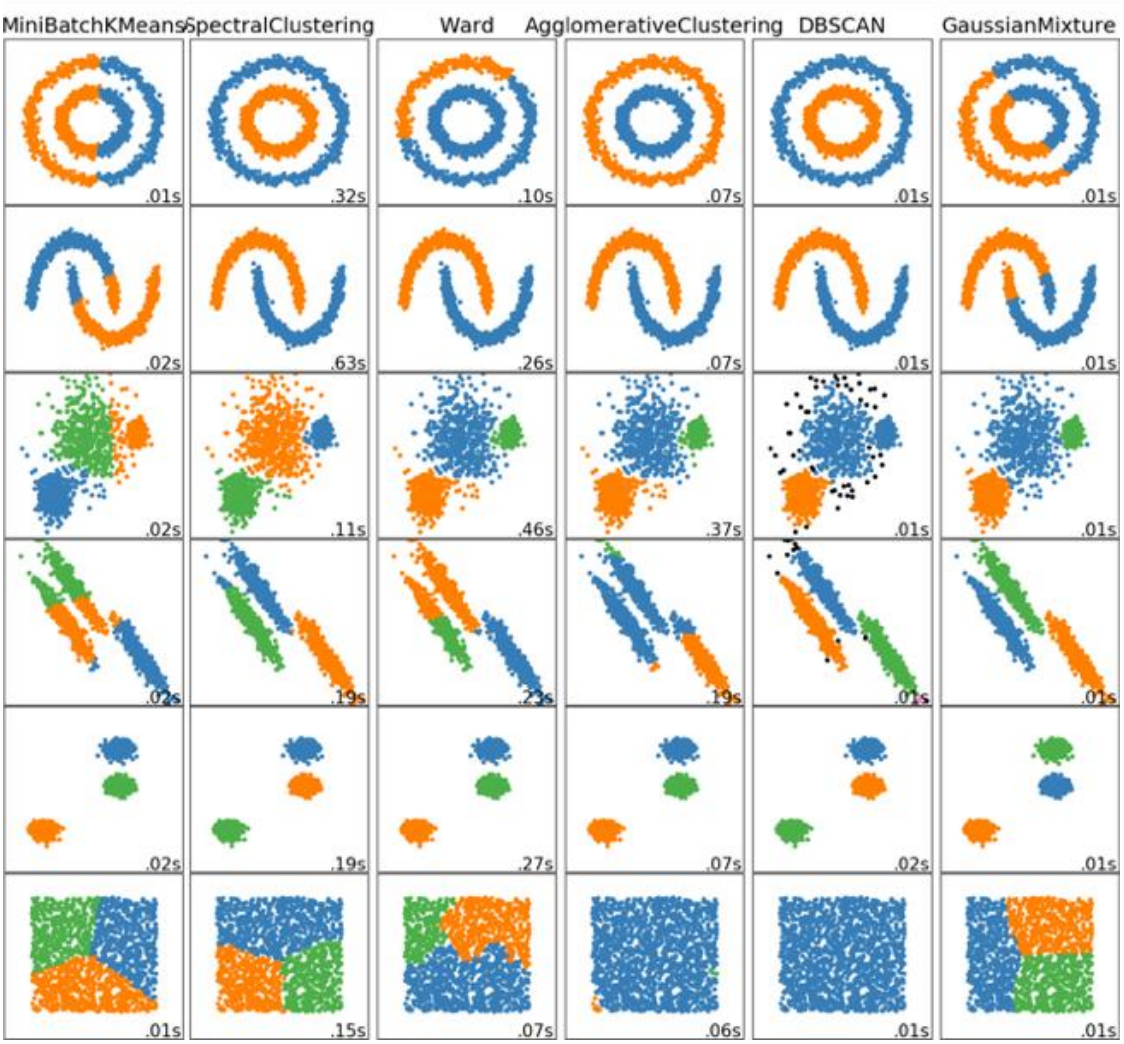

Figure 2.13: Chart showing the different clustering algorithms applied to different types of data and how the data is sorted. Included in the corners are also the computing times for each algorithm. [49]

There are many clustering algorithms out there and so deciding to choose one over another depends on the parameters of the algorithm as well as the input data and what you are specifically looking for. Some of the more commonly used algorithms that are seen in studies are the K-means, spectral, hierarchical, and DBSCAN (density-based spatial clustering of applications with noise). Each algorithm plays to its own advantages and uses a specific method to cluster the data along with different parameters to be used [50].

The K-means clustering algorithm clusters data by minimizing the inertia of each cluster. It works by calculating a centroid for each cluster that will minimize the within cluster sum of squares as such:

$$\sum_{i=0}^{n} \min \left(\| x_i - u_j \|^2 \right)$$

Then once it has chosen a centroid for a cluster, it selects points with the smallest Euclidean distance which in turn results in the smallest sum of squares in relation to that centroid. Then it updates the process over and over again dependent on the number of clusters the user has inputted. However, one of the main issues in using this approach is that it assumes all the clusters to not only be convex but also isotropic, which depending on the input data (as well as what one is searching for) is not necessarily the case. Secondly, due to these assumptions, it then does not work as well on clusters that are not shaped in that specific format [51].

Spectral clustering uses the eigenvalues of the similarity matrix constructed from the input data to create clusters. It does this by first creating a similarity graph based on either of two approaches (nearest-neighbour or epsilon-neighborhood), then the graph is transformed to a low dimensional space by calculating the graph laplacian and obtaining the eigenvalues and eigenvectors, from which then a k-means based clustering is implemented using this to obtain the final clusters.

$$W_{ij} = \begin{cases} \exp\left(-\frac{\left\| y^i - y^j \right\|^2}{2\sigma_f^2} \right) if\ i\ and\ j\ are\ neighbors \\ 0\ otherwise \end{cases}$$

This is represented by the above equation where Wij is the adjacency matrix weighted by the distance between voxels (i and j) and where yi – yj are data points and σ_f^2 is the average squared distance between neighboring voxels. Thus spectral clustering still uses k-means clustering but it essentially does so on a form of an adjacency or similarity matrix of the eigenvalues [52].

DBSCAN clustering uses a density based method of looking at areas of high density versus areas of low density. It essentially treats main points within the cluster as a core and then expands by adding more points to it based on the number of points and their proximity to that core.

Therefore, the closer the points are together, the higher the probability that they will be in the same cluster. This needs two main parameters to be specified by the user however, the first being the minimum number of data points to determine the cluster and the second is the distance between points within the cluster.

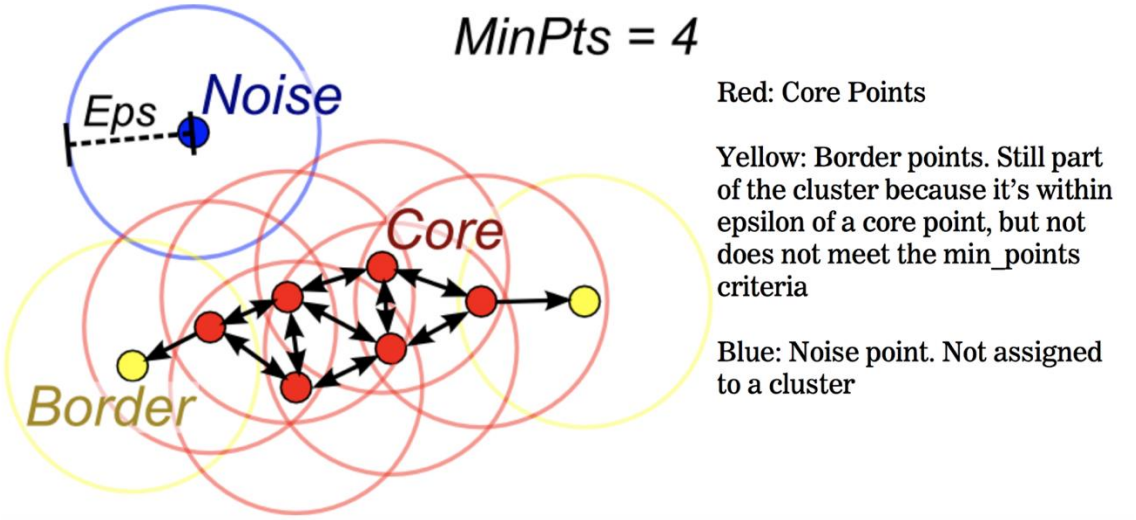

Figure 2.14: Illustration of how DBSCAN clustering works. The red points are shown as the cores which are the main points that get added to the cluster based on proximity. The figure shows that based on a specified distance, the yellow points are considered to be part of the cluster as they are just at the max distance away from the core points but the noise point in blue is not taken into account to be a part of the cluster [53].

Hierarchical clustering can be divided into two different approaches. The first is a top-down approach where everything is considered as one cluster and then recursively splits up into different clusters. This is known as divisive clustering. The second approach is known as agglomerative clustering where each data point is considered as its own cluster and successively merges with other points to form clusters. Both of these methods try to build a hierarchy of clusters which is represented as a dendrogram (Figure 2.14) [54-57].

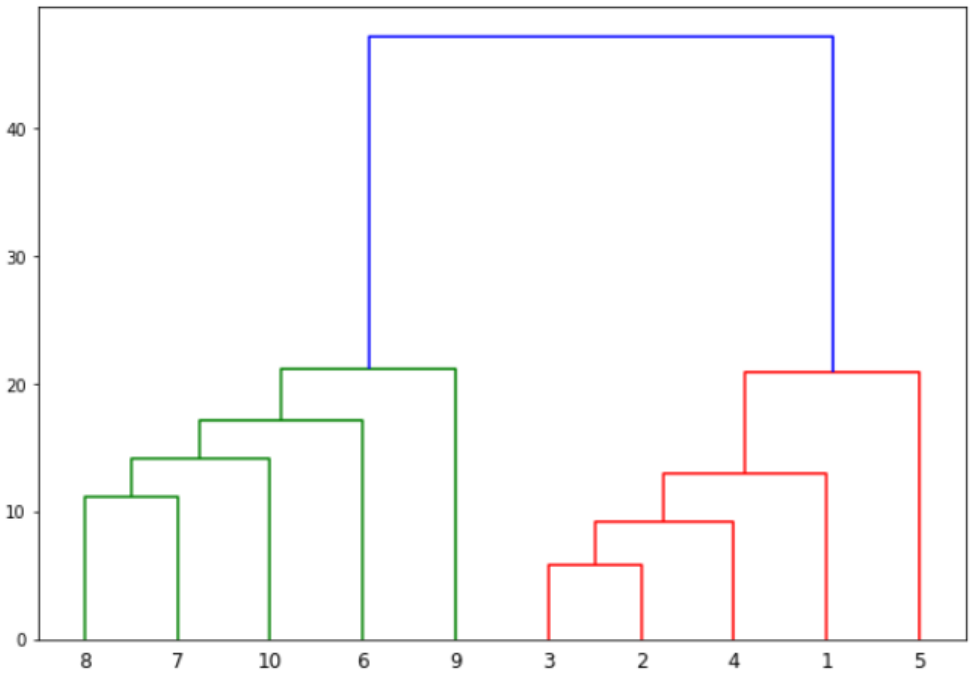

Figure 2.15: An example of the breakdown of agglomerative clustering which is based on a bottom up approach of starting every single point as its own cluster and then moving up the hierarchy to group more and more points together [58].

Agglomerative clustering is the more used one out of the two as it is less expensive in terms of memory, as with dividing down into clusters there are $O(2^n)$ ways to split the clusters whereas in agglomerative clustering there are $O(n^2)$ ways to merge the clusters. Therefore, depending on the size of the input data, divisive could be too overwhelming [59].

Another key component for clustering is the concept of the connectivity matrix. A connectivity matrix (also known as an adjacency matrix) is a matrix that distinguishes which parts of the data are directly located or connected to each other and portrays this in the form of a matrix (example shown in Figure 2.15). Essentially, if two points are next to each other, the matrix would represent that with a 1 and if two points are not next to each other then it would be represented as a 0.

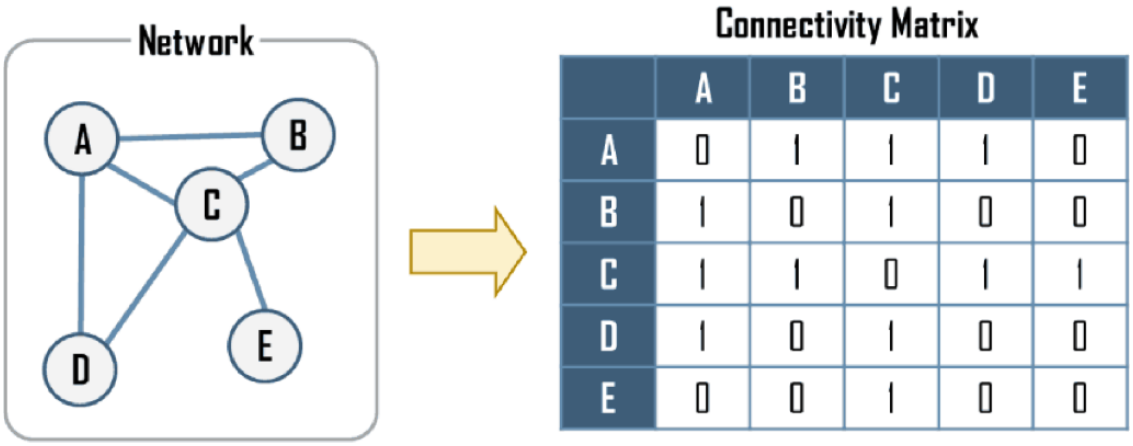

	A	B	C	D	E
A	0	1	1	1	0
B	1	0	1	0	0
C	1	1	0	1	1
D	1	0	1	0	0
E	0	0	1	0	0

Figure 2.16: An example of a connectivity matrix where based on specific points a matrix is assigned with 1s and 0s based off of whether two points are connected to one another (or adjacent to each other) or not [60].

For example, in an image, this would be expressed by the pixels in the image that are directly adjacent to one other or not. What this allows for within the context of clustering is that since we already know that the data within a cluster can only be from those pixels adjacent to it, we can then allow for a defined spatial resolution and delineation yielding more coherent results. It allows for spatial representation and bounds to be set.

As of recently, only very few studies have been undertaken to really ascertain the underlying white matter tracts. Prior to these studies, the studies done to characterize and map the white matter of the spinal cord were done over 40 years ago using older, manual staining techniques as well as limited sample sizes (the paxinos atlas is only based off of one whole rat spinal cord). Moreover, the recent studies undertaken that did some form of investigation on the white matter tracts were done in studies where this was not the main focus of the study. An example of this would be from the study by Benjamini et al. where they were investigating the white matter microstructure using a double diffusion encoding MRI method to map the distribution and variation of axon diameter throughout the white matter on MRI methods [61]. They obtained the maps as shown in Figure 1 below that showed the voxel-weighted and normal-weighted axon diameter distribution maps.

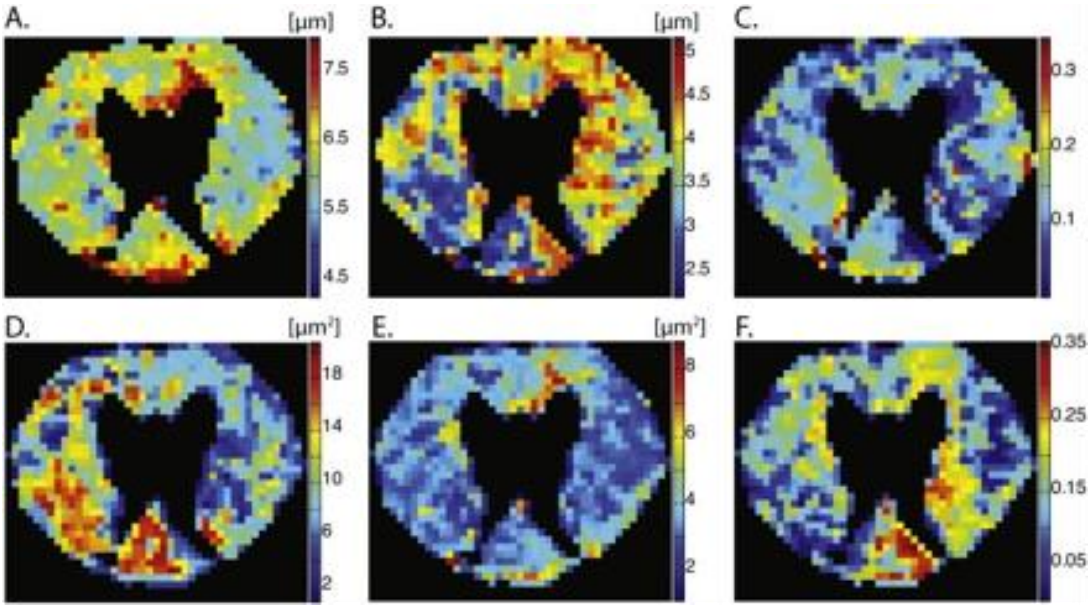

Figure 2.17: The results obtained by Benjamini et al. that illustrates the average volume-weighted and number-weighted axon diameter distribution (a and b) as well as the axon diameter variance from the volume-weighted and the number-weighted axon diameter distribution (d and e). Parts c and f show the extra-axonal volume fraction and the sub-micron fraction maps respectively [61].

Then using these distribution maps, what they ended up doing was applying a k-means clustering algorithm to look at what kind of tracts and groupings would arise from this data. This is shown in Figure 2.17 below.

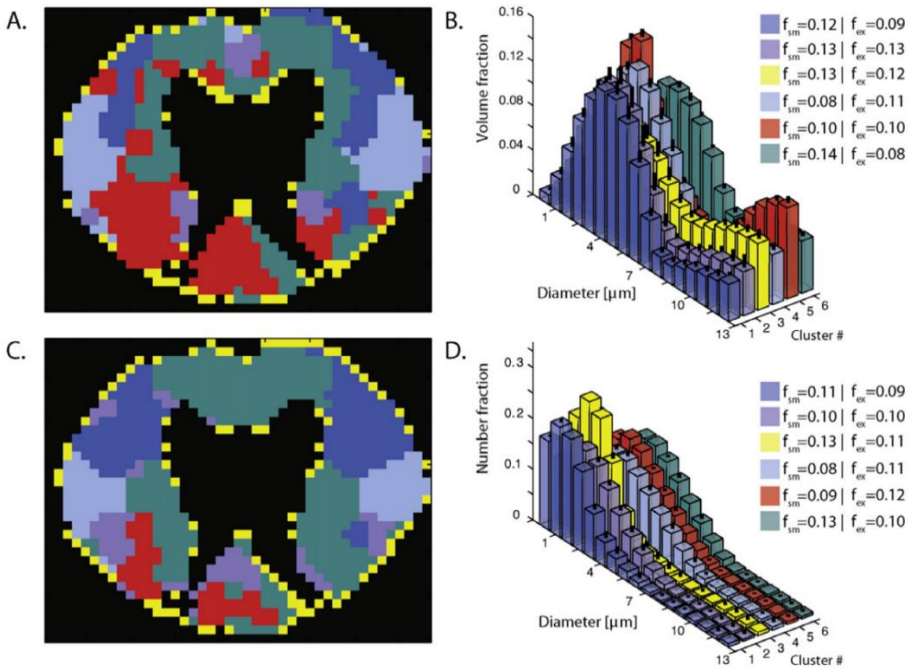

Figure 2.18: The results in (A) show the applied k-means maps on the volume weighted axon diameter distribution and in (C) the volume-weighted axon diameter distribution. Figures B and D show the average axon diameter distribution and extra-axonal and sub-micron volume fractions per cluster [61].

What we see from this is a slight groupings of the data based on the axon diameter distribution. However the paper itself doesn't really go into details outlining what tracts the clusters represent and adding some form of anatomical direction to the data.

Another example of the very few papers out there investigating this is from Assaf et al. Their paper was also on the utilization of diffusion MRI data to establish a method for axon diameter distribution (which they named axcaliber) [62]. The distribution maps they obtained are shown below in Figure 2.18 after which they compared the clustering of their data to the clustering they did on histological stained slices. This was all done on porcine spinal cords so comparatively the tracts may differ a bit from what we saw previously for the anatomy of the rat spinal cord.

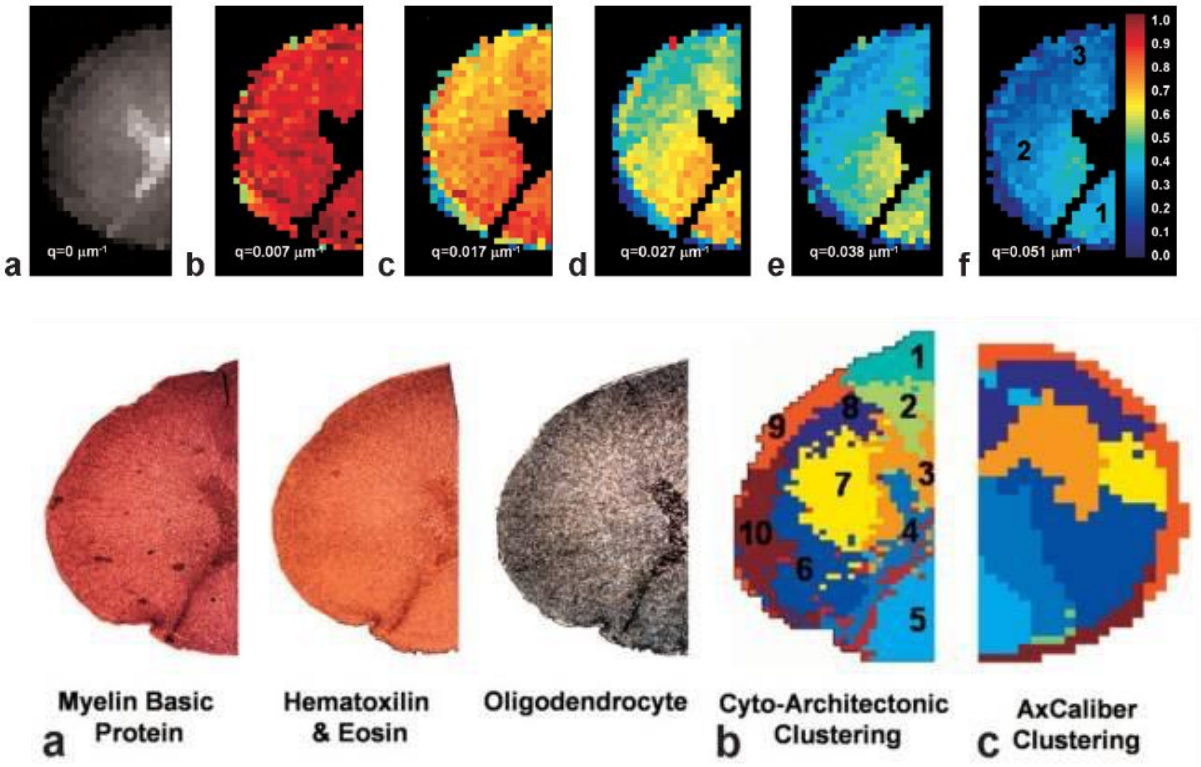

Figure 2.19: i) The data obtained from Assaf et al. on diffusion MRI data ii) Figure showing the various histological staining done (a) which is then clustered using k-means (b) and then compared to the k-means clustering applied on the diffusion MRI data (c) [62].

What we observe form their results is the grouping of the tracts based on a k-means clustering algorithm again. We can see that the tracts are not completely well-defined with pixels overlapping across tracts. This can be observed for the previous study from Benjamini as well. One of the main things it that both studies are using lower resolution data (comparatively to histological data) as well as the fact that both studies are applying a k-means based algorithm which is a bit more simpler as an algorithm. Furthermore, looking at the histological data clustering, we can see that even utilizing this, the clustering algorithm does not do a great job at delineating the tracts as there were sparse pixels distributed throughout regardless of the tracts.

These were the only 2 studies that were found on the application of a clustering algorithm to highlight the cytoarchitecture of the spinal cord. Each had not really explored the different types of algorithms out there to really determine what could yield the best possible results and give the closest semblance to the true anatomy. What is more prevalent in research is the use of these types

of clustering algorithms in brain parcellation studies. Those studies also use a broader range of clustering techniques to delineate the various white matter tracts and fiber tracts in the brain.

One of those studies is the study by Thirion et al. that investigates different clustering algorithms applied to brain f-mri data to observe the functional connectivity patterns [63]. They looked at three different types of algorithms, k-means, spectral and ward and then validated the results based on accuracy and reproducibility of the parcellation. An example of their results is shown in figure 2.20 below.

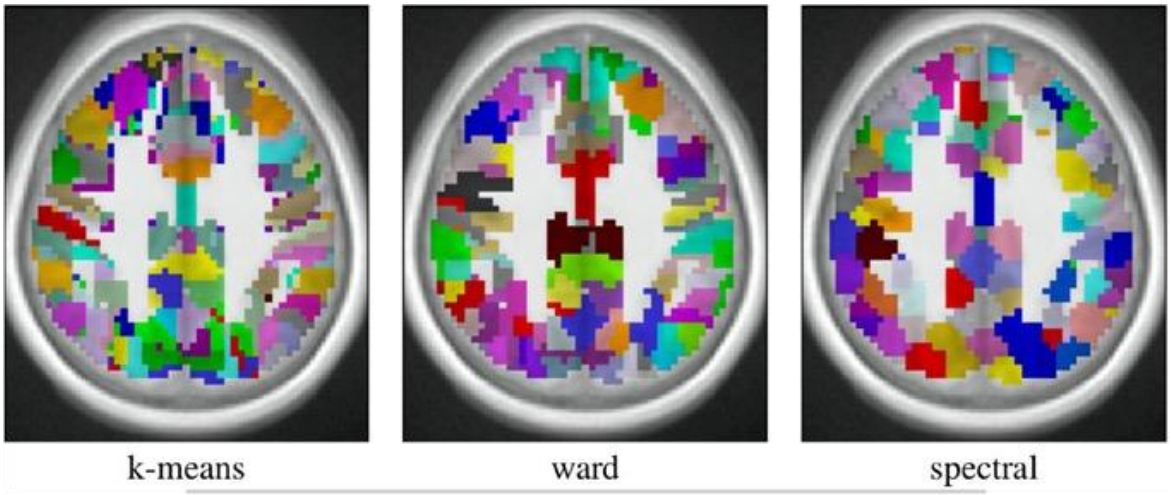

Figure 2.20: A comparison of three different clustering algorithms applied on the brain showing the variations in how each algorithm clusters the white matter fibre tracts [63].

They were able to conclude based on their results that ward clustering obtained the best results when taking into account accuracy and reproducibility. They also showed however that there is still some form of trade-off in trying to maximize the accuracy or reproducibility and thus a compromise needs to be made in order to obtain viable results.

A second study done on brain using diffusion tensor imaging data was done by Zhang et al using hierarchical clustering as their main method to determine the brain fiber tracts [64]. They essentially looked at various thresholds that they could tweak in order to try and obtain the most anatomically relevant clustering of the fiber bundles as shown in figure 2.21 below.

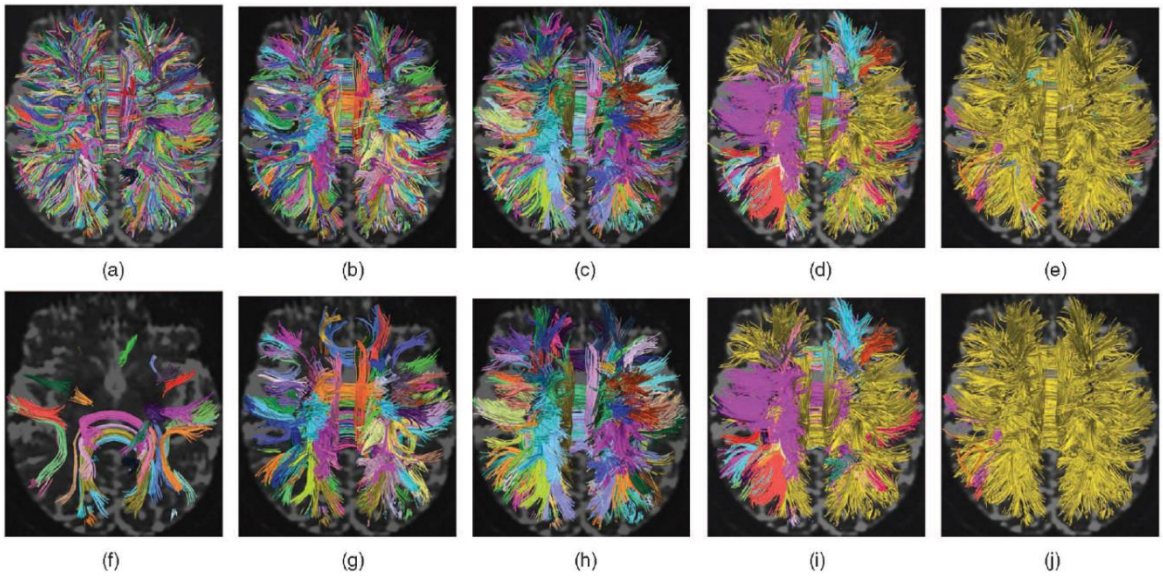

Figure 2.21: The results show the clustering using agglomerative clustering tweaked with their own model with different parameters. From figures (a)-(e) the thresholding for the fibre thickness was set to 1.5 mm, 2.5 mm, 3.5 mm, 4.5 mm, and 5.5 mm respectively. For figures (f)-(j) the same thresholding applied for each image but then set with a minimum cluster size of k=10 [64].

They were able to obtain anatomically relevant and precise fiber bundles based on using proximity thresholds between fibers as their main parameter as well as the number of clusters they were looking for.

Thus from these examples we can see that there have been more exhaustive approaches in clustering and parcellation of the white matter in the brain as opposed to spinal cord. Our aim is to change that by exploring and implementing clustering algorithms on spinal cord as the main focus of the study. We had explored a few types of clustering algorithms applied to our datasets to see what would yield the best results.

2.4 Clustering Validation

As with anything that produces a result, there is always the question of whether that result is correct or not and how would one be able to define or validate whether it is indeed correct. One of the most used tools as a means of validation, especially in neuroimaging, is the concept of the ground truth. It is defined as an evidence obtained empirically or directly visualized such that it is concrete evidence. Therefore, one could always compare obtained results with this ground truth to

see if what they are observing is correct. Depending on context, this can be interchanged with the term gold standard as well, but generally speaking, a gold standard is essentially an imperfect ground truth whereby it is as close to the ground truth as possible based on limited constraints. In the context of this specific research project, as has been mentioned earlier, it is very difficult to truly have a ground truth comparison for the white matter tracts as already it is not 100% certain on the positions or sizes, as well as the fact that there is no digital resources available on histological images that could be used for comparison. Therefore, trying to compare whether the clusters are in fact correct or not has to rely on the intrinsic properties of the clusters themselves.

There are a few methods in the way this can be done without the use of ground truths. The first is the silhouette coefficient technique that measures the intra-cluster distance and the mean nearest cluster distance for every single data point to evaluate how well that data point fits within the cluster. It is given by the following equation:

$$s = \frac{b - a}{\max(a, b)}$$

Where a is the mean distance between a point and all other points in the same cluster and b is the mean distance between a point and all the other points in the cluster closest to the cluster that point is contained in. It outputs a score between -1 to 1 where -1 means the point does not belong to the cluster at all and 1 means the point fits perfectly in its assigned cluster [65].

The second technique that could be used to validate the clusters without ground truths is the Calinski-Harabasz index. It is also known as the variance ratio criterion and it evaluates the ratio of the between-clusters dispersion mean and the within-cluster dispersion. It is given by the following formula:

$$s(k) = \frac{Tr(Bk)}{Tr(Wk)} \times \frac{N - k}{k - 1}$$

where

$$Bk = \sum_q nq(cq - c)(cq - c)^T \text{ and } Wk = \sum_{q=1}^{k} \sum_{x \in Cq} (x - cq)(x - cq)^T$$

Where k is the number of clusters, Bk is the between group dispersion matrix and Wk is the within-cluster dispersion matrix, and N is the number of total data points, Cq is the set of points within a cluster q, cq is the centroid of a cluster, c is the center of E and nq is the number of points

in a cluster. The higher the values of the Calinski-Harabasz score (s) the better the clusters fit within that model [66].

The last evaluation method that could be used to validate the clustering results is the Davies-Bouldin Index. It looks at the similarities between clusters and gives a score to which a lower value represents a model with better separation between the clusters. The lowest score that can be obtained is zero which indicates perfect separation between clusters, thus the closer the score is to zero the better the clustering. It is defined by the following formulae:

$$R_{ij} = \frac{s_i + s_j}{d_{ij}}$$

$$DB = \frac{1}{k}\sum_{i=1}^{k} \max_{i \neq j} R_{ij}$$

Where R is the similarity calculated by s, the average distance between the points in a cluster and the cluster centroid and d, the distance between two different clusters. Using R, the Davies-Bouldin index is then calculated where k is the maximum number of clusters [67].

CHAPTER 3 METHODS

This project was a continuation of a previous project I had worked on (for the master's project of another student) in which the data acquired was used to first create a quantitative rat spinal cord atlas, after which the clustering was applied to the atlas. The perfusion and extraction of the spinal cords were done by Ariane Saliani. The preparation of the samples as well as the solutions were done by Ariane Saliani and myself. The image acquisition was done by Ariane Saliani. The image analysis and processing of the data was done by Ariane Saliani, Aldo Zaimi and myself. The core clustering script was written by Christian Perone and myself and the analysis and application of the clustering algorithms was done by myself. The clustering algorithms used were already in place and taken as is from scikit-learn and thus the clustering script was mostly used to process the images so the clustering algorithms could be applied on them with ease.

The data was collected across five Sprague Dawley rats (2 females and 3 males). The experimental procedure and protocol was approved by the Animal Research Ethics Committee of the Montreal Heart Institute.

The methodologies chapter is split into 4 different sections. The first consists of obtaining and preparing the spinal cord, which includes the fixation process, the extraction process, the post fixation steps as well as preparation for imaging. The second section consists of acquiring the image using scanning electron microscopy and the third consists of treating the images using various in-house MATLAB scripts to put everything into the same space, obtaining the metric maps and averaging them across all five rats. The fourth section deals with the application of the clustering algorithm on the metric maps and the various parameters used to optimize the algorithm.

3.1 Spinal cord extraction and preparation

3.1.1 Fixation and Extraction

The fixative solution used for the fixation of the tissue needs to be prepared on the day the rats are to be sacrificed and fixed. The solution is made from a mixture of 3% paraformaldehyde and 3% glutaraldehyde with the rest of the solution being Phosphate buffer solution (PBS). Approximately 200 mL of fixative solution is used per rat to ensure that the tissues are well preserved. The volumes and the percentages used for the perfusion as well as the future sample

preparation steps were determined through using previous literature along with testing and experimenting on some of the samples to see which combination of percentages would give the best result. (done by Tanguy Duval and Ariane Saliani) [68].

The rats were put under anesthesia using a 3% concentration of isofluorane, and then the thoracic cage and heart was exposed in order to euthanize the rat by intracardiac perfusion using the PBS solution. Once the rat was deemed to be sacrificed, the fixation step via perfusion was done using the aforementioned fixative solution. Once the rat was observed to be preserved (by observing the rigidity of the organs and tissue), the spinal cord was then extracted. Upon extraction the cords were placed in a post-fixative solution for 2 days and then transferred to a PBS solution to be washed out for a few days prior to being permanently stored in PBS.

3.1.2 Staining, Dehydration and Embedding

The spinal cords were then cut up into 31 slices corresponding to the 31 levels of the spinal cord. Each level was then placed into a separate microtube which were then filled with 40 mL of 2% osmium tetroxide which is the main staining agent used for myelin identification for SEM. The samples were left for a minimum of 5 hours on a rotator and covered as osmium tetroxide reacts poorly with light.

Once the samples were stained, they were then dehydrated by taking out the osmium tetroxide in each microtube and replacing it with varying concentrations of acetone for 30 minutes at each concentration (10%, 35%, 50%, 75%, 85%, 90% and 100%).

The next step was to further dehydrate the samples using a mixture of the embedding resin and acetone. The samples were placed in a 1:1 concentration of the epoxy resin to acetone overnight followed by an immersion for 6 hours in just the epoxy resin. The epoxy resin is a mixture of Embed812, dodecenyl succinic anhydride (DDSA), nadic methyl anhydride (NMA) and 2,4,6-{tri(dimehtylaminoethyl)phenol} (DMP-30). The samples were then finally embedded in the resin following the technical data sheet for the resin kit (EMbed 812 kit) shown in table 1 below. The initial 6 hours of immersion was done with a medium amount, and then for the final embedding the large amount was used and the samples were left to be cured at 60° C for 48 hours.

Table 3.1: Different Mixture amounts for Resin embedding

	Small Amount	Medium Amount	Large Amount
Mixture A:			
EMbed 812 DDSA	5 ml 8 ml	20 ml 31 ml	62 ml 100 ml
Mixture B:			
EMbed 812	8 ml	20 ml	100ml
NMA	7 ml	17 ml	90 ml
Final Embedding Mixture:			
Mixture A:	13 ml	51 ml	162 ml
Mixture B:	15 ml	37 ml	190 ml
DMP-30*	.42-.56 ml	1.3-1.7 ml	5.3-7.0 ml

3.2 Image Acquisition

3.2.1 Polishing and gold coating

Once the spinal cords were fully embedded, the next step was to obtain the images using scanning electron microscopy. To do this, the samples first needed to be polished and smoothed, which was done using three different grit papers from coarse to fine; 600 um, 1 um and 0.05 um. At 1 um a monocrystalline diamond suspension was used to aid in the polishing and at 0.05 um a colloidal alumina suspension was used to achieve a finer surface smoothness. Once the samples were polished, they were coated in gold using a Polaron Sputter Coater SC502 for 5 minutes to first vacuum the compartment, and then an additional 20 seconds to allow the gold to coat the surface of the samples.

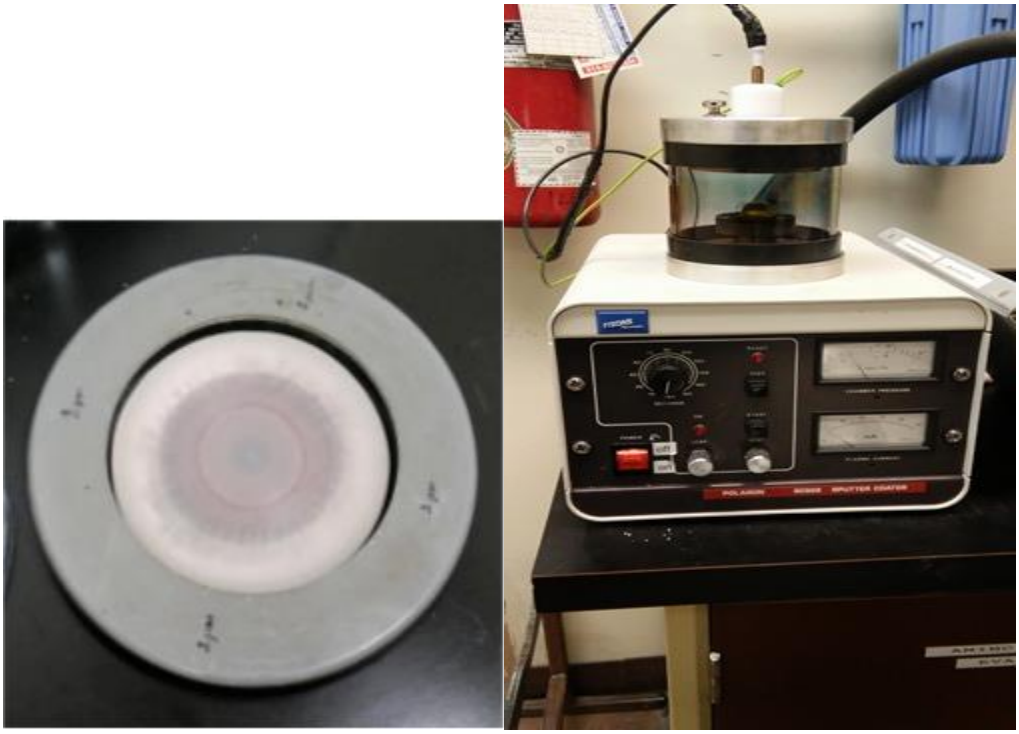

Figure 3.1: Left: Polishing table used to polish the samples at 1 um grit. Right: Gold sputter coater.

3.2.2 Scanning Electron Microscopy

The samples were then prepared to be scanned using the SEM. The scanning was done on a JEOL JSM7600F in conjunction with the Aztec 3.2 software to control the placement of the sample and obtain mosaic images. The parameters for the scanning were as follows: the image size was 8192x5632 pixels (573 um x 394 um) with the pixel size being 0.070 um per pixel, with an overlap of about 15%, a low-angle backscattered electron detector (LABE) mode was used, with a magnification of 200x, an aperture of 70 um, with a working distance of 30 mm, acceleration voltage of 15 kV, emission current of 140 uA, and a pixel dwell time of 2 us. The parameters were chosen as a means of trying to reduce the scan time while still trying to obtain high resolution images without damaging the samples. This will be further discussed in chapter 5 of the thesis in the discussion section. Due to the relatively large size of the spinal cord (3-4 mm) the samples were imaged in sub sections first, which were then combined together into the full image using the Fiji stitching software combined with in-house matlab scripts.

Figure 3.2: JEOL JSM7600F scanning electron microscope [69].

3.3 Image Processing

The next step upon acquiring the images was to segment them in order to obtain all the various metrics and values. An overview of the entire process is found at the end of the section (Figure 3.4). The metrics were obtained using the AxonSeg software to segment the axons for each sub-image prior to the stitching (in order to save on computation time and memory) [2]. The AxonSeg software works by using two main features. The first is the intensity of the image by looking for the contrast in intensities between the axon and the myelin due to the staining. The second feature the software looks at is the morphological structure of the axon. The software first conducts an initial segmentation on the axon based on an inputted threshold value the user defines. The user then has to use thresholding sliders for the various features (minimal size, solidity, ellipticity) to remove the false positive axons that are initially segmented by the software. The myelin is then segmented on these accepted axons by using a minimal-path and maximal path algorithm to determine the borders of the myelin sheath. There were 6 main metrics that were outputted by the software which will eventually be the main inputs used for the clustering. The first was the Axonal density, then the axon equivalent diameter, the g-ratio, the myelin thickness, the

myelin volume fraction and the axon volume fraction. The metrics and how they are calculated are as follows:

- Axon Density: $\frac{Naxons}{pixel\ area}$
- Axon Diameter: $d = 2\sqrt{\frac{Aaxon}{\pi}}$
- Myelinated fiber equivalent diameter: $D = 2\sqrt{\frac{Afiber}{\pi}}$
- g-ratio: $g = d/D$
- Myelin thickness: $m = \frac{(D-d)}{2}$
- Myelin volume fraction: $\frac{Amyelin}{Atotal}$
- Axonal volume fraction: $\frac{Aaxon}{Atotal}$
- Where $Atotal = \left(\frac{50}{0.07}\right)^2 = 510,204\ pixels$

Naxons represents the number of axons, and the axon density therefore represents the number of axons per 50x50um downsampled area. Axon diameter is simply measured by using the area of the segmented axon (Aaxon) and extrapolating the diameter from it. The same can be said with the Myelinated fiber equivalent diameter, except that it uses the diameter of the entire fiber (Afiber) to extrapolate the myelin diameter. The g-ratio can therefore be calculated by just using the ratios of the axon diameter to the myelinated fiber equivalent diameter. And the myelin thickness can then be calculated by simply subtracting the two diameters. The volume fractions can be calculated by looking at the total number of pixels occupied by myelin or axons and then dividing by the overall number of pixels (Atotal) in the spinal cord slice (i.e. C1, C2 etc). Atotal simply comes from the fact that the maps are downsampled at 50x50 um2 with a pixel size of 0.07. The segmentation of a slice can be seen below in figure 3.3 with a zoom in of an area showing the individual myelin segmented.

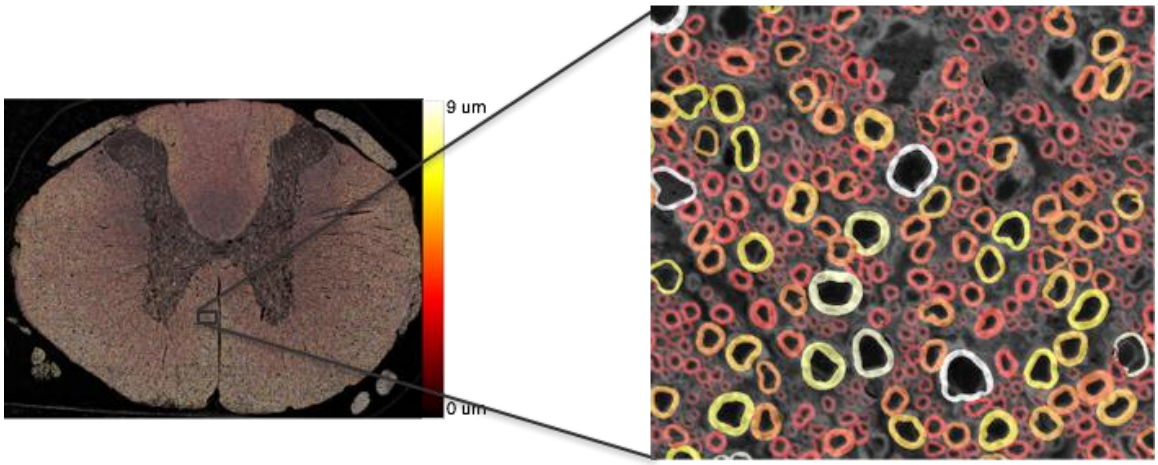

Figure 3.3: Left: SEM spinal cord slice segmented with AxonSeg. Right: Close up of an area on the spinal cord showing the variations in diameters.

Each of the metrics are presented as a map overlayed on the spinal cord images to give a representation of the distribution of the values on each sample. These maps were downsampled at a 50x50 um2 resolution so as to allow for quicker processing times while still maintaining a reasonable resolution. Once the maps were obtained, the next step was to process the maps in order to get them in the same space so that they could be averaged across all the rats. The averaging was done by taking the value of one metric for each rat at one pixel and calculating the mean from the pixel and then doing this again for each metric to have 6 averaged metric maps. This was done using custom matlab scripts using functions from the sct toolbox [70]. The first step was to create white matter masks for each rat for every level of one of the metrics (in this case we used Axon density as it was the most easily distinguishable). This was done using the custom matlab functions to obtain the regions of interest. Once the masks were created, the next step was to place all of them into the same space which was again done using custom matlab scripts. The next step was to generate an averaged template of all the masks using the ANTS multivariate template construction script (with the following parameters: gradient step of 0.15, BSplineSyN mesh grid of 2 mm, a shrink factor of 8x4x2, zero smoothing, 200x50x2 for the number of iterations for pairwise registration, a mean square difference for the similarity metric). After which the outputted warping fields from template generation was then applied onto all the metrics so that they would all be in the same space and averaged. And then lastly the metrics were then cleaned to remove any background noise and pixels and then symmetrized to obtain left-right symmetry.

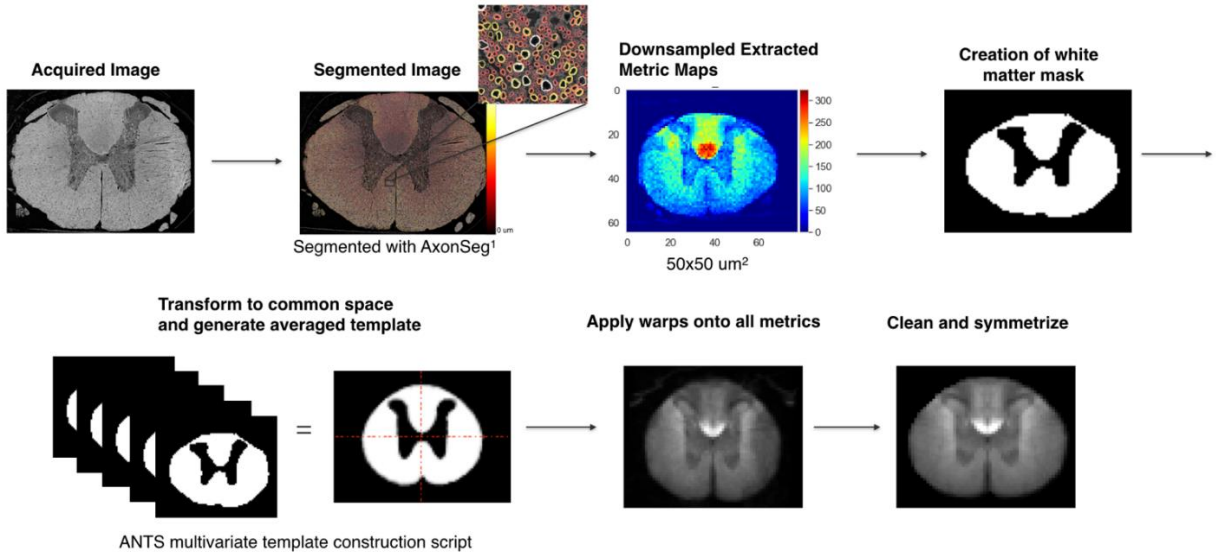

Figure 3.4: Workflow of the image segmentation, metric extraction, template generation and atlas generation.

3.4 Clustering

A few clustering algorithms were tested and applied on the data to test which method would yield the best results. An overview of the entire methodology is shown at the end of this section in Figure 3.5. This part of the study was done using python to be able to make better use of the algorithms as everything is already incorporated in the pre-made functions. Before being able to apply the algorithm directly on our data, a few things needed to be done first to ensure optimal results. The maps that were used as inputs for the clustering were the axon density, axon diameter, axon volume fraction, g-ratio, myelin thickness and myelin volume fraction. Using these metric maps, a connectivity matrix was created in order to have spatial priors for the clustering to optimize the results which would allow for the pixels adjacent to each other to be taken into account for the clustering. Then the metric maps were normalized so that all of the metric maps would be taken into account at an equal weight for the clustering.

Then once all of this was done the clustering algorithms from scikit-learn were applied [49]. The algorithms for spectral clustering and k-means were applied as is, as there were not too many parameters to tune and the default values seemed suitable to run (apart from the number clusters which was consistent between all methods). For agglomerative clustering, a few parameters can be varied based on user inputs. The parameters used to obtain the final results were found through a

heuristic approach due to the fact that there is no literature specific to spinal cord clustering to draw inspiration from. For our needs, we used the following: number of clusters was 5-29, the affinity was Euclidean, the connectivity was the connectivity matrix created and the linkage used was ward. The number of clusters was set at this broad range just as means to have a visual representation of all the broad possibilities of the clusters. Based on the theory and background knowledge, there should only be 13-14 tracts spinal cord and therefore the number of clusters should vary around those numbers. However, since this is an investigative study, having a broader range allows for more interpretation and to see whether other tracts may be apparent that have not been seen in prior studies or atlases. The connectivity matrix as mentioned earlier is just a means to be able to have a spatial reference for which the clusters can adhere to based on the adjacency of the pixels and how only neighboring pixels could belong to one specific cluster. The affinity is a metric that is used to calculate the linkages. Essentially what it looks at is based on the linkage criterion, how should the distances between clusters that are being merged be calculated. There are six main affinity types that the algorithm can use, which are: Euclidean, l1, l2, manhattan, cosine or pre-computed. The pre-computed one is essentially a custom made one if the user decides to use another method of computing the distance. Since we are using ward linkage, the only affinity type that can be used is Euclidean based on the algorithm.

The linkage is the metric used that will calculate how the clusters will merge together. There are four main types of linkage that the algorithm can use (Figure 3.4).

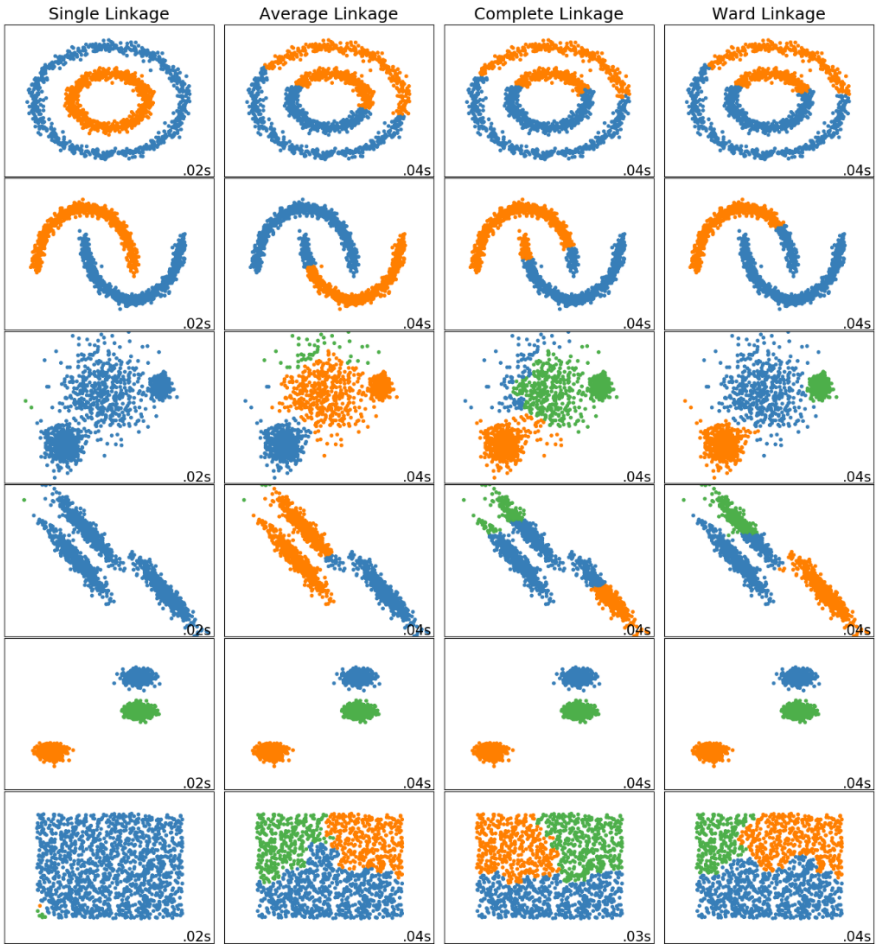

Figure 3.5: The 4 different linkage types that are possible to use with the agglomerative clustering algorithm. Each row is for a different type of data set with the results being shown for each type of linkage. The computational time is also shown in each box for each type of linkage and dataset [49].

The first is ward linkage which minimizes the variance of the clusters being merged. In essence, it works by theoretically merging two clusters (or points if its starting off from no clusters) and calculating a centroid for the theoretical resultant cluster, and then looking at the sum of the squared deviations of all the points with regards to that centroid. Therefore, it does this for all the clusters and then chooses the lowest sum of the squared deviation between two clusters and then will merge those together. The second linkage type is single linkage which looks at the closest points between clusters and merges those clusters together. So if you have multiple clusters in an area, single linkage will evaluate the distance of the points between all those clusters and will merge the two clusters that have the shortest distance between the two closest points. The next type of

linkage is complete linkage, which is the opposite of single linkage, in that it looks at the two points between clusters that are the furthest apart from each other and uses that as the criterion to pick which clusters will merge. In doing so, this linkage forces more spherical clusters as with the two furthest points this metric essentially acts like the diameter (think two points on opposite ends of a circle). The last linkage type is called average linkage. Average linkage calculates the distance between two clusters as the average distance between the pairwise points in the clusters. All the linkage types were tested on the samples but the best results were shown by ward linkage. The last step in the process of the clustering was to validate the results. Two different validation methods were implemented on the results to try and cross-reference the best method; these were silhouette score and the davies-bouldin index. Both were implemented using the sci-kit learn algorithms.

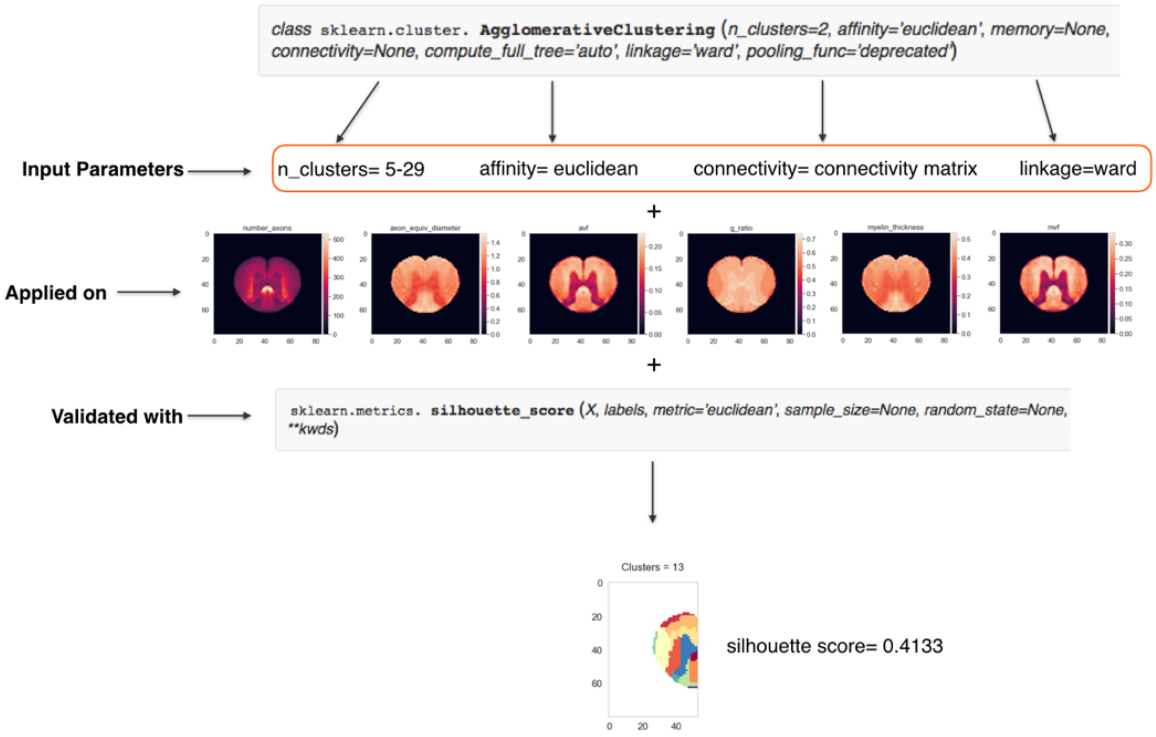

Figure 3.6: Clustering workflow for which the algorithm and parameters are chosen to then be applied onto the metric maps and then validated with one of the validation algorithms to give the final clustering result. This is an example using agglomerative clustering and silhouette score, but the same methodology applies to the other algorithms.

CHAPTER 4 RESULTS

The results section for the thesis is split up into two main sections. The first is the results of the metric maps that are important to understand as these are the inputs to be used for the clustering. And the second is the actual clustering results which includes the initial results between each algorithm, the t-sne plots, the comparison between the single rats and the average across all the rats, as well as the comparison to the literature.

4.1 Metric Maps

As mentioned earlier, 6 main metric maps were obtained to be used as the inputs for the clustering. An example of the metric maps obtained are shown below in Figure 4.1.

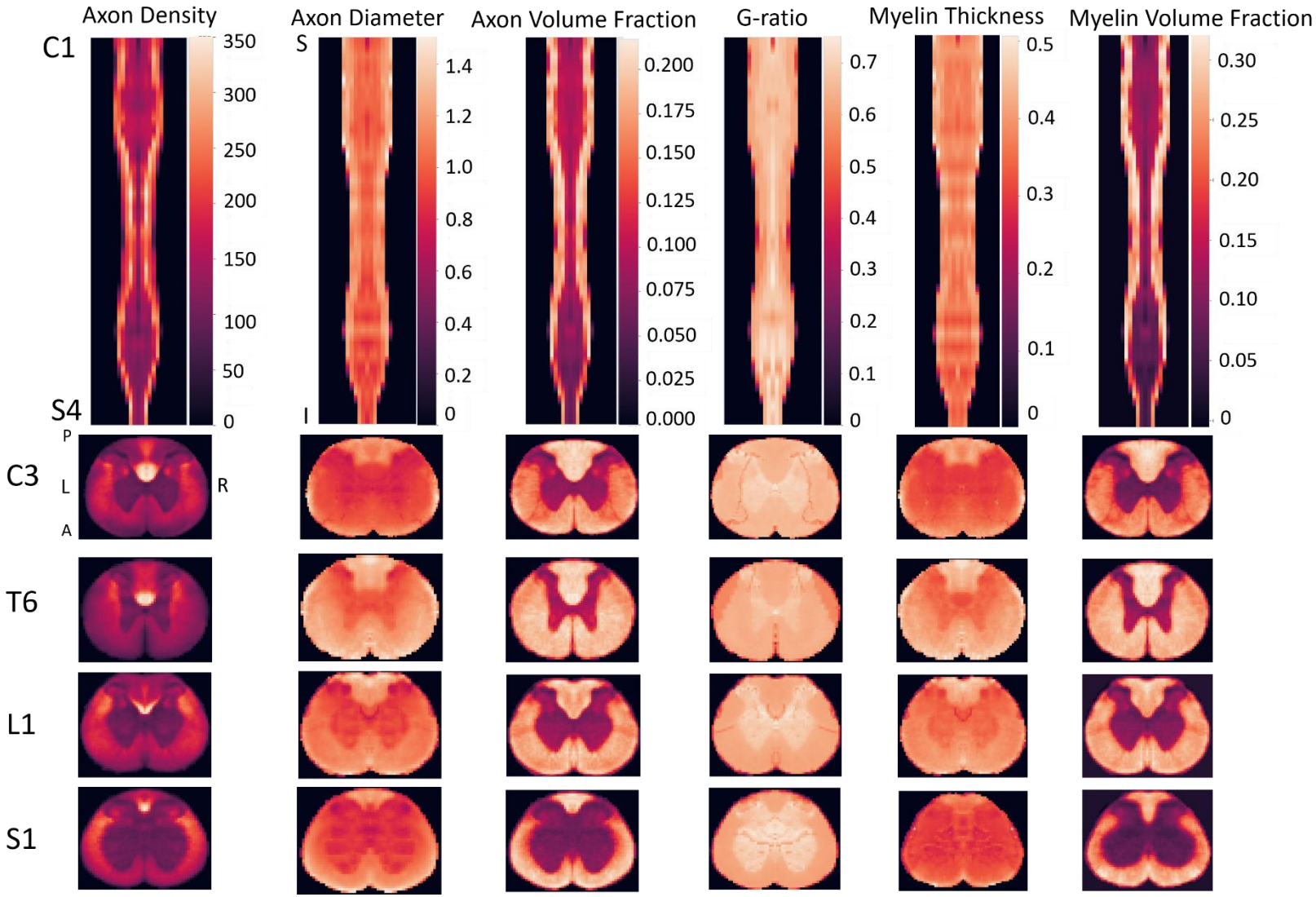

Figure 4.1: The 6 metric maps. Top Row: The 3D volume for each metric map for the entire spinal cord (from C1 to S4). Bottom rows: Example axial slices for each metric from each section of the spinal cord (Cervical, Thoracic, Lumbar, Sacral)

We can observe the differences of the distribution of the metrics around the spinal cord depending on which tract the metric falls under. We can see that certain areas have higher or more dense axon concentration or diameters.

4.2 Clustering Results

The results for the clustering are split up into various sections. The first section shows the overall results for an example level of the clustering. It shows the progression of the clusters from 5-29 and shows the differences that arise as the clusters progress. It also gives an example of the silhouette score at each cluster level, thereby showing at what number of clusters the best score is given, which could be an indication of choosing the optimal number of clusters. The second section shows an example of the t-distributed stochastic neighbour embedding (t-SNE), which is essentially a distribution map for the different clusters and enables a visual representation of how close the points in the clusters are to each other and how different they are from the other clusters. The section after that compares the differences between just a single non-averaged sample to one of the averaged samples. And then the last two sections are also comparison, the first one being a comparison between agglomerative clustering versus k-means that was also applied on our data. And the last is a comparison between the literature atlases and our results.

4.2.1 Initial Results and validation results

The initial clustering results are shown below for one example level. The results show the complete clustering output from 5-29 clusters and the following table proceeds to show the silhouette score and the davies-bouldin score for each cluster. The calinski-harabasz index was not shown in the end due to technical limitations in getting the algorithm to work appropriately on our data. We did the same for a few other clustering techniques such as the spectral clustering and k-means clustering, both of which are 2 of the more commonly used techniques that can also have some sort of implementation of a connectivity matrix.

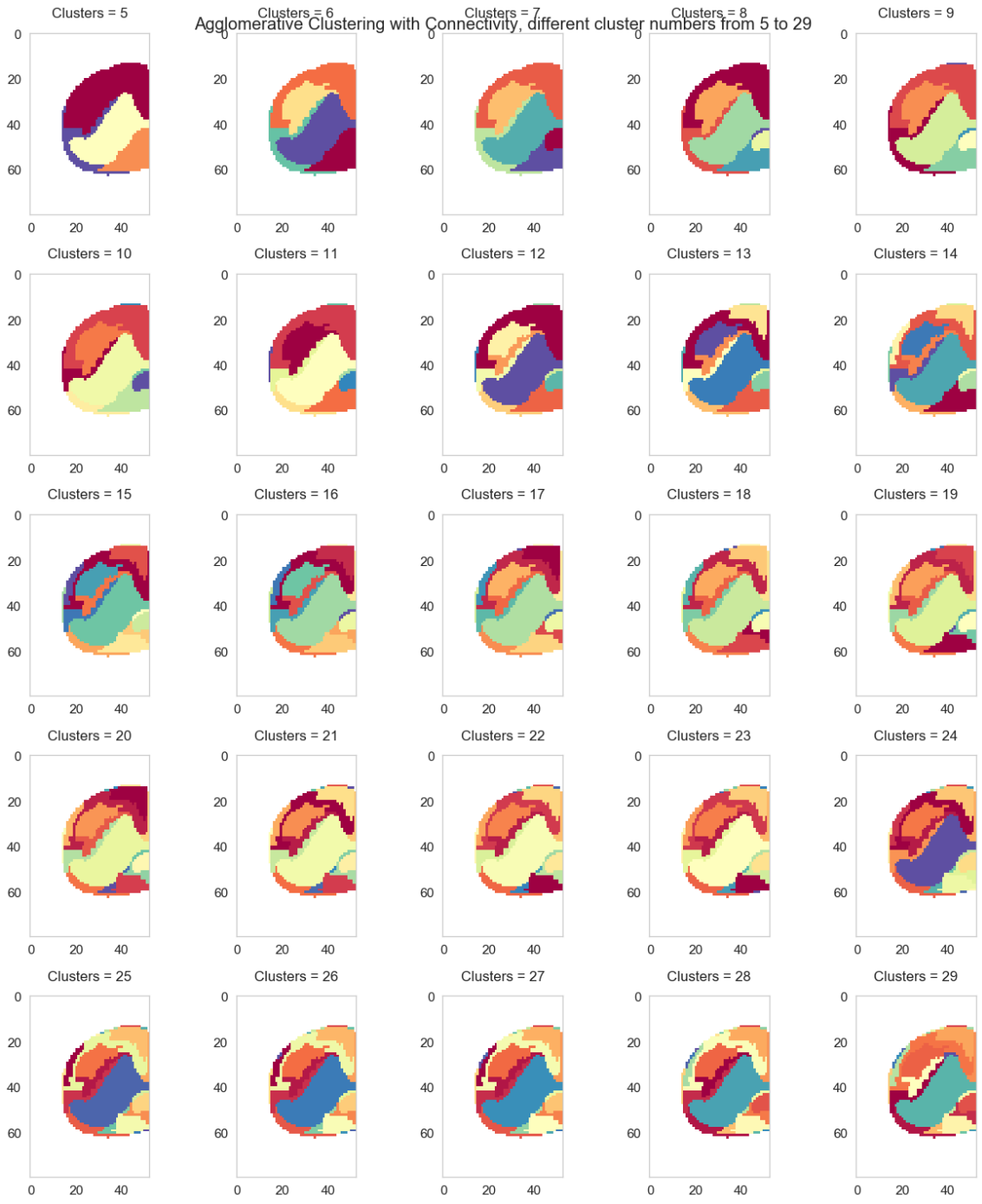

Figure 4.2: Example of the clustering outputs for one level (C1) for the half spinal cords for agglomerative clustering

Table 4.1: Validation score outputs for example level of C1 for agglomerative clustering

Clusters	Silhouette Score	Davies-Bouldin
5	0.426	1.728
6	0.422	3.829
7	0.424	1.610
8	0.405	1.833
9	0.400	1.776
10	0.406	1.908
11	0.409	1.904
12	0.389	1.842
13	0.371	1.960
14	0.381	2.023
15	0.386	2.568
16	0.378	2.633
17	0.374	2.613
18	0.375	2.588
19	0.364	2.776
20	0.367	2.828
21	0.368	3.048
22	0.366	3.389
23	0.362	3.384
24	0.354	3.269
25	0.355	3.395
26	0.356	3.338
27	0.357	3.412
28	0.356	3.652
29	0.353	3.635

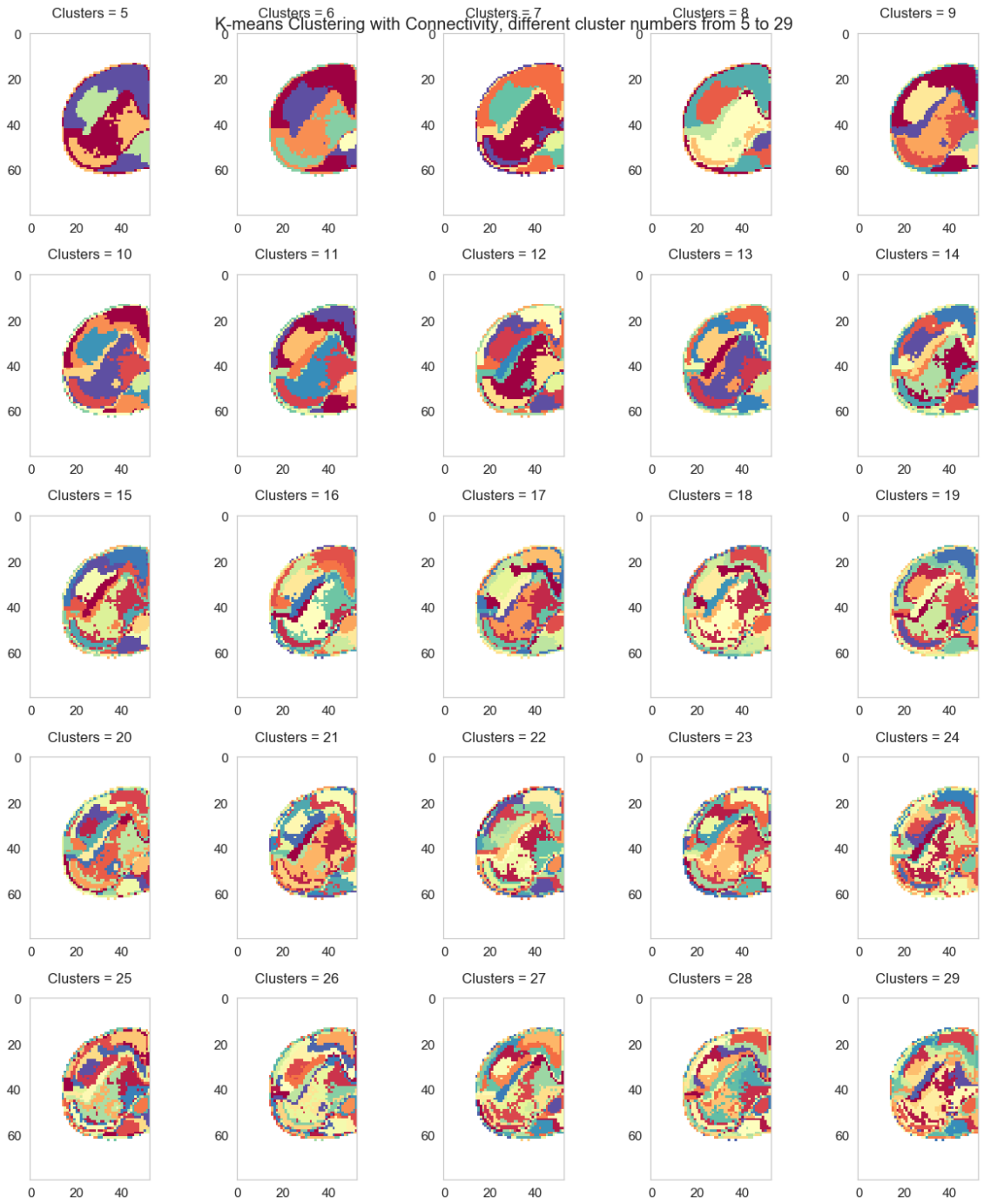

Figure 4.3: Example of the K-means clustering output on half-spinal cords from clusters 5-29

Table 4.2: Validation score outputs for example level of C1 for K-means clustering

Clusters	Silhouette Score	Davies-Bouldin
5	0.381	0.833
6	0.374	0.807
7	0.398	0.803
8	0.413	0.763
9	0.402	0.718
10	0.358	0.815
11	0.366	0.836
12	0.354	0.786
13	0.335	0.824
14	0.359	0.859
15	0.341	0.871
16	0.341	0.873
17	0.336	0.864
18	0.343	0.872
19	0.342	0.869
20	0.326	0.867
21	0.321	0.882
22	0.313	0.885
23	0.309	0.877
24	0.312	0.901
25	0.321	0.913
26	0.314	0.938
27	0.312	0.939
28	0.318	0.924
29	0.315	0.905

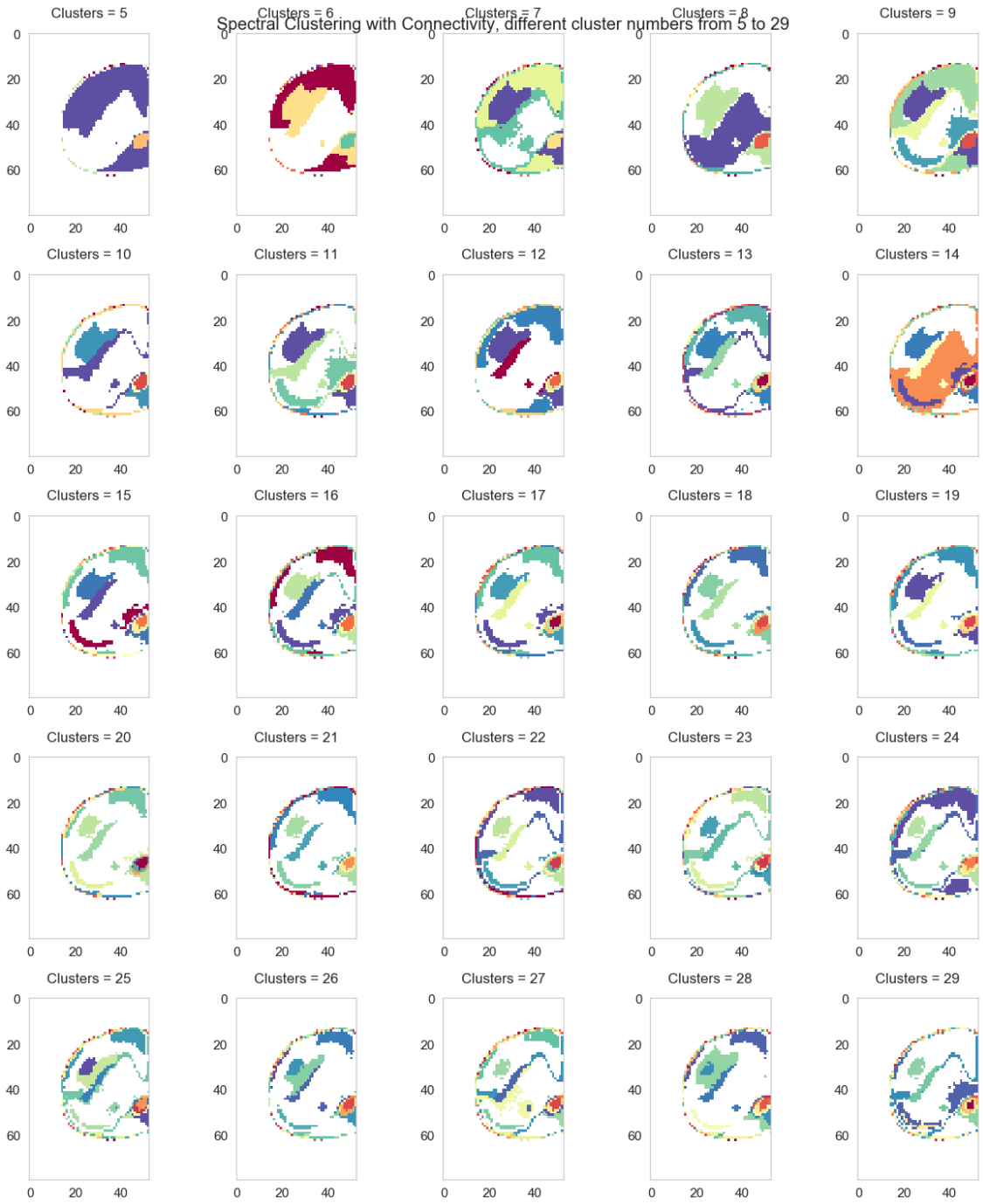

Figure 4.4: Example of the spectral clustering outputs for an example level from clusters 5-29

Table 4.3: Validation score outputs for examples level of C1 for spectral clustering

Clusters	Silhouette Score	Davies-Bouldin
5	0.585	0.644
6	0.415	0.836
7	0.426	0.726
8	0.421	0.780
9	0.405	0.946
10	0.414	0.872
11	0.367	0.951
12	0.561	0.834
13	0.433	0.971
14	0.462	0.876
15	0.474	0.830
16	0.311	0.904
17	0.469	0.916
18	0.407	0.945
19	0.307	0.890
20	0.455	0.839
21	0.410	0.906
22	0.503	0.885
23	0.483	0.838
24	0.476	0.935
25	0.449	0.908
26	0.460	0.909
27	0.363	0.894
28	0.400	0.861
29	0.384	0.878

4.2.2 t-SNE Plots

The various t-sne plots for each type of the clustering explored are shown below. We can see that the distribution based on the background taking up a good majority of the clusters and then the various spread between the other clusters. A clustering number of 10 clusters was chosen for

each plot seeing as it is at around that point that the clustering for each of the algorithms is most similar/representative of the actual white matter tracts. Based on this we can also see that since the background plays a large part of the clusters, it is important to remove this for the calculation of the validation methods or else they would be heavily biased.

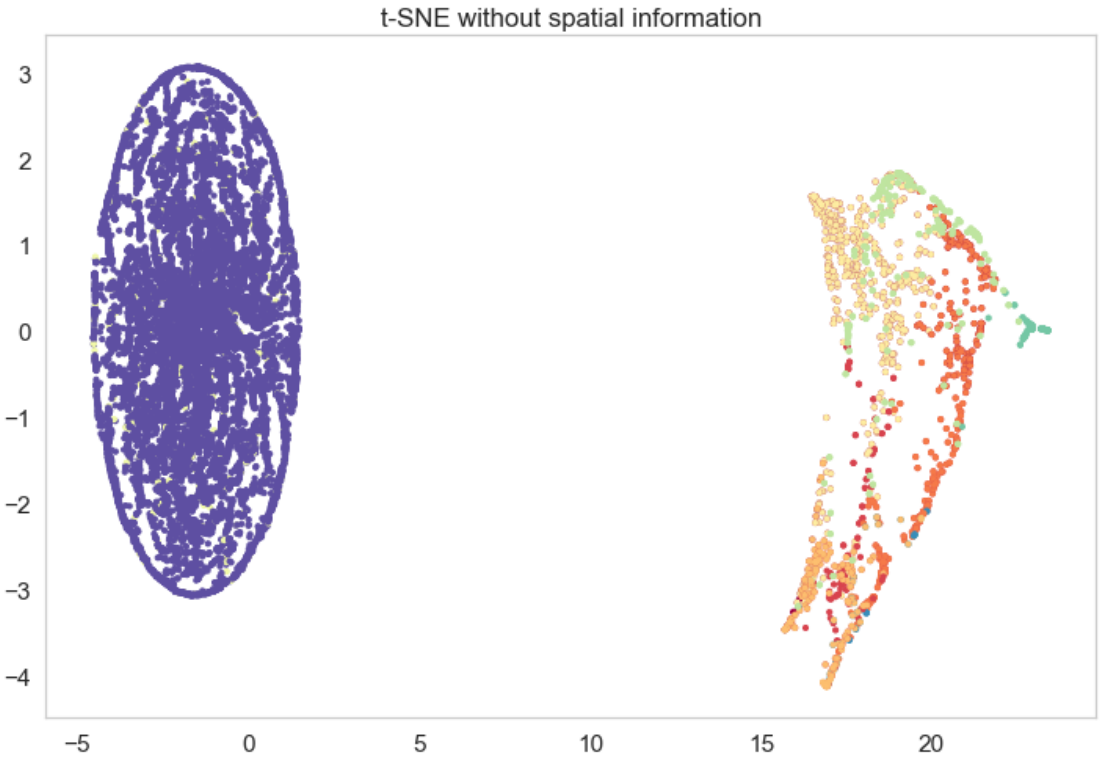

Figure 4.5: t-SNE plot for agglomerative clustering at 10 clusters

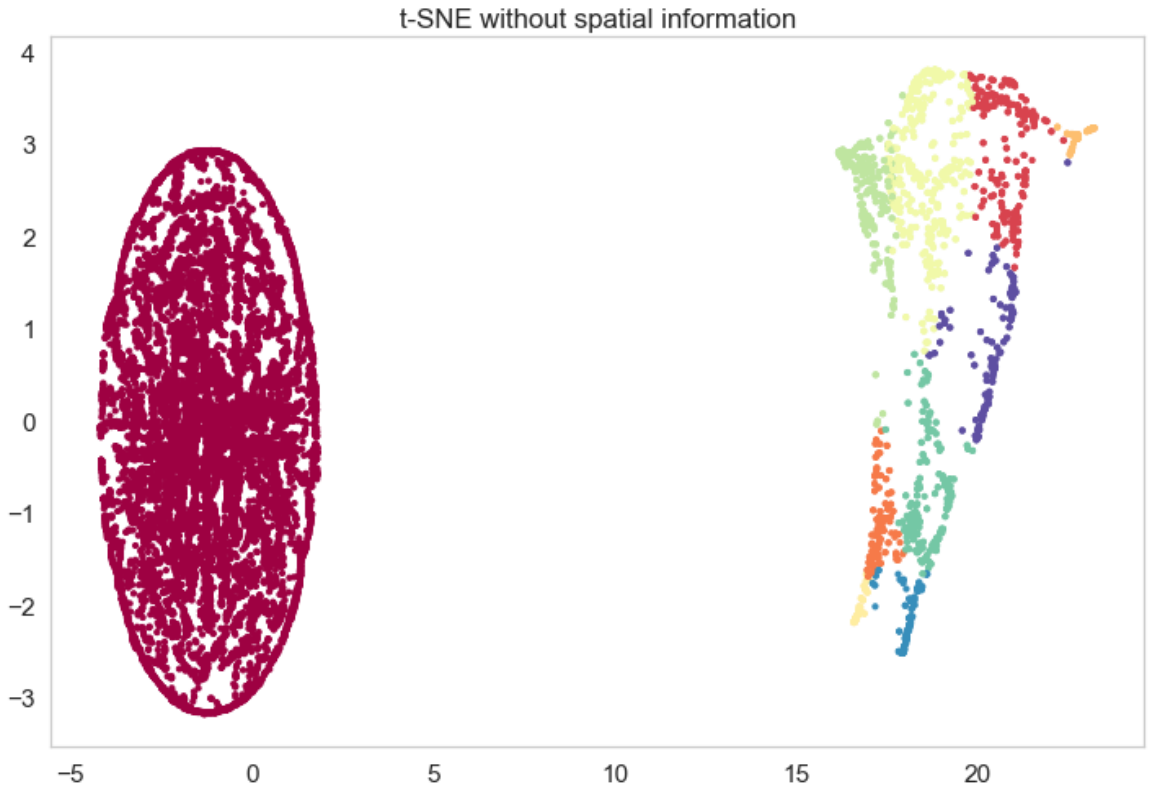

Figure 4.6: t-SNE plots for k-means clustering at 10 clusters

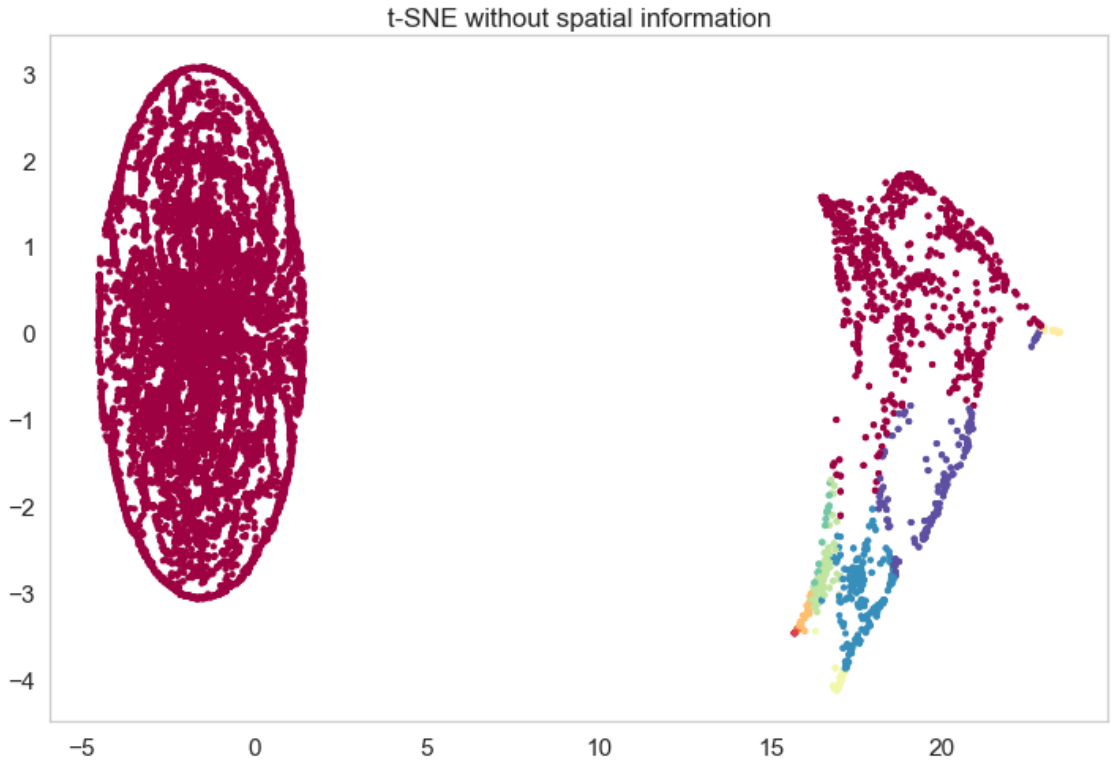

Figure 4.7: t-SNE plot for spectral clustering at 10 clusters

4.2.3 Comparison Plots

The results below show the differences not only between the 5 rats used but also between the average of the 5 rats as well. Each of the samples below are shown with the agglomerative clustering applied on them for an example level of C3.

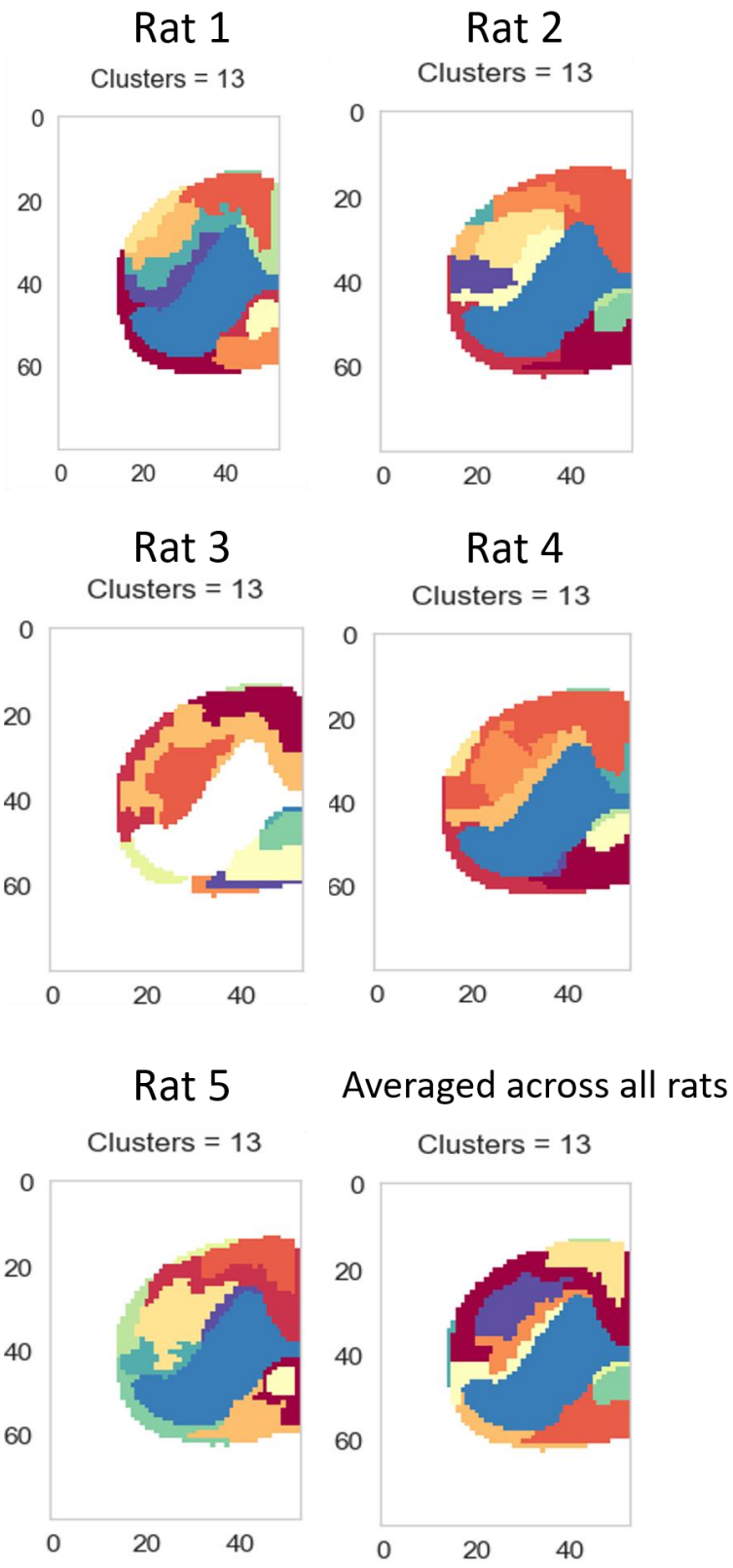

Figure 4.8: Comparison of the 5 different rat samples on level C1 for 13 clusters as well as the cluster averaged across all 5 rats for agglomerative clustering

4.2.4 Comparison between Rat atlas and results

The Paxinos atlas, being the major gold standard for rat atlases at the moment, is one of the means that we compare our results to. We can see in figure 4.9 the visual comparison for an example of each level chosen at 9 clusters for each level for each of the clustering methods that we tested. There are many stark differences that we can see between each clustering algorithm and the Paxinos rat atlas with each algorithm focusing on different areas to bring about the clusters.

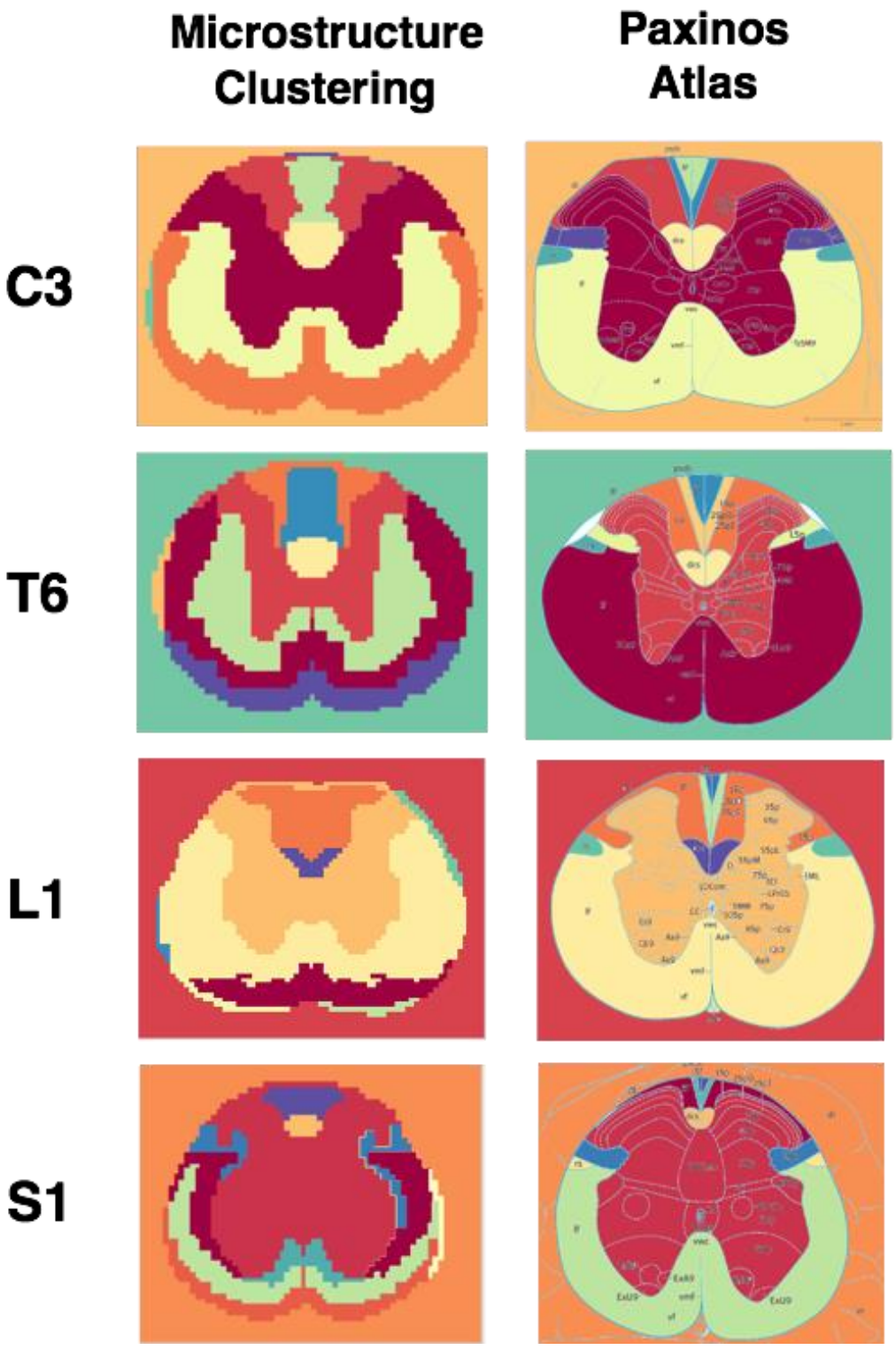

Figure 4.9: Comparison of the various clustering methods measured against the gold standard paxinos atlas for one level per section [10]

CHAPTER 5 DISCUSSION

The results obtained will be discussed by first evaluating the actual methodology of the clustering and the values obtained from the validation and then comparing the obtained results to literature and discussing the various limitations that arose during the study.

5.1 Metric Maps

Based on the functionality of the white matter tracts in the spinal cord, there is a spread of the various metrics. We can see that in tracts that are responsible for higher processing and major motor pathways, such as the corticospinal tract, have a higher density of axons but at a medium to smaller size. The theory this ties in to is the fact that larger axons normally have faster conduction speeds due to the thicker myelin sheath. Therefore, areas with higher axon diameters and myelin diameters tend to be areas where the functions are reliant on the information travelling much more quickly.

5.2 Comparison between clustering methods

The use of agglomerative clustering for determining the white matter tracts showed the delineation of a lot of the major tracts in the rat. When observing the progression of the tracts as new clusters are added however, we start to see that after 15 clusters the clusters start to generate at arbitrary positions taking into account smaller and isolated pixels as well as the gray matter. However, looking at the clusters prior to 15, we can see that the results are quite comparable to the Paxinos atlas that we are using as a reference. Majority of the larger tracts, the corticospinal tract and the fasciculus gracilis and fasciculus cuneatus are well defined. However, once we start look at the smaller levels of tracts, we can see that the algorithm stops being as precise. This is notable for the postsynaptic dorsal column that normally is present on the dorsal side of the spinal cord and separates the gracilis and cuneatus tracts, which we do not observe on the clustering results. The other smaller tracts that are notably missing are the rubrospinal tract and the lateral spinothalamic tract, both of which sit on the left and right sides of the spinal cord. However, if we were to look at this in contrast to the K-means and spectral clustering, we see an opposite trend of where those algorithms are more sensitive to the smaller tracts as opposed to the larger tracts. This is especially true as the number of clusters progress; the larger tracts break down more and more into smaller

numerous clusters. In comparison to the agglomerative clustering algorithm, we see that rather than dividing the larger clusters into smaller clusters as the number of clusters increase, it seeks out more isolated groups of pixels to start turning into additional clusters.

Delving into the validation methods for each clustering algorithm, we can see that in general the numbers do not vary too much for the silhouette score. The average for all the clusters for agglomerative, k-means and spectral clustering were 0.38, 0.37 and 0.43 respectively, and for the clusters 5-15 (which would be more indicative of the white matter tracts) the averages were 0.40, 0.37, and 0.45 respectively. Therefore based off of this, we can see that the k-means clustering had a lower overall score but still very close to the other two techniques, whereas spectral seemed to have performed slightly better than agglomerative clustering. If we were to compare the results of the davies-bouldin scores, the averages were 2.68, 0.85 and 0.87 for all the clusters, and 2.09, 0.81 and 0.84 for the 5-15 cluster averages respectively. For the davies-bouldin score, a lower number indicates better partitioned clusters, and thus we see that between k-means and spectral clustering the results are very similar whereas the score for agglomerative clustering is much higher. This would indicate that there are a lot more pixels between clusters that are overlapping or could be equally placed into either of the two clusters that pixel is adjacent to.

5.3 Comparison with literature

Furthermore, something that we do not see in the rat Paxinos atlas but is shown in our results is the division of the ventral tract, adding more than one tract to the area. What we do see however, when comparing our results with the literature of various other species white matter tracts, notably the mouse, we see stark similarities that we do not observe between our results and the rat Paxinos results (see Figure 5.1). Notably, if we look at the figure below, we see that the tracts in the ventral side that are shown in the mouse paxinos atlas that were not observable in the rat paxinos atlas. These are the vestibulospinal tract and rostral reticulospinal tract. Furthermore tracts like the dorsolateral spinothalamic tract and the lateral spinothalamic tract seem to be more apparent in the clusters that we observed as opposed to the rat paxinos atlas as well. This seems to at the very least show that the results are promising in terms of obtaining representative tracts without having to actually individually stain for various cell bodies and components.

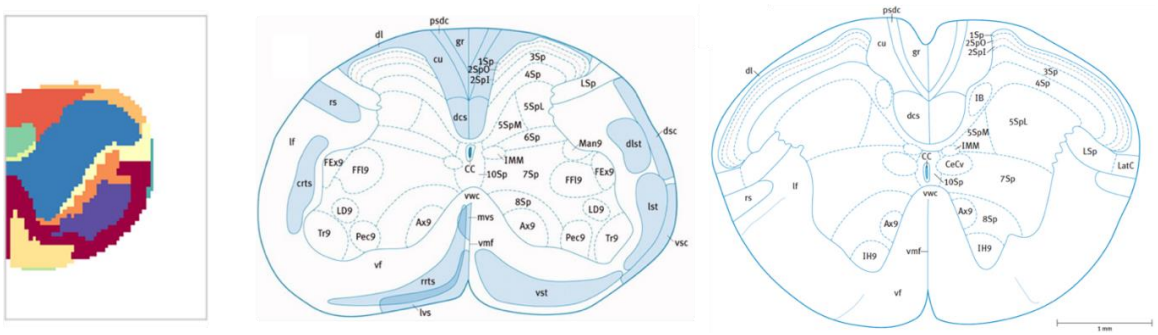

Figure 5.1: Comparison between the agglomerative clustering results (at k=13), the mouse paxinos atlas and the rat paxinos atlas [19]

5.4 Comparison between samples and averaged results

When looking at the results that show a comparison between the 5 different rats as well as the results averaged across the five rats, we seem some differences in the composition of the clusters as well as their shapes and sizes. Theoretically speaking, since the clusters are being applied to the same levels the differences shouldn't be very apparent from sample to sample, but this can be due to multiple things. The first thing is that it could have been due to is the fact that some of the samples may have had holes or areas that were distorted due to the sample preparation (see section limitations sample preparation). This would have created distortions in the metric maps due to the missing information and thus would cause extra clusters or change the shapes of the clusters between samples. And since these defects were present on a few of the rats (though not on every level) this would cause differences to be observed between each sample.

5.5 Limitations

5.5.1 Sample Preparation

One of the major limitations of the study was the preparation of the samples. If the samples are not prepared to near perfection in terms of fixation, polishing and smoothing, this would affect the images obtained through microscopy which would therefore end up affecting the final metric maps and thus affecting the final clustering outputs. One of the issues has to do with the initial steps of fixation. If the samples are not properly fixed, this would mean that the Myelin integrity would not be preserved throughout the rest of the preparation and processing steps. This would ultimately affect the myelin volume fraction and myelin thickness which could alter the groupings

of the clustering. Secondly, throughout the entire process of fixation, PBS storage, dehydration, staining and embedding, there could have been various moments of either improper dehydration which could have caused myelin and cell shrinkage or myelin swelling due to the osmolarity differences caused by these steps. Furthermore, the polishing and the smoothing of the samples caused destruction of certain areas of the tissue leading to some loss of microstructural information, and perhaps influencing the clusters in those areas.

5.5.2 Microscopy and Image Processing

Though the benefits of SEM are quite valuable to obtain high resolution and high magnification images, there are still some drawbacks or limitations that arise with this technique. The first limitation that we saw was that trying to get towards an even higher resolution resulted in images losing focus and thus creating blurring around the edges of the images. Since no autofocus feature is available this would entail having to refocus each individual mosaic tile manually which would thus mean staying for the entirety of the scan. This also ties into the fact that the scan time for a single slice was between 1-2 hours (depending on the slice) and therefore doing this for an entire spinal cord itself would take roughly 45-60 hours total at a magnification of 200X. Therefore, going for a higher magnification and resolution would yield even more increasing scan times as well as larger data files to store and process. One of the reasons that the metric maps were downsampled was because of the fact that the file sizes were too large and that processing them would have taken much too long. The focus also ties into the preparation of the sample as mentioned earlier seeing as if the sample itself is not perfectly well polished and flat the SEM will have a hard time obtaining proper images. It was also noticed that even with these resolutions, there were still some smaller sized axons that were not visually clear and blurred which would affect the segmentation because the software would not take these axons into account. These were mostly axons at around the 1 um diameter size, which would mean that axons of that size would also not be taken into account for the clustering algorithm. If that is the case, then it means if there are smaller clusters containing mostly smaller axons these would not show up in the final clustering results.

Downsampling as well could have played a part in perhaps not delineating some of the smaller tracts as the clusters are being applied to these lower resolution metric maps. Therefore

another thing to consider would perhaps be to try and do this on a non-downsampled sample and observe if any differences in the metric maps as well as the clustering show up.

One of the other potential issues that we see with the imaging and the metrics is what is known as myelin incisures or Schmidt-Lanterman incisures [71]. These incisures are gaps in the Myelin sheath caused by cytoplasm that fills the gaps due to oligodendrocytes (in the CNS or Schwann cells in the PNS) during the myelination process. What outcome this has on the results is that this would increase the thickness of the myelin sheath and would therefore be overestimated when being segmented by the AxonSeg software and ultimately skewing the myelin metric maps. Further investigation is still required to look into how this could be taken into account and how to tune the segmentation software to deal with this. We would also need to see how much of an actual impact this would have on the quantitative metric maps.

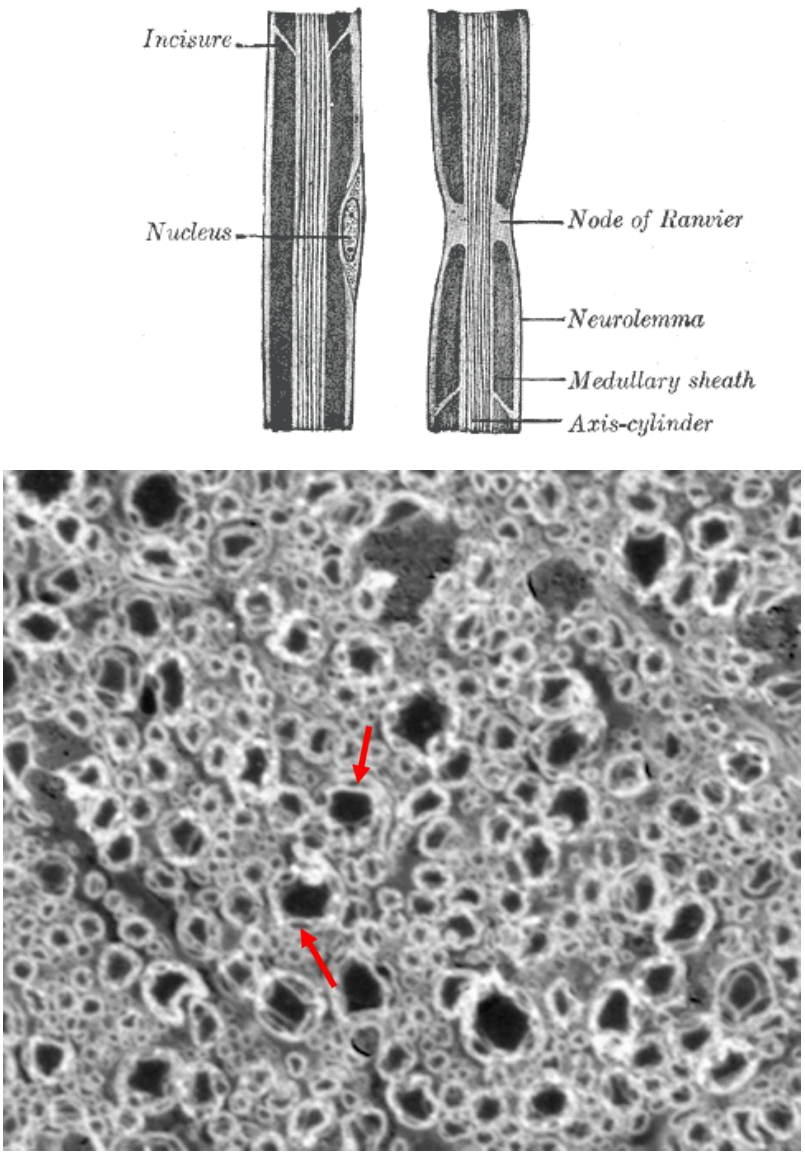

Figure 5.2: Top: Myelin Incisures in a longitudinal slice of an axon [72]. Bottom: An axial slice of an axon obtained through SEM showing different types of incisures.

5.5.3 Clustering Algorithm

One of the limitations of the clustering algorithm is that it relies solely on the intrinsic patterns of the initial inputs and therefore if there are issues with these inputs then the final clustering results will not reflect what is actually there and give less accurate results. This is what we see from above and how if sample preparation is off or the imaging is not perfect then everything else downstream

gets affected. Another issue is that what we see for agglomerative clustering is that despite giving comparable results to the gold standards for the larger tracts, it is less sensitive to a lot of the smaller tracts present. This is in contrast to some of the other clustering algorithms that we saw (K-means and spectral) which are too overly sensitive to smaller clusters and therefore create very intricate clustering groups that may not necessarily reflect what is actually there. Furthermore, we see that in the spectral clustering the clusters are simply not being assigned as well as the other two algorithms. After testing various parameters, the problem was still not resolved as to why this is occurring. It could be due to the fact that the assignment of clusters is assigning the ventral portion of the spinal cord and the background as the same cluster, and thus it ignores this area when clustering further. Thus, a measure needs to be implemented to try and assign different clusters to the background and ventral portion of the spinal cord.

Though it wasn't shown in the Paxinos rat atlas, if we look at the mouse atlas we'll see that there are some tracts that overlap with each other, especially on the ventral side. This is something that the clustering can't fully take into account since the algorithms try and partition the clusters rather than overlapping.

Validation is one of the tougher challenges for clustering. One of the easiest methods for determining whether the results are accurate or not is by comparing it to a gold standard. As mentioned in the literature review section, some of the validation methods involve using a ground truth to insert into the validation functions. However in our particular case, since we are investigating and in a sense validating the gold standards, we can't use them for the validation of our clusters (especially considering that the Paxinos atlas for the rat does not contain all the clusters either), only as a comparison. Furthermore, since there are variations that we see between different atlases, choosing which one to use would also be a problem (this applies to other species seeing as the rat itself has only one atlas as of right now). Another issue with the quantifiable validation methods is that they are just innate measures of whether the points belong in that cluster based solely off of distance measurements and metrics as opposed to verifying whether the positioning and size of the clusters are anatomically correct. It is tough to truly identify what the validation values represent and this also led to the difficulty in choosing the optimal number of clusters quantitatively.

CHAPTER 6 CONCLUSION AND RECOMMENDATIONS

To conclude, we were able to implement and develop a pipeline that would cluster the white matter tracts based solely on quantitative metrics obtained from high resolution SEM images. We were able to obtain tracts that the gold standard atlas used at this moment was unable to do with their multiple staining techniques. We observed missing tracts such as the ventral spinothalamic tract and the reticulospinal tract which are seen in other species (such as the mouse and human) and therefore having a high likelihood of being present in the rat as well. The algorithm that showed to give the best overall representation of the atlas was the agglomerative clustering algorithm. Unfortunately, as of right now, we can only estimate that the best number of clusters to use would be 14-15 based on what we know from the literature on how many tracts there are supposed to be. On a quantitative note however, we were not able to establish a guaranteed way of determining this. Of course, there are still some constraints especially with the acquisition of the input data that could have potentially affected the final clustering results and perhaps the exclusion of smaller tracts due to missing information. However, since there is a methodology and pipeline in place, we could easily re-test and verify this on other data sets of higher quality to which we could compare the results to a gold standard being used at the moment as well. This would be of interest because instead of having to visually identify the tracts using different types of stains for different bodies we could easily just use one set of data that was prepared with one stain that yields quantitative information which could then be implemented in the pipeline.

The pipeline could also be tweaked to be applied to other modalities to help with investigations on non-histological images that are perhaps non-invasive such as quantitative magnetic resonance imaging that gives metric maps as outputs. This would allow for the use of the pipeline in potentially clinical situations in order to be able to understand how the white matter tracts are being affected by either pathology or trauma. Our pipeline would also be relevant if other gold standard atlases would be constructed for different species in order to have a quantitative and digital representation of what the cytoarchitecture of the white matter looks like. Having this type of atlas would allow for the registration of other types of images (like MRI) onto the atlas for purpose of comparison within the space.

Though the study so far gives good results, there are still many improvements that could be made and further investigations to be done. These would consist of firstly applying a z-correlation

approach to correlate pixels in the z direction (i.e. between levels) to see if the tracts correspond along the entirety of the length of the spinal cord (or at least between a few levels). This would be done by registering the levels for each section of the spinal cord on a common level and then exploring the clustering on these areas. The second approach would be to apply what is known as a multi-layer network which would essentially apply a correlation matrix in the z-direction to try and figure out the corresponding pixels superior-inferiorly and then applying the clustering algorithm onto this. Of course, this is something that could potentially work only across a few levels as we know that in the z-direction axons are not entirely straight going down and can curve [48]. Another thing to implement is a more robust method for quantifying if the clusters are indeed grouped appropriately or not. This is crucial so as to gain a better understanding of how the clustering algorithm works and what would need to be improved to obtain even better results to be closer to the anatomic truth.

BIBLIOGRAPHY

[1] A. Laird, "Autonomic dysreflexia following high level spinal cord injury: time course, mechanisms and possible intervention," 08/23 2019.

[2] A. Zaimi, T. Duval, A. Gasecka, D. Côté, N. Stikov, and J. Cohen-Adad, "AxonSeg: Open Source Software for Axon and Myelin Segmentation and Morphometric Analysis," (in eng), *Frontiers in neuroinformatics*, vol. 10, pp. 37-37, 2016.

[3] S. Standring, *Gray's anatomy : the anatomical basis of clinical practice*. 2016.

[4] U. de Girolami and T. A. Bale, "Spinal cord," *Handbook of clinical neurology*, vol. 145, p. 405, 2017.

[5] Nervous System Cells [Online]. Available: https://basicmedicalkey.com/nervous-system-cells/ - f6

[6] B. c. staff, "Medical gallery of Blausen Medical 2014," ed: WikiJournal of Medicine, 2014.

[7] S. Hochman, "Spinal cord," *Current Biology*, vol. 17, no. 22, pp. R950-R955, 2007/11/20/ 2007.

[8] J. V. Priestley, "Neuroanatomy of the spinal cord: current research and future prospects," *Spinal Cord*, vol. 25, no. 3, pp. 198-204, 1987/06/01 1987.

[9] (2015, July 1). *The spinal cord and peripheral nerves*. Available: https://clinicalgate.com/the-spinal-cord-and-peripheral-nerves/

[10] C. W. I. T. G. P. Gulgun Sengul, *Atlas of the Spinal Cord - 1st Edition*. Academic Press, 2015.

[11] R. Burstein, R. J. Dado, and G. J. Giesler, "The cells of origin of the spinothalamic tract of the rat: a quantitative reexamination," *Brain Research*, vol. 511, no. 2, pp. 329-337, 1990/03/19/ 1990.

[12] D. Tracey, "CHAPTER 7 - Ascending and Descending Pathways in the Spinal Cord," in *The Rat Nervous System (Third Edition)*, G. Paxinos, Ed. Burlington: Academic Press, 2004, pp. 149-164.

[13] R. Deumens, G. C. Koopmans, and E. A. J. Joosten, "Regeneration of descending axon tracts after spinal cord injury," *Progress in Neurobiology*, vol. 77, no. 1, pp. 57-89, 2005/09/01/ 2005.

[14] P. A. Axderson, "The Vestibular Nuclei and Their Connections, Anatomy and Functional Correlations," *Journal of Neuropathology & Experimental Neurology*, vol. 23, no. 2, pp. 388-389, 1964.

[15] B. W. Peterson, R. A. Maunz, and K. Fukushima, "Properties of a new vestibulospinal projection, the caudal vestibulospinal tract," (in eng), *Exp Brain Res*, vol. 32, no. 2, pp. 287-92, Jun 19 1978.

[16] L. W. Kneisley, M. P. Biber, and J. H. LaVail, "A study of the origin of brain stem projections to monkey spinal cord using the retrograde transport method," *Experimental Neurology*, vol. 60, no. 1, pp. 116-139, 1978/05/15/ 1978.

[17] J. A. Buford and A. G. Davidson, "Movement-related and preparatory activity in the reticulospinal system of the monkey," *Experimental Brain Research,* journal article vol. 159, no. 3, pp. 284-300, December 01 2004.

[18] B. W. Peterson, "Reticulospinal Projections to Spinal Motor Nuclei," *Annual Review of Physiology,* vol. 41, no. 1, pp. 127-140, 1979.

[19] C. Watson and M. Harrison, "The location of the major ascending and descending spinal cord tracts in all spinal cord segments in the mouse: actual and extrapolated," *Anat. Rec.,* vol. 295, no. 10, pp. 1692-1697, 2012/10 2012.

[20] G. Kayalioglu, "Chapter 10 - Projections from the Spinal Cord to the Brain," in *The Spinal Cord*, C. Watson, G. Paxinos, and G. Kayalioglu, Eds. San Diego: Academic Press, 2009, pp. 148-167.

[21] E. D. Al-Chaer, Y. Feng, and W. D. Willis, "Comparative Study of Viscerosomatic Input Onto Postsynaptic Dorsal Column and Spinothalamic Tract Neurons in the Primate," *Journal of Neurophysiology,* vol. 82, no. 4, pp. 1876-1882, 1999.

[22] B. L. Whitsel, L. M. Petrucelli, G. Sapiro, and H. Ha, "Fiber sorting in the fasciculus gracilis of squirrel monkeys," *Experimental Neurology,* vol. 29, no. 2, pp. 227-242, 1970/11/01/ 1970.

[23] E. D. Al-Chaer, N. B. Lawand, K. N. Westlund, and W. D. Willis, "Pelvic visceral input into the nucleus gracilis is largely mediated by the postsynaptic dorsal column pathway," *Journal of Neurophysiology,* vol. 76, no. 4, pp. 2675-2690, 1996.

[24] P. R. Burgess and K. W. Horch, "The distinction between the short and intermediate ascending pathways in the fasciculus gracilis of the cat," *Brain Research,* vol. 151, no. 3, pp. 579-580, 1978/08/11/ 1978.

[25] M. C. SMITH and P. DEACON, "TOPOGRAPHICAL ANATOMY OF THE POSTERIOR COLUMNS OF THE SPINAL CORD IN MAN: THE LONG ASCENDING FIBRES," *Brain,* vol. 107, no. 3, pp. 671-698, 1984.

[26] G. J. Giesler and K. D. Cliffer, "Postsynaptic dorsal column pathway of the rat. II. Evidence against an important role in nociception," *Brain Research,* vol. 326, no. 2, pp. 347-356, 1985/02/11/ 1985.

[27] G. J. Bennett, N. Nishikawa, G.-W. Lu, M. J. Hoffert, and R. Dubner, "The morphology of dorsal column postsynaptic spinomedullary neurons in the cat," *Journal of Comparative Neurology,* vol. 224, no. 4, pp. 568-578, 1984.

[28] A. V. Apkarian and C. J. Hodge, "Primate spinothalamic pathways: II. The cells of origin of the dorsolateral and ventral spinothalamic pathways," *J. Comp. Neurol.,* vol. 288, no. 3, pp. 474-492, 1989/10/15 1989.

[29] A. V. Apkarian and C. J. Hodge, "Primate spinothalamic pathways: I. A quantitative study of the cells of origin of the spinothalamic pathway," *Journal of Comparative Neurology,* vol. 288, no. 3, pp. 447-473, 1989.

[30] X. Zhang, C. N. Honda, and J. Glenn J. Giesler, "Position of Spinothalamic Tract Axons in Upper Cervical Spinal Cord of Monkeys," *Journal of Neurophysiology*, vol. 84, no. 3, pp. 1180-1185, 2000.

[31] R. T. Stevens, A. V. Apkarian, and C. J. Hodge, "The Location of Spinothalamic Axons within Spinal Cord White Matter in Cat and Squirrel Monkey," *Somatosensory & Motor Research*, vol. 8, no. 2, pp. 97-102, 1991/01/01 1991.

[32] J. H. Kim, T. J. Ebner, and J. R. Bloedel, "Comparison of response properties of dorsal and ventral spinocerebellar tract neurons to a physiological stimulus," *Brain Research*, vol. 369, no. 1, pp. 125-135, 1986/03/26/ 1986.

[33] S. A. Edgley and E. Jankowska, "Information processed by dorsal horn spinocerebellar tract neurones in the cat," (in eng), *The Journal of physiology*, vol. 397, pp. 81-97, 1988.

[34] S. A. Edgley and G. M. Grant, "Inputs to spinocerebellar tract neurones located in Stilling's nucleus in the sacral segments of the rat spinal cord," *Journal of Comparative Neurology*, vol. 305, no. 1, pp. 130-138, 1991.

[35] C. Watson and A. R. Harvey, "Chapter 11 - Projections from the Brain to the Spinal Cord," in *The Spinal Cord*, C. Watson, G. Paxinos, and G. Kayalioglu, Eds. San Diego: Academic Press, 2009, pp. 168-179.

[36] N. D. Jeffery and M. Fitzgerald, "Lack of topographical organisation of the corticospinal tract in the cervical spinal cord of the adult rat," *Brain Research*, vol. 833, no. 2, pp. 315-318, 1999/07/03/ 1999.

[37] I. Q. Whishaw, B. Gorny, and J. Sarna, "Paw and limb use in skilled and spontaneous reaching after pyramidal tract, red nucleus and combined lesions in the rat: behavioral and anatomical dissociations," *Behavioural Brain Research*, vol. 93, no. 1, pp. 167-183, 1998/06/01/ 1998.

[38] V. J. Wilson *et al.*, "The vestibulocollic reflex," (in eng), *J Vestib Res*, vol. 5, no. 3, pp. 147-70, May-Jun 1995.

[39] O. Pompeiano, "Spinovestibular Relations: Anatomical and Physiological Aspects," in *Progress in Brain Research*, vol. 37, A. Brodal and O. Pompeiano, Eds.: Elsevier, 1972, pp. 263-296.

[40] T. R. Corle and G. S. Kino, "CHAPTER 1 - Introduction," in *Confocal Scanning Optical Microscopy and Related Imaging Systems*, T. R. Corle and G. S. Kino, Eds. Burlington: Academic Press, 1996, pp. 1-66.

[41] R. F. Egerton, "An Introduction to Microscopy," in *Physical Principles of Electron Microscopy: An Introduction to TEM, SEM, and AEM*Boston, MA: Springer US, 2005, pp. 1-25.

[42] R. F. Egerton, "Electron Optics," in *Physical Principles of Electron Microscopy: An Introduction to TEM, SEM, and AEM*Boston, MA: Springer US, 2005, pp. 27-55.

[43] R. F. Egerton, *Physical Principles of Electron Microscopy: An Introduction to TEM, SEM, and AEM*. Springer, Boston, MA, 2005.

[44] T. F. S. P.-W. BV. (2018, July 20). *How to Mix Backscattered and Secondary Electron Images.* Available: https://www.azom.com/article.aspx?ArticleID=16390.

[45] Q. Wan *et al.*, "Angle selective backscattered electron contrast in the low-voltage scanning electron microscope: Simulation and experiment for polymers," *Ultramicroscopy*, vol. 171, pp. 126-138, 2016/12/01/ 2016.

[46] JEOL. (2011, July 20). *JEOL Application Data Sheet*. Available: https://www.jeol.co.jp/en/applications/pdf/sm/465_en.pdf

[47] J. A. Kiernan, "Formaldehyde, Formalin, Paraformaldehyde And Glutaraldehyde: What They Are And What They Do," *Microscopy Today*, vol. 8, no. 1, pp. 8-13, 2000.

[48] S. Mikula and W. Denk, "High-resolution whole-brain staining for electron microscopic circuit reconstruction," *Nature Methods*, Article vol. 12, p. 541, 04/13/online 2015.

[49] G. V. Fabian Pedregosa, Alexandre Gramfort, Vincent Michel, Bertrand Thirion, Olivier Grisel, Mathieu Blondel, Peter Prettenhofer, Ron Weiss, Vincent Dubourg, Jake Vanderplas, Alexandre Passos, David Cournapeau, Matthieu Brucher, Matthieu Perrot, Édouard Duchesnay, "Scikit-learn: Machine Learning in Python," *Journal of Machine Learning Research*, vol. 12, pp. 2825-2830, 2011.

[50] A. K. Jain, "Data clustering: 50 years beyond K-means," *Pattern Recognition Letters*, vol. 31, no. 8, pp. 651-666, 2010/06/01/ 2010.

[51] H.-H. Bock, "Clustering Methods: A History of k-Means Algorithms," in *Selected Contributions in Data Analysis and Classification*, P. Brito, G. Cucumel, P. Bertrand, and F. de Carvalho, Eds. Berlin, Heidelberg: Springer Berlin Heidelberg, 2007, pp. 161-172.

[52] A. Y. Ng, M. I. Jordan, and Y. Weiss, "On spectral clustering: Analysis and an algorithm," in *Advances in neural information processing systems*, 2002, pp. 849-856.

[53] M. Ester, H.-P. Kriegel, J. Sander, and X. Xu, "A density-based algorithm for discovering clusters in large spatial databases with noise," in *Kdd*, 1996, vol. 96, no. 34, pp. 226-231.

[54] A. Bouguettaya, Q. Yu, X. Liu, X. Zhou, and A. Song, "Efficient agglomerative hierarchical clustering," *Expert Systems with Applications*, vol. 42, no. 5, pp. 2785-2797, 2015/04/01/ 2015.

[55] W. H. E. Day and H. Edelsbrunner, "Efficient algorithms for agglomerative hierarchical clustering methods," *J. Classification*, vol. 1, no. 1, pp. 7-24, 1984/12/1 1984.

[56] F. Murtagh, "A Survey of Recent Advances in Hierarchical Clustering Algorithms," *The Computer Journal*, vol. 26, no. 4, pp. 354-359, 1983.

[57] F. Murtagh and P. Legendre, "Ward's Hierarchical Agglomerative Clustering Method: Which Algorithms Implement Ward's Criterion?," *Journal of Classification*, journal article vol. 31, no. 3, pp. 274-295, October 01 2014.

[58] U. Malik. (2018, July 20). *Hierarchical Clustering with Python and Scikit-Learn*. Available: https://stackabuse.com/hierarchical-clustering-with-python-and-scikit-learn/

[59] M. Roux, "A Comparative Study of Divisive and Agglomerative Hierarchical Clustering Algorithms," *Journal of Classification*, journal article vol. 35, no. 2, pp. 345-366, July 01 2018.

[60] J.-P. Rodrigue, C. Comtois, and B. Slack, *The geography of transport systems*. 2017.

[61] D. Benjamini, M. E. Komlosh, L. A. Holtzclaw, U. Nevo, and P. J. Basser, "White matter microstructure from nonparametric axon diameter distribution mapping," *NeuroImage*, vol. 135, pp. 333-344, 2016/07/15/ 2016.

[62] Y. Assaf, T. Blumenfeld-Katzir, Y. Yovel, and P. J. Basser, "Axcaliber: A method for measuring axon diameter distribution from diffusion MRI," *Magnetic Resonance in Medicine*, vol. 59, no. 6, pp. 1347-1354, 2008.

[63] B. Thirion, G. Varoquaux, E. Dohmatob, and J.-B. Poline, "Which fMRI clustering gives good brain parcellations?," (in English), *Frontiers in Neuroscience*, Original Research vol. 8, no. 167, 2014-July-01 2014.

[64] S. Zhang, S. Correia, and D. H. Laidlaw, "Identifying White-Matter Fiber Bundles in DTI Data Using an Automated Proximity-Based Fiber-Clustering Method," *IEEE Transactions on Visualization and Computer Graphics*, vol. 14, no. 5, pp. 1044-1053, 2008.

[65] P. J. Rousseeuw, "Silhouettes: A graphical aid to the interpretation and validation of cluster analysis," *Journal of Computational and Applied Mathematics*, vol. 20, pp. 53-65, 1987/11/01/ 1987.

[66] U. Maulik and S. Bandyopadhyay, "Performance evaluation of some clustering algorithms and validity indices," *IEEE Transactions on Pattern Analysis and Machine Intelligence*, vol. 24, no. 12, pp. 1650-1654, 2002.

[67] D. L. Davies and D. W. Bouldin, "A Cluster Separation Measure," *IEEE Transactions on Pattern Analysis and Machine Intelligence*, vol. PAMI-1, no. 2, pp. 224-227, 1979.

[68] T. Duval *et al.*, "Axons morphometry in the human spinal cord," *NeuroImage*, vol. 185, pp. 119-128, 2019/01/15/ 2019.

[69] JEOL. (2019, July 20). *JSM-7600F Schottky Field Emission Scanning Electron Microscope*. Available: https://www.jeol.co.jp/en/products/detail/JSM-7600F.html

[70] B. De Leener *et al.*, "SCT: Spinal Cord Toolbox, an open-source software for processing spinal cord MRI data," *NeuroImage*, vol. 145, pp. 24-43, 2017/01/15/ 2017.

[71] J. R. Small, M. N. Ghabriel, and G. Allt, "The development of Schmidt-Lanterman incisures: an electron microscope study," (in eng), *Journal of anatomy*, vol. 150, pp. 277-286, 1987.

[72] H. Gray and W. H. Lewis, *Anatomy of the human body*. Philadelphia: Lea & Febiger, 1918.

APPENDIX A – CLUSTERS FOR EACH LEVEL

The section in the appendix will show the rest of the clustering outputs for every single level for each algorithm. This shows only the spread between 5-15 clusters as those tend to be the most relevant clusters.

C1

Agglomerative Clustering

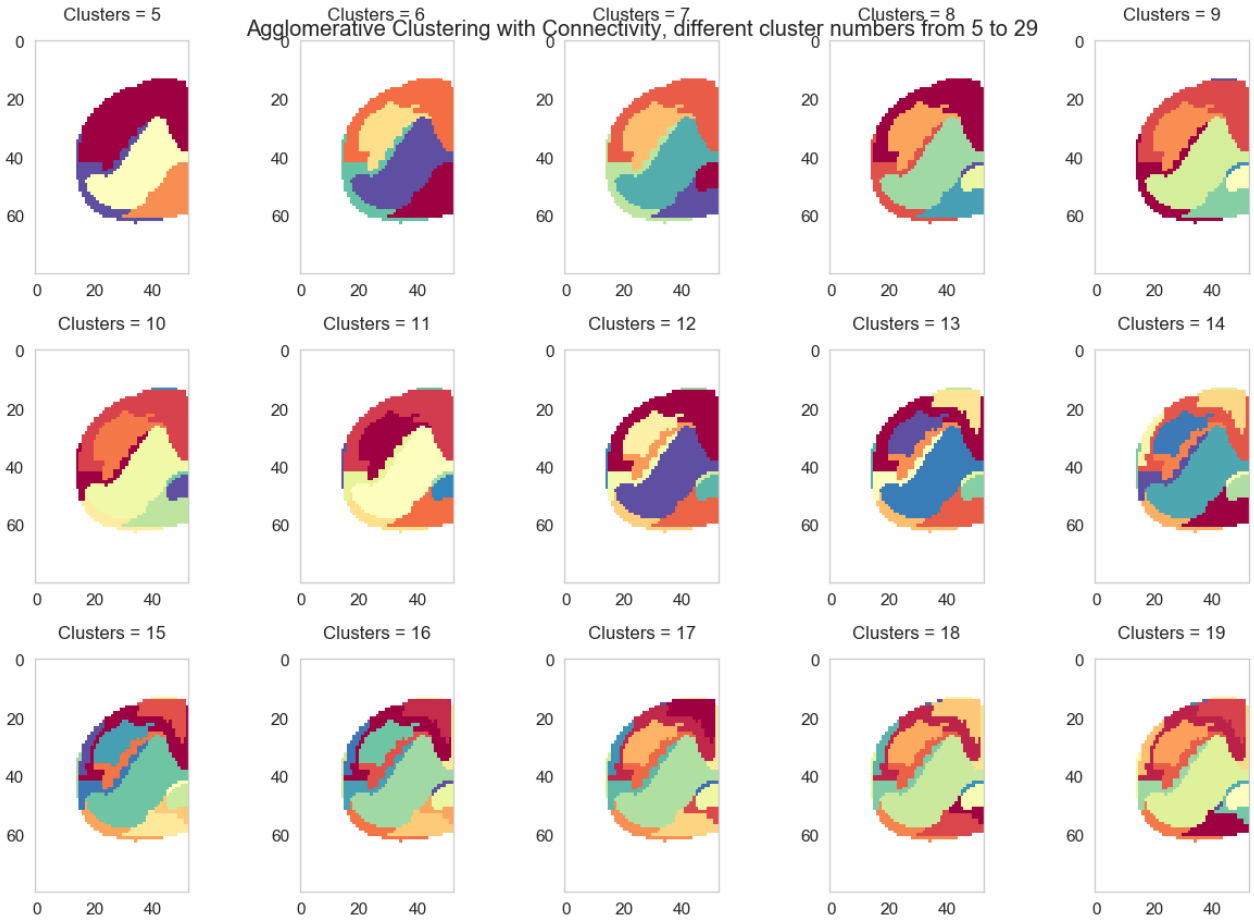

C2

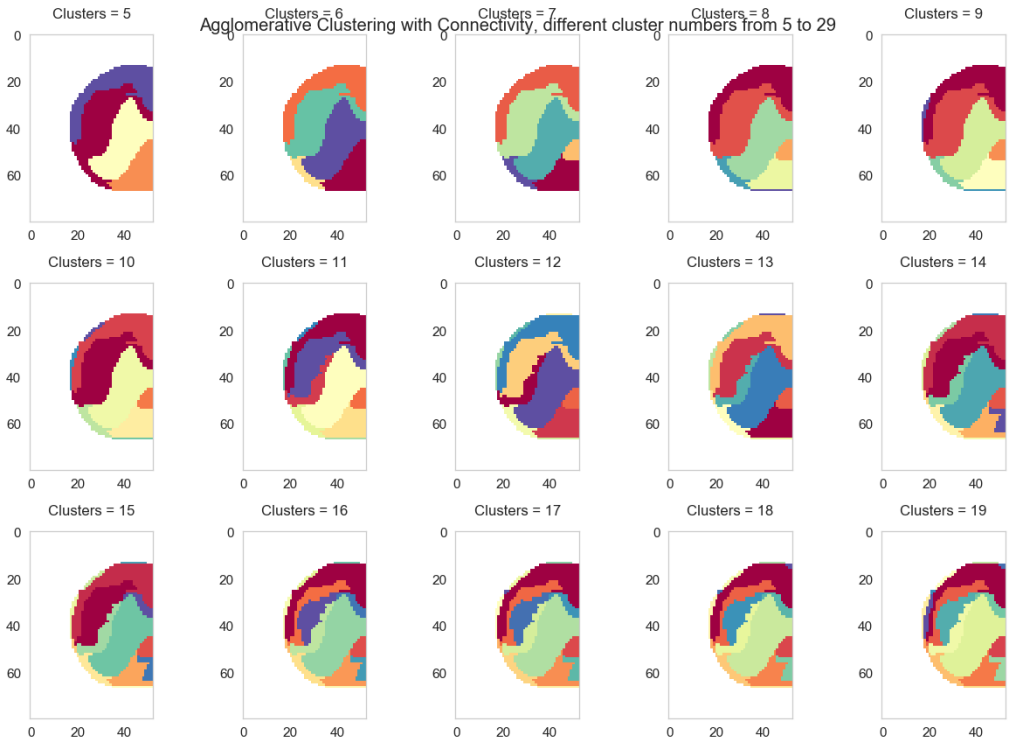
Agglomerative Clustering with Connectivity, different cluster numbers from 5 to 29
Clusters = 5
Clusters = 6
Clusters = 7
Clusters = 8
Clusters = 9
Clusters = 10
Clusters = 11
Clusters = 12
Clusters = 13
Clusters = 14
Clusters = 15
Clusters = 16
Clusters = 17
Clusters = 18
Clusters = 19

C3

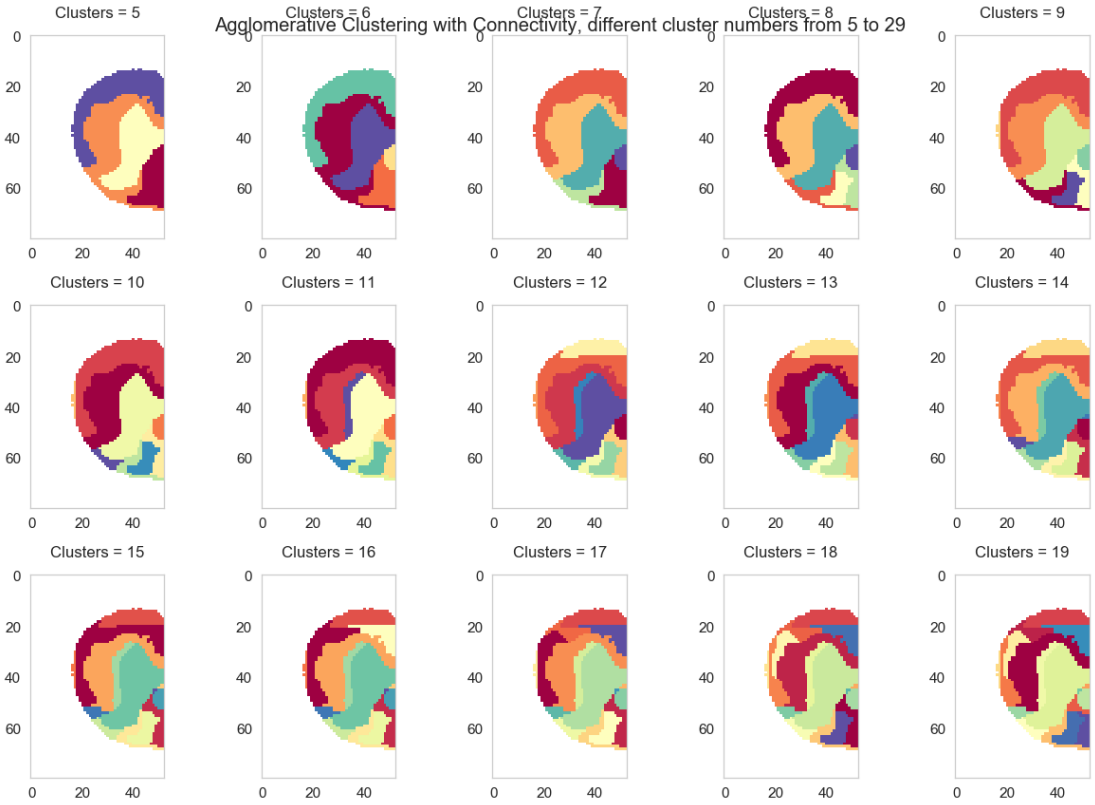
Agglomerative Clustering with Connectivity, different cluster numbers from 5 to 29
Clusters = 5
Clusters = 6
Clusters = 7
Clusters = 8
Clusters = 9
Clusters = 10
Clusters = 11
Clusters = 12
Clusters = 13
Clusters = 14
Clusters = 15
Clusters = 16
Clusters = 17
Clusters = 18
Clusters = 19

C4

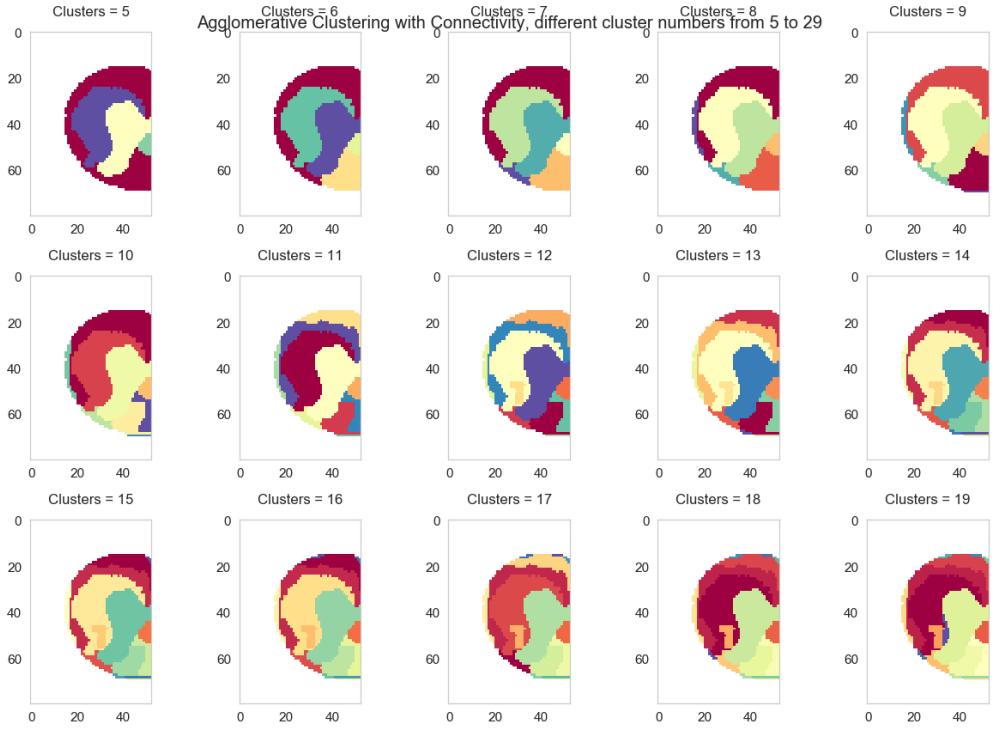
Agglomerative Clustering with Connectivity, different cluster numbers from 5 to 29
Clusters = 5
Clusters = 6
Clusters = 7
Clusters = 8
Clusters = 9
Clusters = 10
Clusters = 11
Clusters = 12
Clusters = 13
Clusters = 14
Clusters = 15
Clusters = 16
Clusters = 17
Clusters = 18
Clusters = 19

C5

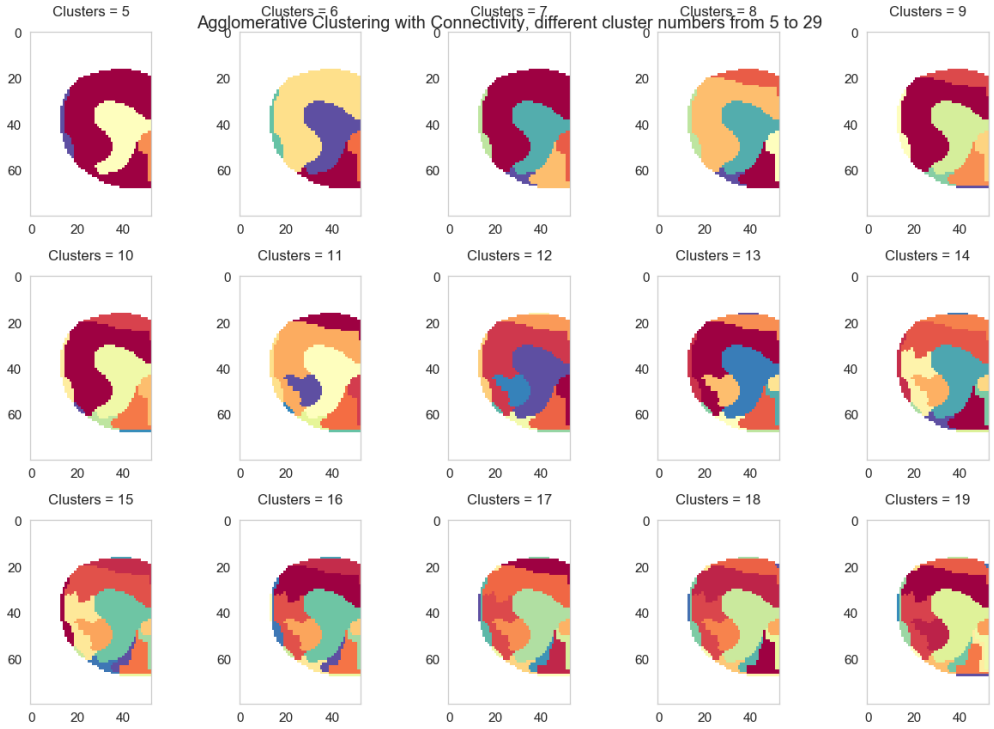
Agglomerative Clustering with Connectivity, different cluster numbers from 5 to 29
Clusters = 5
Clusters = 6
Clusters = 7
Clusters = 8
Clusters = 9
Clusters = 10
Clusters = 11
Clusters = 12
Clusters = 13
Clusters = 14
Clusters = 15
Clusters = 16
Clusters = 17
Clusters = 18
Clusters = 19

C6

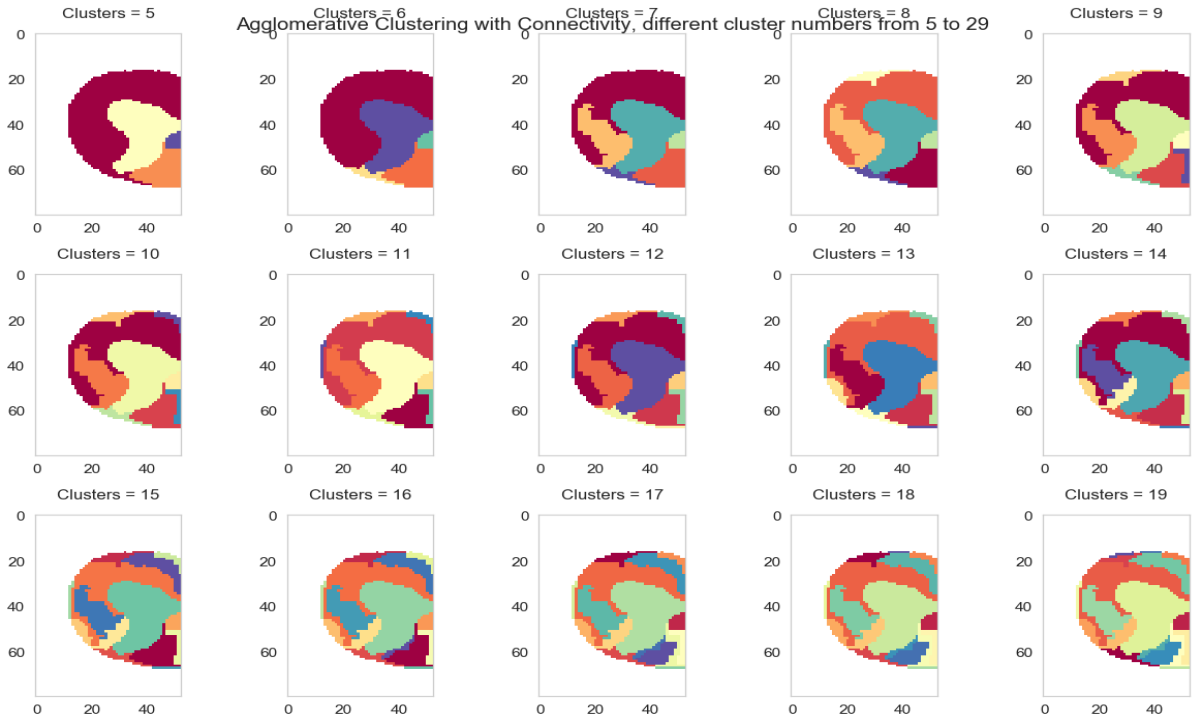
Agglomerative Clustering with Connectivity, different cluster numbers from 5 to 29
Clusters = 5
Clusters = 6
Clusters = 7
Clusters = 8
Clusters = 9
Clusters = 10
Clusters = 11
Clusters = 12
Clusters = 13
Clusters = 14
Clusters = 15
Clusters = 16
Clusters = 17
Clusters = 18
Clusters = 19

C7

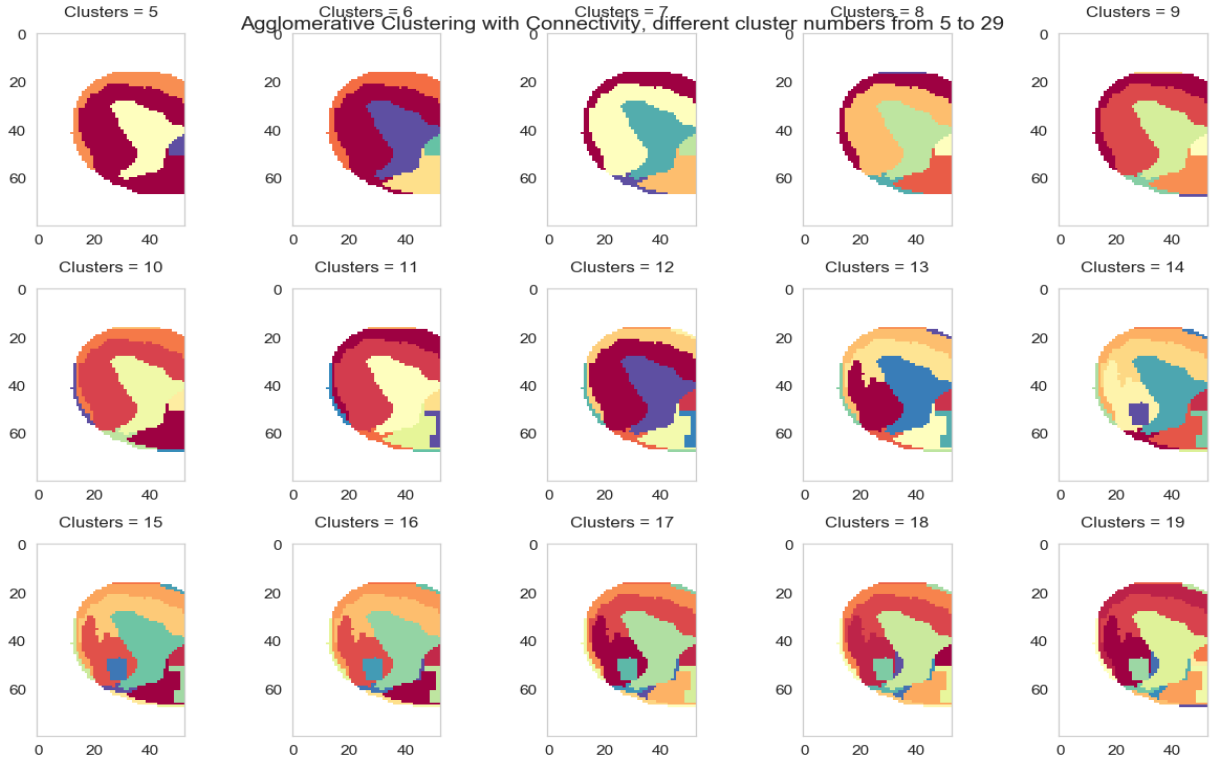
Agglomerative Clustering with Connectivity, different cluster numbers from 5 to 29
Clusters = 5
Clusters = 6
Clusters = 7
Clusters = 8
Clusters = 9
Clusters = 10
Clusters = 11
Clusters = 12
Clusters = 13
Clusters = 14
Clusters = 15
Clusters = 16
Clusters = 17
Clusters = 18
Clusters = 19

C8

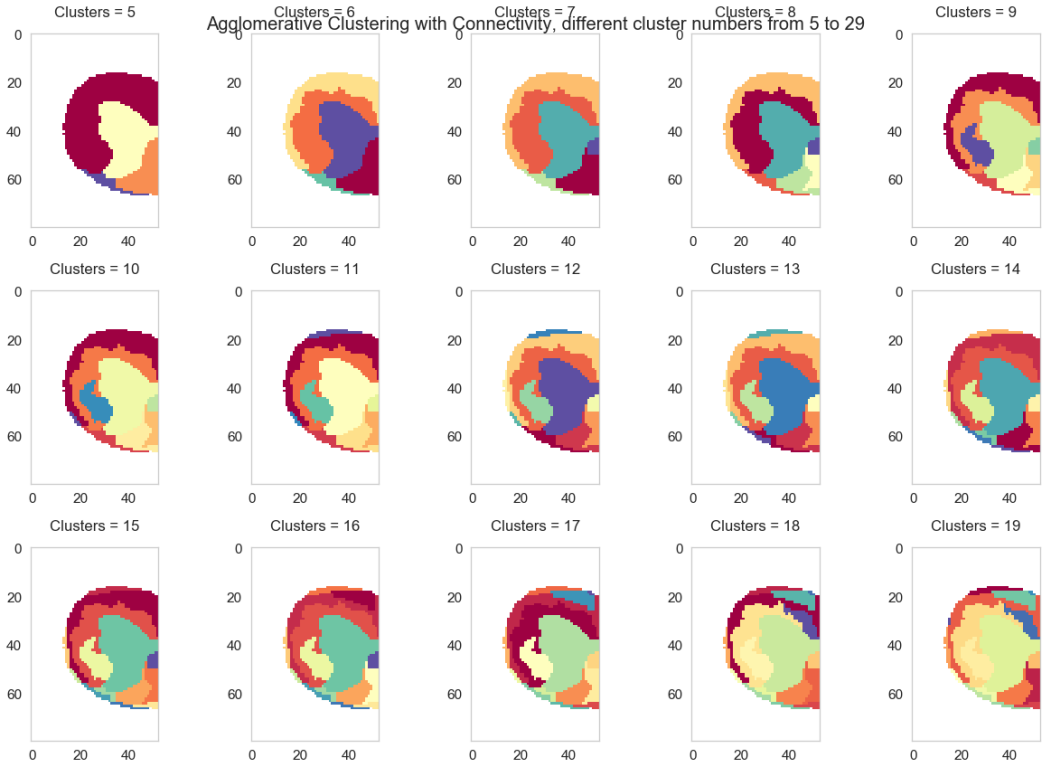
Agglomerative Clustering with Connectivity, different cluster numbers from 5 to 29
Clusters = 5
Clusters = 6
Clusters = 7
Clusters = 8
Clusters = 9
Clusters = 10
Clusters = 11
Clusters = 12
Clusters = 13
Clusters = 14
Clusters = 15
Clusters = 16
Clusters = 17
Clusters = 18
Clusters = 19

T1

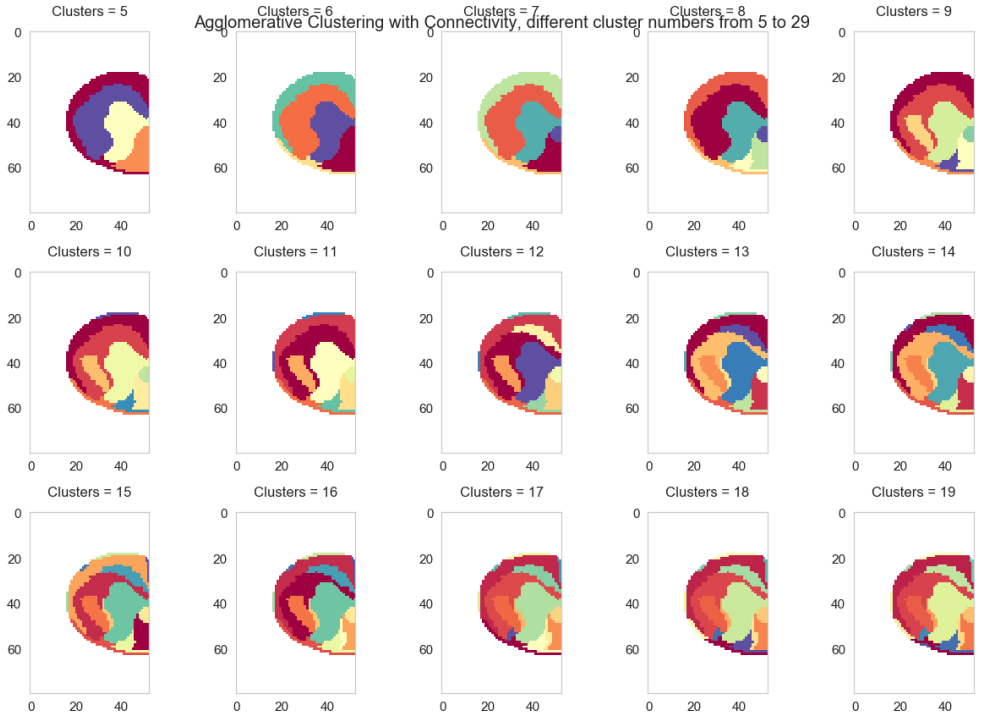
Agglomerative Clustering with Connectivity, different cluster numbers from 5 to 29
Clusters = 5
Clusters = 6
Clusters = 7
Clusters = 8
Clusters = 9
Clusters = 10
Clusters = 11
Clusters = 12
Clusters = 13
Clusters = 14
Clusters = 15
Clusters = 16
Clusters = 17
Clusters = 18
Clusters = 19

T2

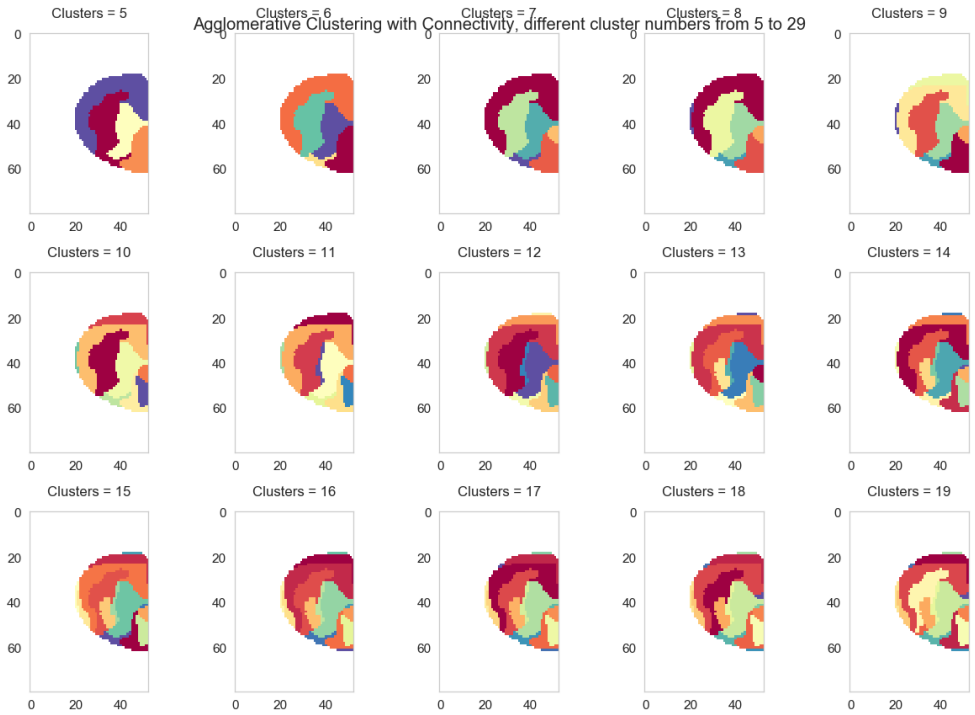
Agglomerative Clustering with Connectivity, different cluster numbers from 5 to 29
Clusters = 5
Clusters = 6
Clusters = 7
Clusters = 8
Clusters = 9
Clusters = 10
Clusters = 11
Clusters = 12
Clusters = 13
Clusters = 14
Clusters = 15
Clusters = 16
Clusters = 17
Clusters = 18
Clusters = 19

T3

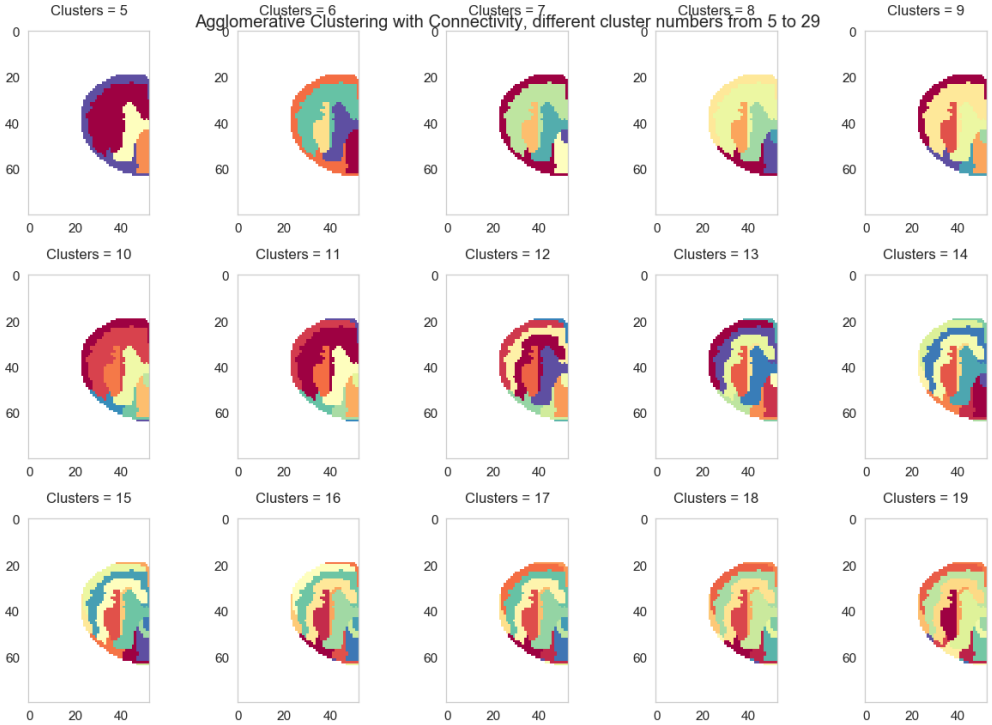
Agglomerative Clustering with Connectivity, different cluster numbers from 5 to 29
Clusters = 5
Clusters = 6
Clusters = 7
Clusters = 8
Clusters = 9
Clusters = 10
Clusters = 11
Clusters = 12
Clusters = 13
Clusters = 14
Clusters = 15
Clusters = 16
Clusters = 17
Clusters = 18
Clusters = 19

T4

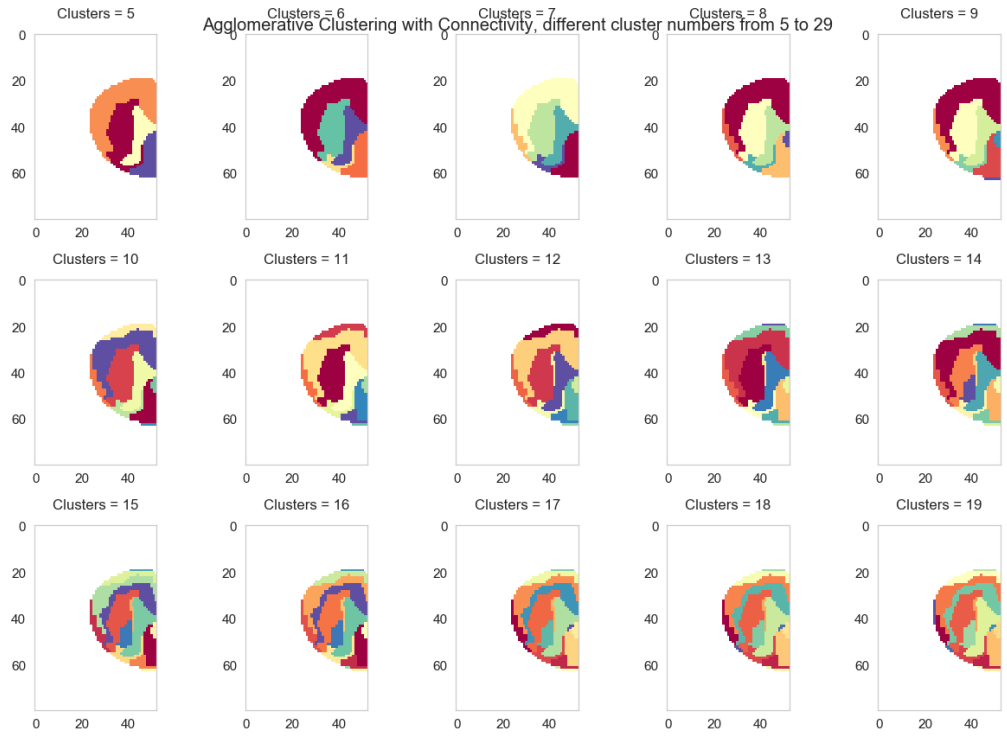
Agglomerative Clustering with Connectivity, different cluster numbers from 5 to 29
Clusters = 5
Clusters = 6
Clusters = 7
Clusters = 8
Clusters = 9
Clusters = 10
Clusters = 11
Clusters = 12
Clusters = 13
Clusters = 14
Clusters = 15
Clusters = 16
Clusters = 17
Clusters = 18
Clusters = 19

T5

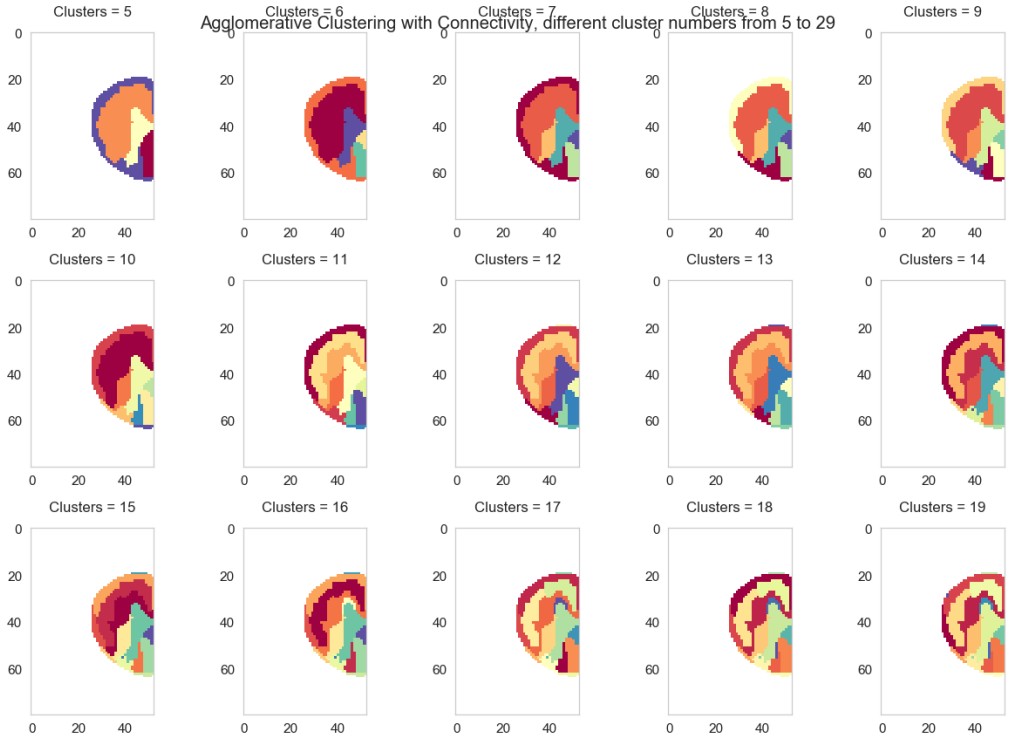
Agglomerative Clustering with Connectivity, different cluster numbers from 5 to 29
Clusters = 5
Clusters = 6
Clusters = 7
Clusters = 8
Clusters = 9
Clusters = 10
Clusters = 11
Clusters = 12
Clusters = 13
Clusters = 14
Clusters = 15
Clusters = 16
Clusters = 17
Clusters = 18
Clusters = 19

T6

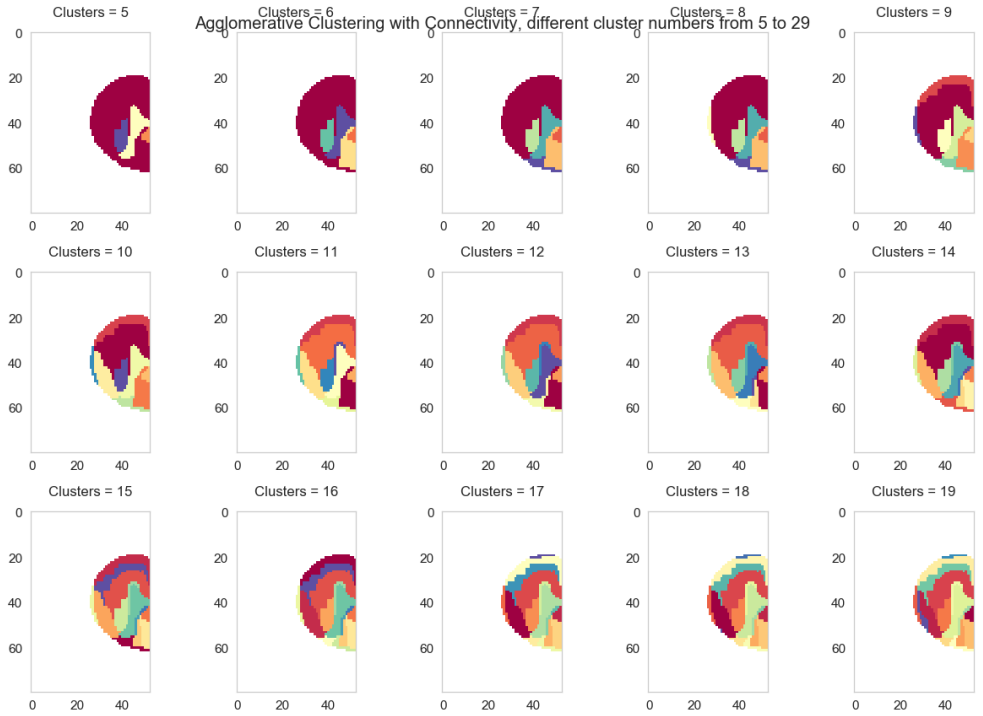
Agglomerative Clustering with Connectivity, different cluster numbers from 5 to 29
Clusters = 5
Clusters = 6
Clusters = 7
Clusters = 8
Clusters = 9
Clusters = 10
Clusters = 11
Clusters = 12
Clusters = 13
Clusters = 14
Clusters = 15
Clusters = 16
Clusters = 17
Clusters = 18
Clusters = 19

T7

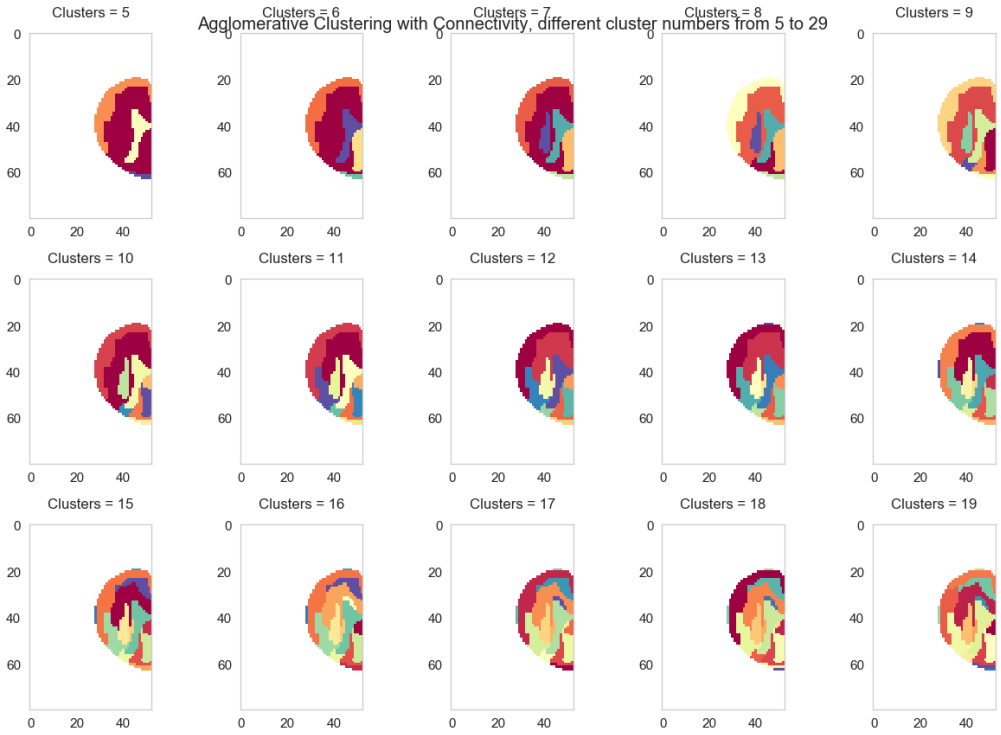
Agglomerative Clustering with Connectivity, different cluster numbers from 5 to 29
Clusters = 5
Clusters = 6
Clusters = 7
Clusters = 8
Clusters = 9
Clusters = 10
Clusters = 11
Clusters = 12
Clusters = 13
Clusters = 14
Clusters = 15
Clusters = 16
Clusters = 17
Clusters = 18
Clusters = 19

T8

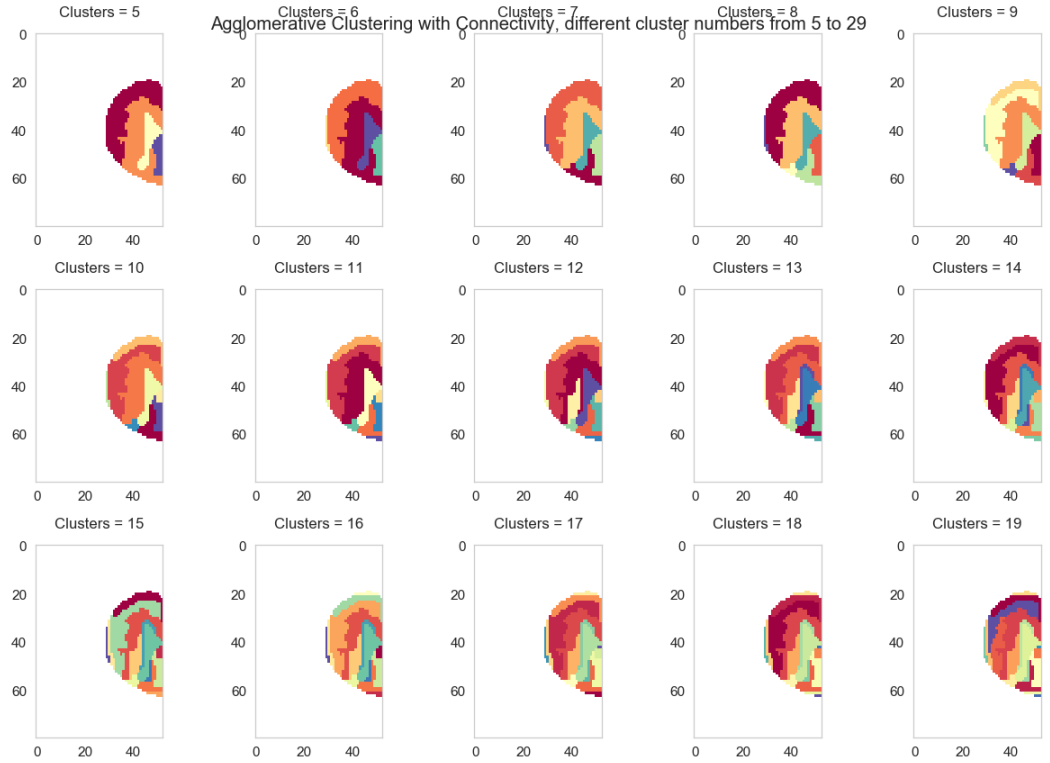
Agglomerative Clustering with Connectivity, different cluster numbers from 5 to 29
Clusters = 5
Clusters = 6
Clusters = 7
Clusters = 8
Clusters = 9
Clusters = 10
Clusters = 11
Clusters = 12
Clusters = 13
Clusters = 14
Clusters = 15
Clusters = 16
Clusters = 17
Clusters = 18
Clusters = 19

T9

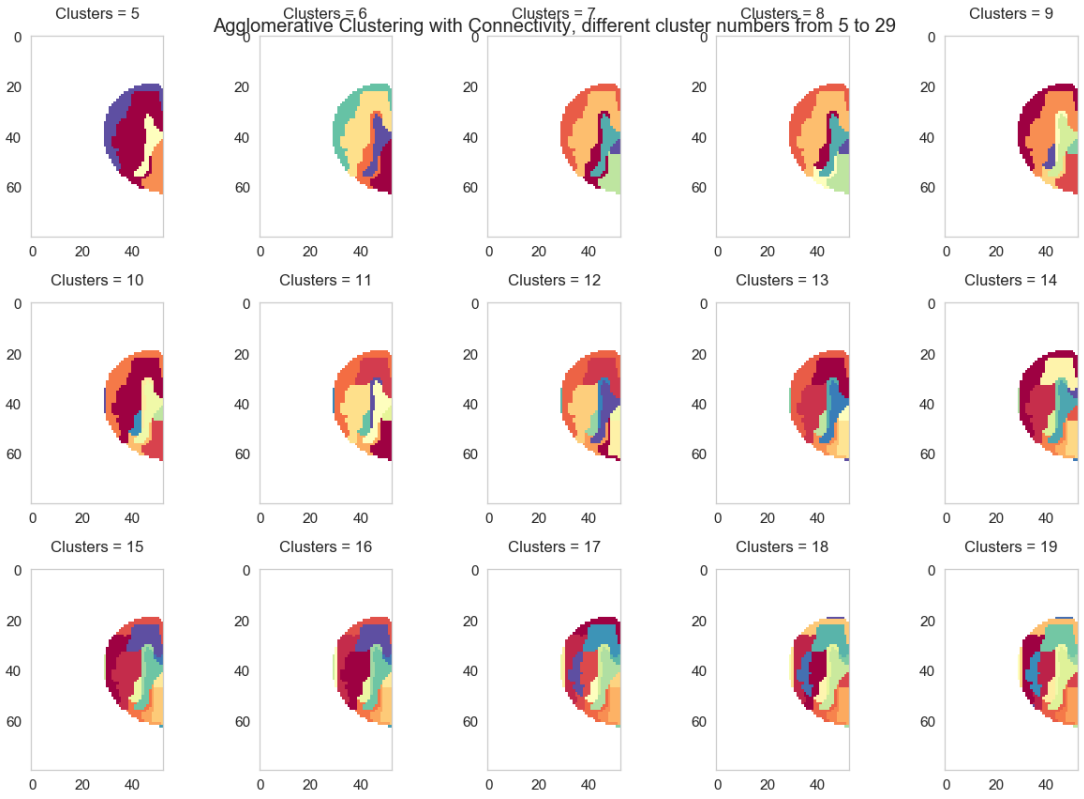
Agglomerative Clustering with Connectivity, different cluster numbers from 5 to 29
Clusters = 5
Clusters = 6
Clusters = 7
Clusters = 8
Clusters = 9
Clusters = 10
Clusters = 11
Clusters = 12
Clusters = 13
Clusters = 14
Clusters = 15
Clusters = 16
Clusters = 17
Clusters = 18
Clusters = 19

T10

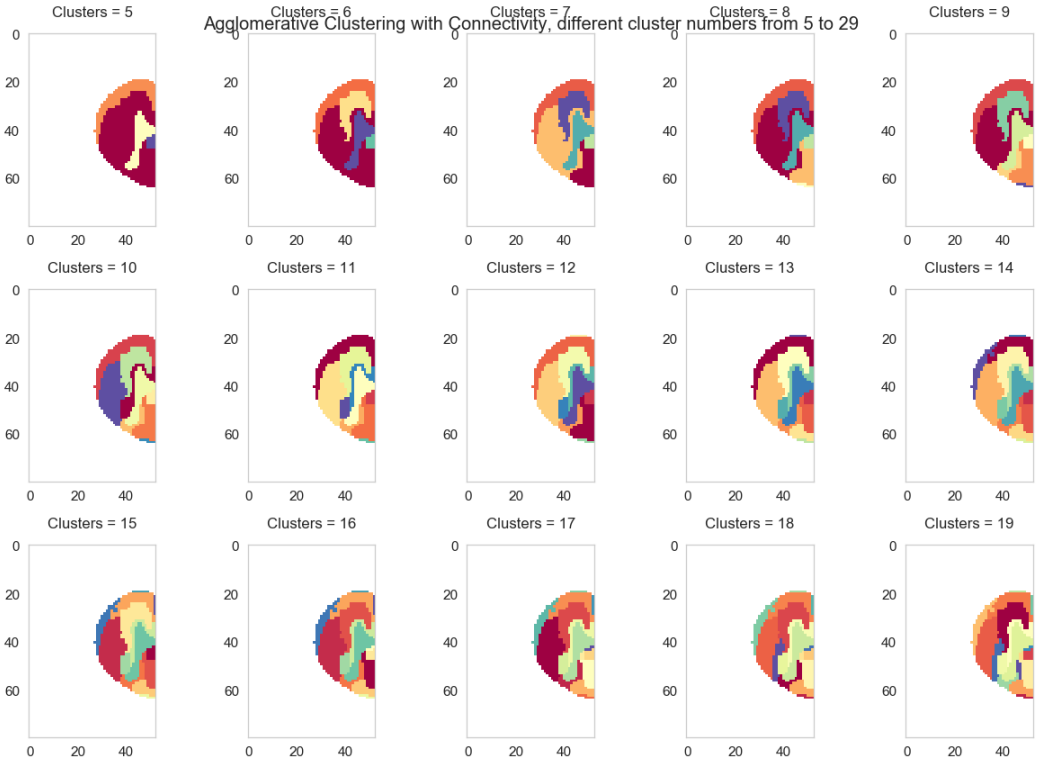
Agglomerative Clustering with Connectivity, different cluster numbers from 5 to 29
Clusters = 5
Clusters = 6
Clusters = 7
Clusters = 8
Clusters = 9
Clusters = 10
Clusters = 11
Clusters = 12
Clusters = 13
Clusters = 14
Clusters = 15
Clusters = 16
Clusters = 17
Clusters = 18
Clusters = 19

T11

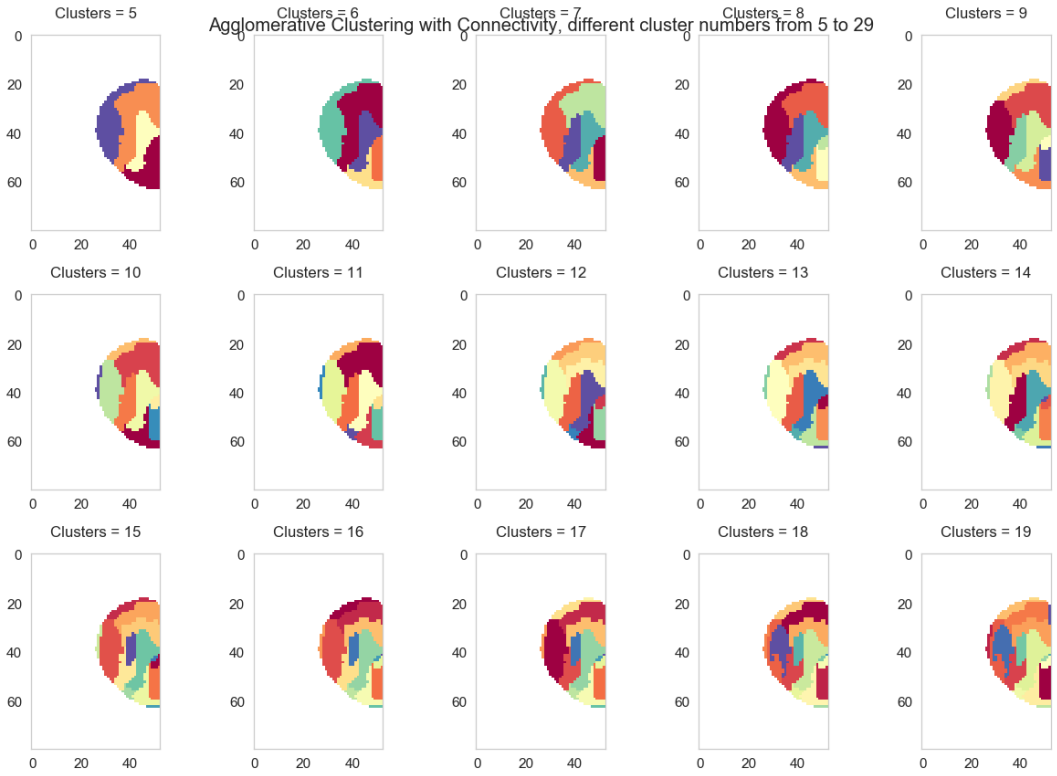
Agglomerative Clustering with Connectivity, different cluster numbers from 5 to 29
Clusters = 5
Clusters = 6
Clusters = 7
Clusters = 8
Clusters = 9
Clusters = 10
Clusters = 11
Clusters = 12
Clusters = 13
Clusters = 14
Clusters = 15
Clusters = 16
Clusters = 17
Clusters = 18
Clusters = 19

T12

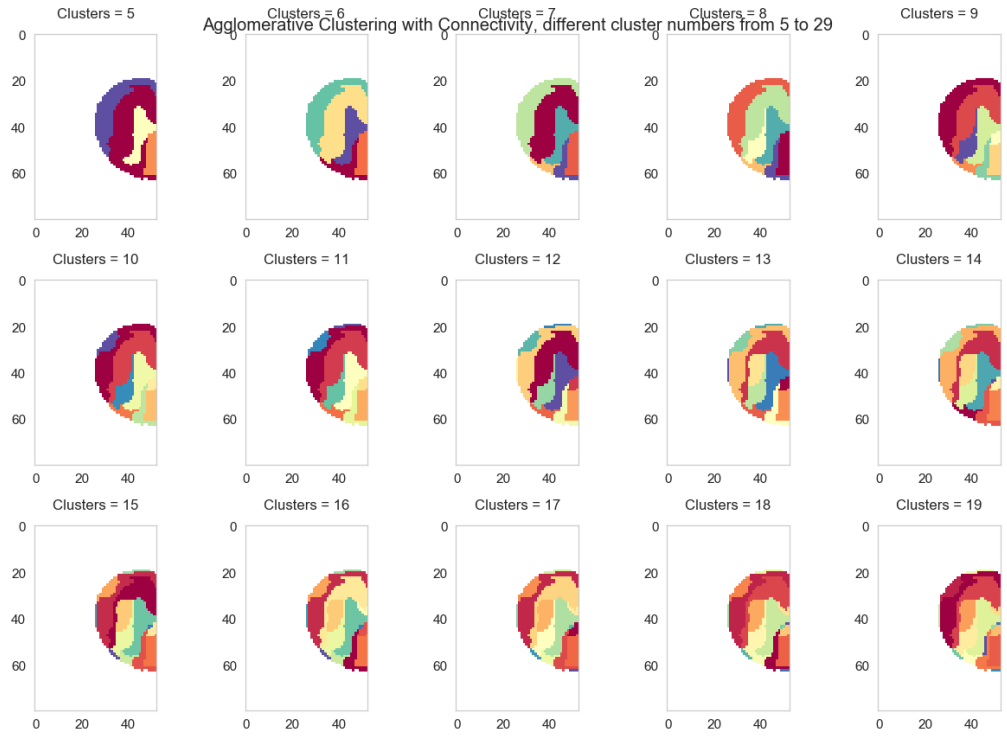
Agglomerative Clustering with Connectivity, different cluster numbers from 5 to 29
Clusters = 5
Clusters = 6
Clusters = 7
Clusters = 8
Clusters = 9
Clusters = 10
Clusters = 11
Clusters = 12
Clusters = 13
Clusters = 14
Clusters = 15
Clusters = 16
Clusters = 17
Clusters = 18
Clusters = 19

T13

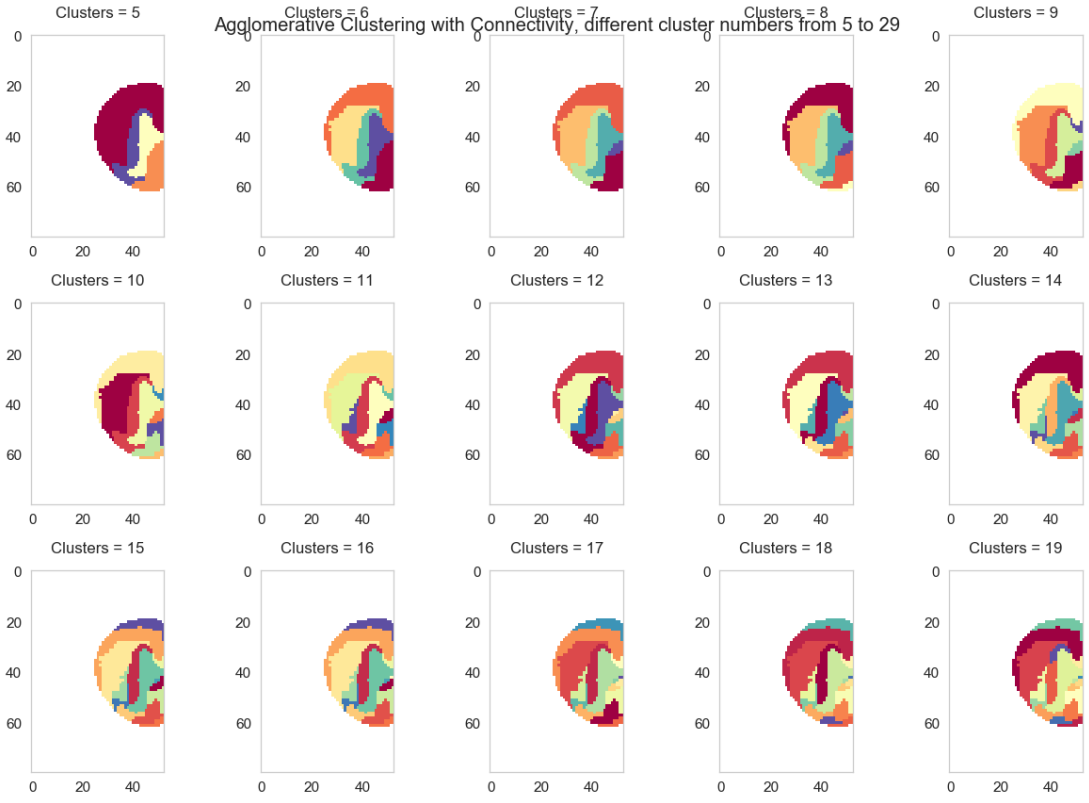
Agglomerative Clustering with Connectivity, different cluster numbers from 5 to 29
Clusters = 5
Clusters = 6
Clusters = 7
Clusters = 8
Clusters = 9
Clusters = 10
Clusters = 11
Clusters = 12
Clusters = 13
Clusters = 14
Clusters = 15
Clusters = 16
Clusters = 17
Clusters = 18
Clusters = 19

L1

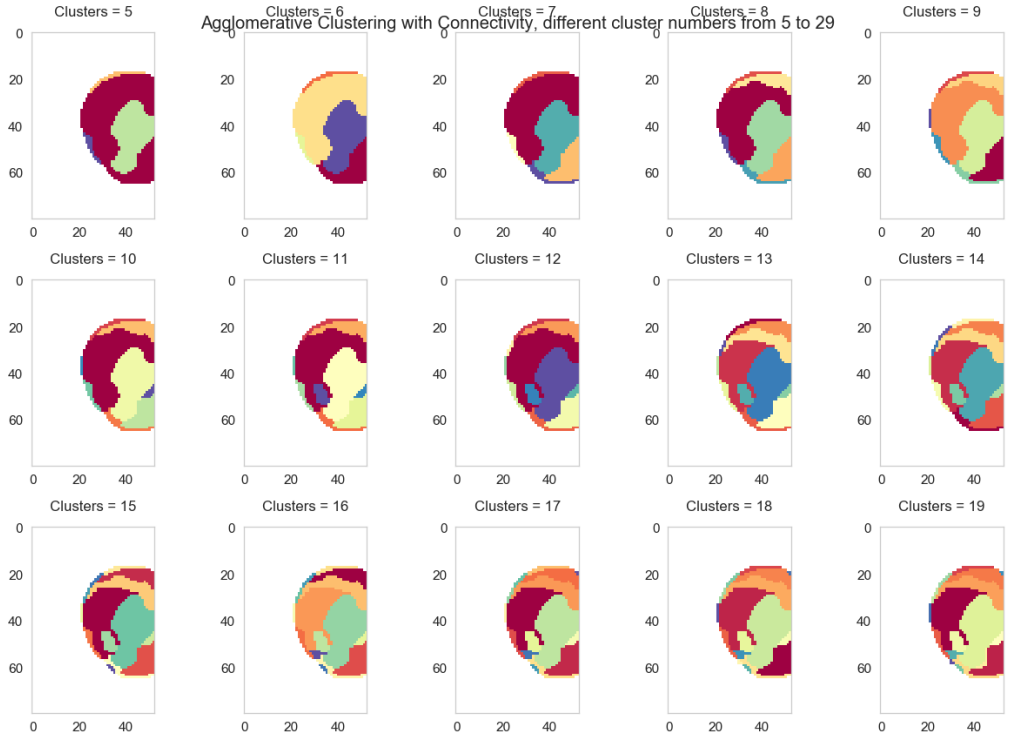
Agglomerative Clustering with Connectivity, different cluster numbers from 5 to 29
Clusters = 5
Clusters = 6
Clusters = 7
Clusters = 8
Clusters = 9
Clusters = 10
Clusters = 11
Clusters = 12
Clusters = 13
Clusters = 14
Clusters = 15
Clusters = 16
Clusters = 17
Clusters = 18
Clusters = 19

L2

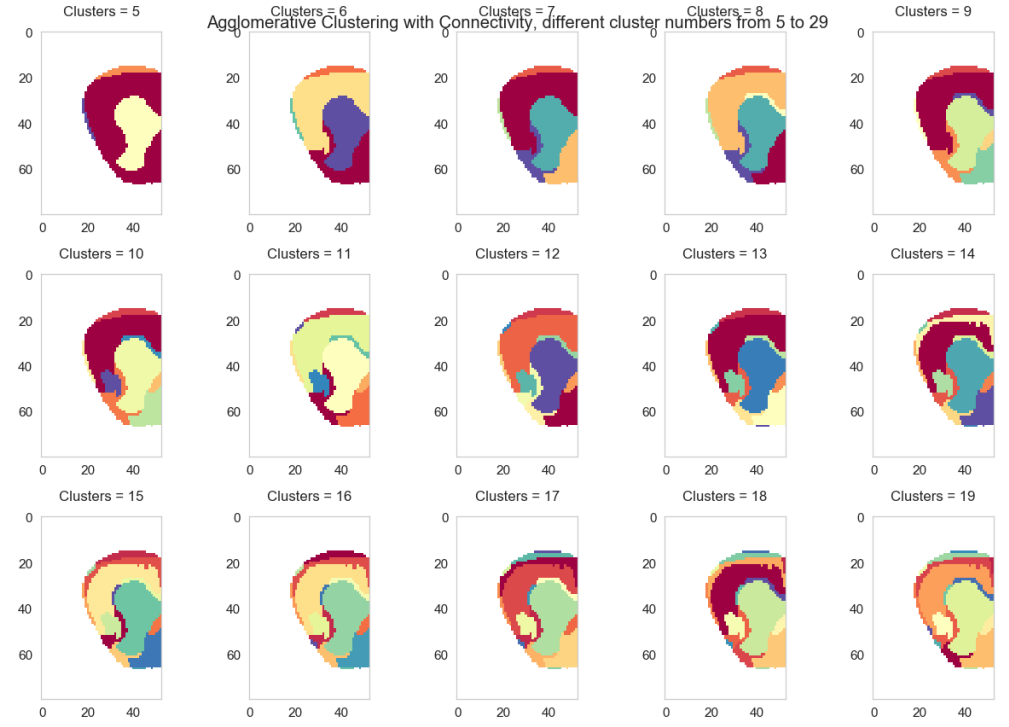
Agglomerative Clustering with Connectivity, different cluster numbers from 5 to 29
Clusters = 5
Clusters = 6
Clusters = 7
Clusters = 8
Clusters = 9
Clusters = 10
Clusters = 11
Clusters = 12
Clusters = 13
Clusters = 14
Clusters = 15
Clusters = 16
Clusters = 17
Clusters = 18
Clusters = 19

L3

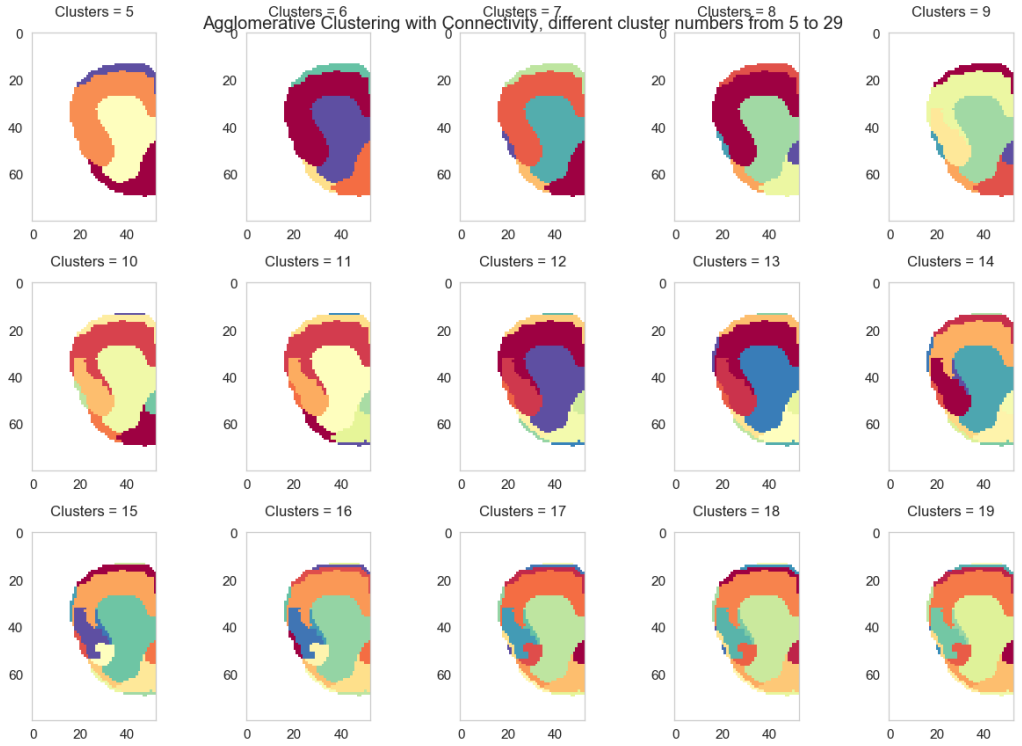
Agglomerative Clustering with Connectivity, different cluster numbers from 5 to 29
Clusters = 5
Clusters = 6
Clusters = 7
Clusters = 8
Clusters = 9
Clusters = 10
Clusters = 11
Clusters = 12
Clusters = 13
Clusters = 14
Clusters = 15
Clusters = 16
Clusters = 17
Clusters = 18
Clusters = 19

L4

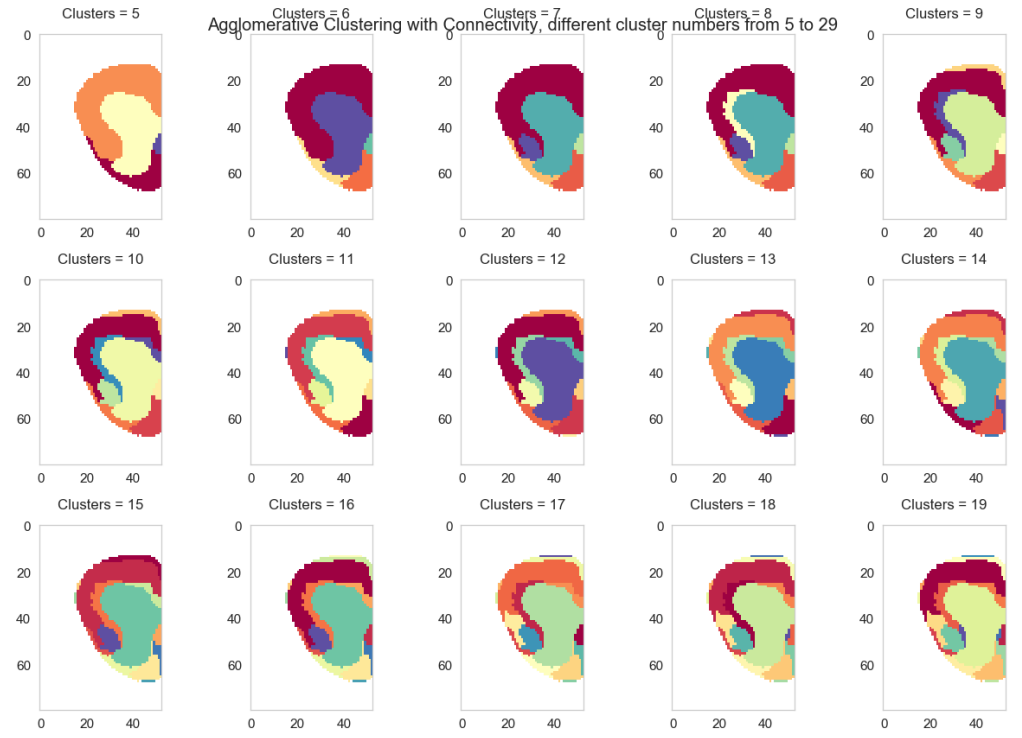
Agglomerative Clustering with Connectivity, different cluster numbers from 5 to 29
Clusters = 5
Clusters = 6
Clusters = 7
Clusters = 8
Clusters = 9
Clusters = 10
Clusters = 11
Clusters = 12
Clusters = 13
Clusters = 14
Clusters = 15
Clusters = 16
Clusters = 17
Clusters = 18
Clusters = 19

L5

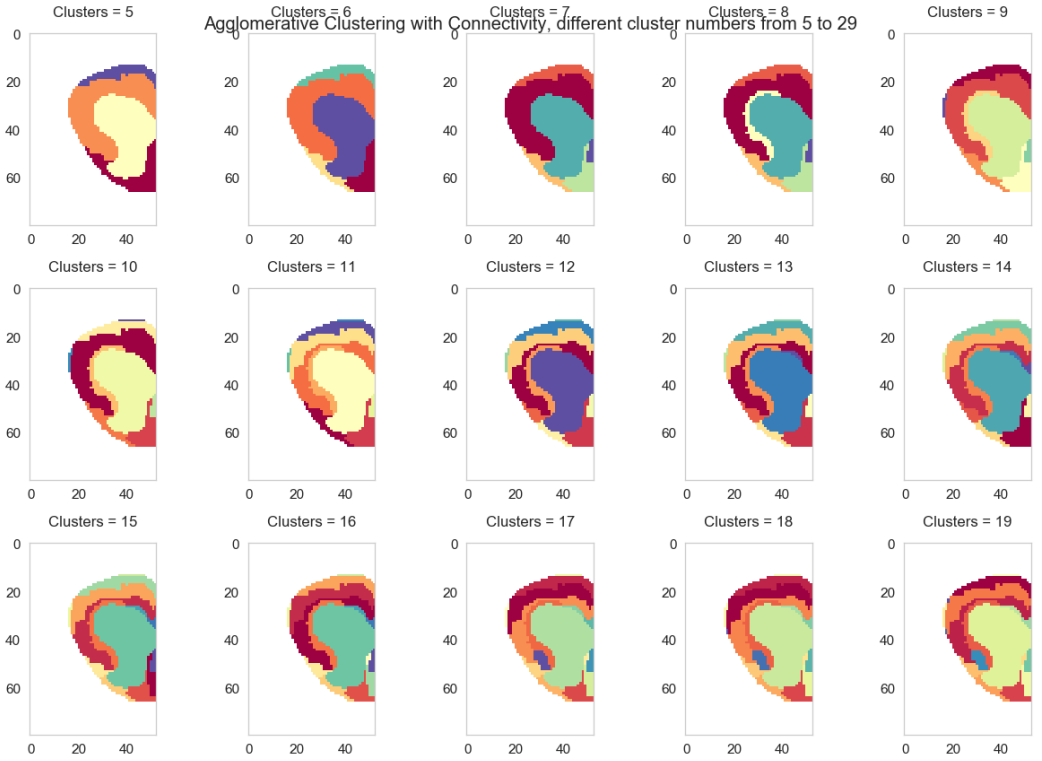
Agglomerative Clustering with Connectivity, different cluster numbers from 5 to 29
Clusters = 5
Clusters = 6
Clusters = 7
Clusters = 8
Clusters = 9
Clusters = 10
Clusters = 11
Clusters = 12
Clusters = 13
Clusters = 14
Clusters = 15
Clusters = 16
Clusters = 17
Clusters = 18
Clusters = 19

L6

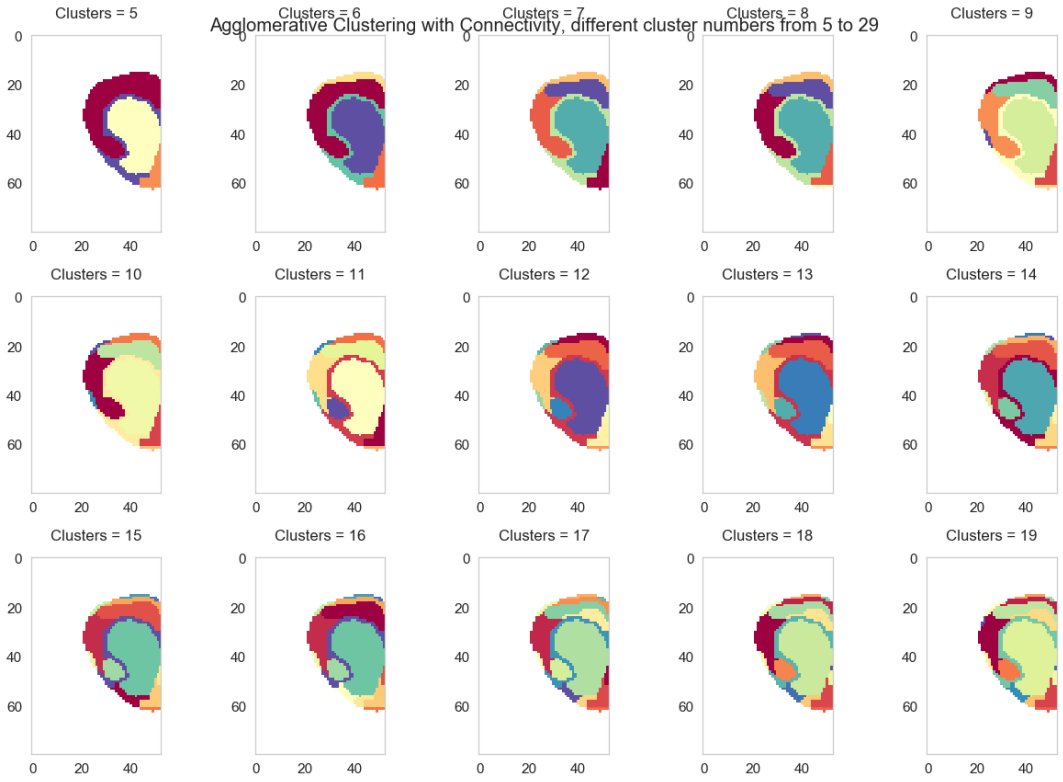
Agglomerative Clustering with Connectivity, different cluster numbers from 5 to 29
Clusters = 5
Clusters = 6
Clusters = 7
Clusters = 8
Clusters = 9
Clusters = 10
Clusters = 11
Clusters = 12
Clusters = 13
Clusters = 14
Clusters = 15
Clusters = 16
Clusters = 17
Clusters = 18
Clusters = 19

S1

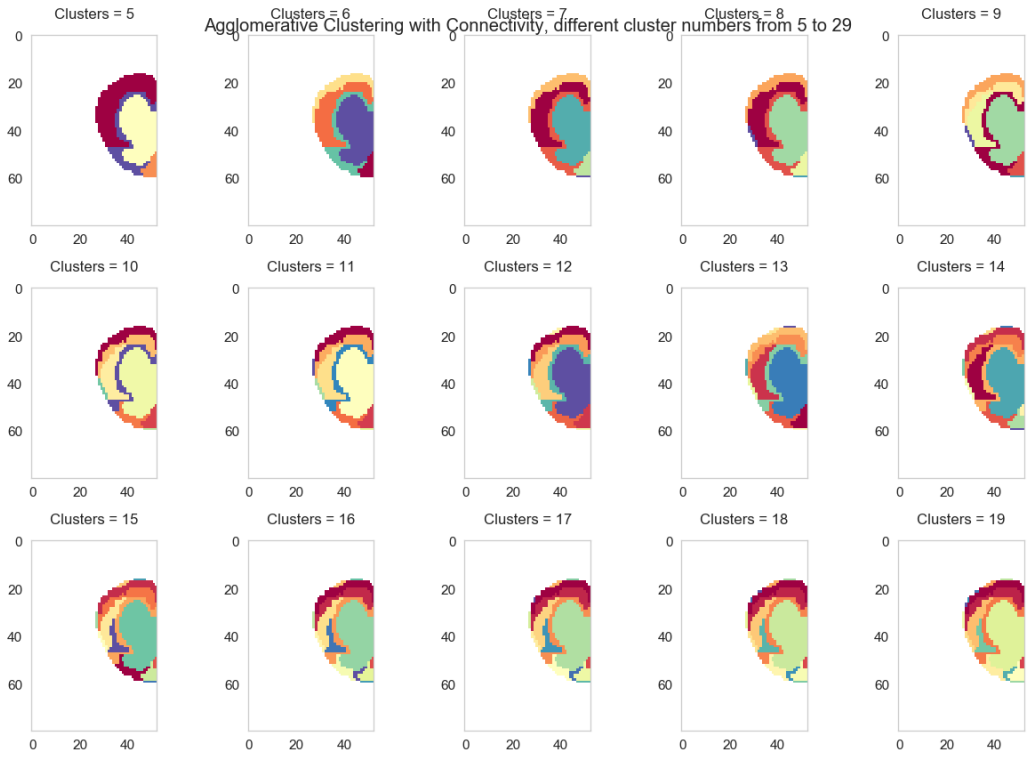
Agglomerative Clustering with Connectivity, different cluster numbers from 5 to 29
Clusters = 5
Clusters = 6
Clusters = 7
Clusters = 8
Clusters = 9
Clusters = 10
Clusters = 11
Clusters = 12
Clusters = 13
Clusters = 14
Clusters = 15
Clusters = 16
Clusters = 17
Clusters = 18
Clusters = 19

S2

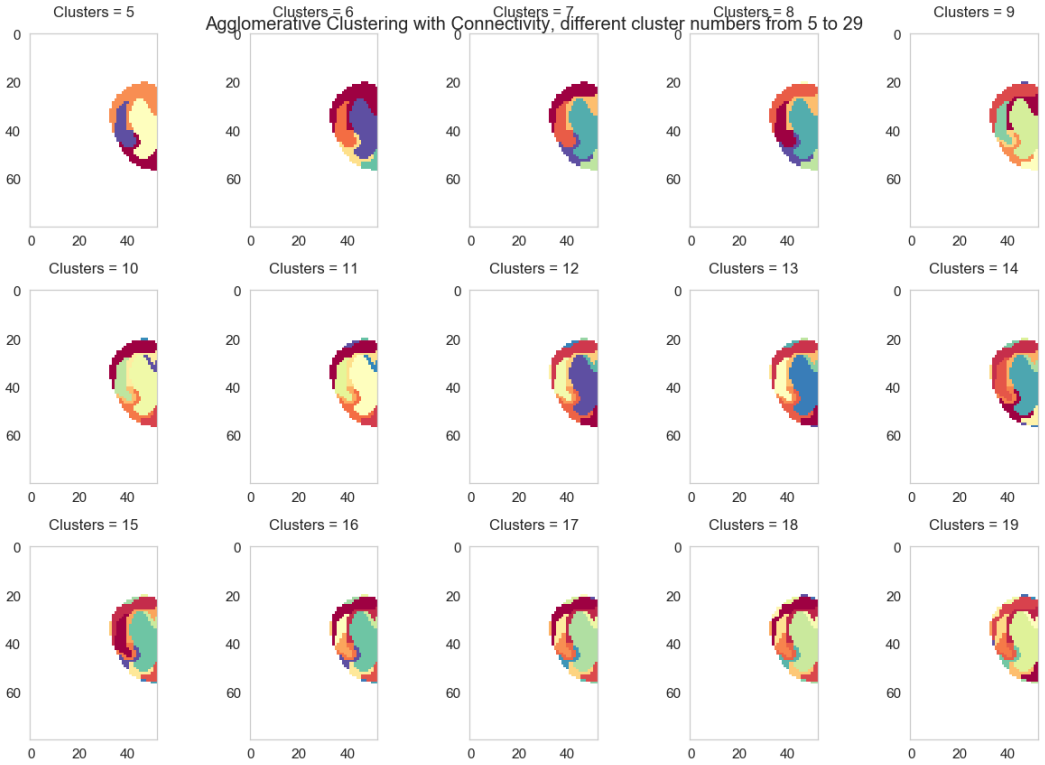
Agglomerative Clustering with Connectivity, different cluster numbers from 5 to 29
Clusters = 5
Clusters = 6
Clusters = 7
Clusters = 8
Clusters = 9
Clusters = 10
Clusters = 11
Clusters = 12
Clusters = 13
Clusters = 14
Clusters = 15
Clusters = 16
Clusters = 17
Clusters = 18
Clusters = 19

S3

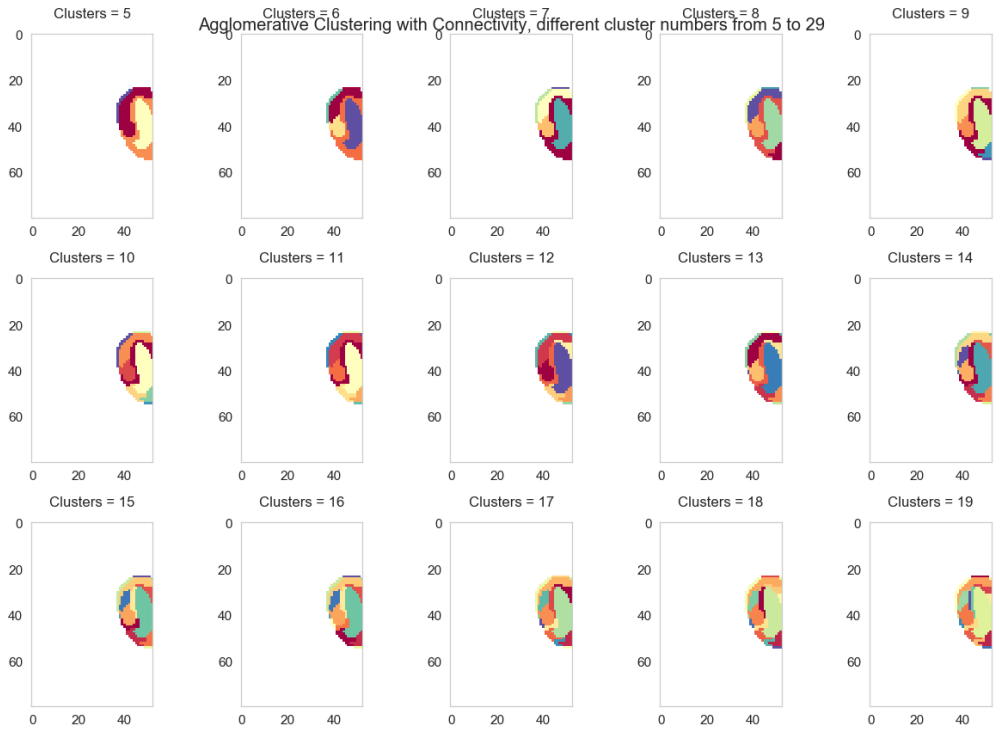
Agglomerative Clustering with Connectivity, different cluster numbers from 5 to 29
Clusters = 5
Clusters = 6
Clusters = 7
Clusters = 8
Clusters = 9
Clusters = 10
Clusters = 11
Clusters = 12
Clusters = 13
Clusters = 14
Clusters = 15
Clusters = 16
Clusters = 17
Clusters = 18
Clusters = 19

S4

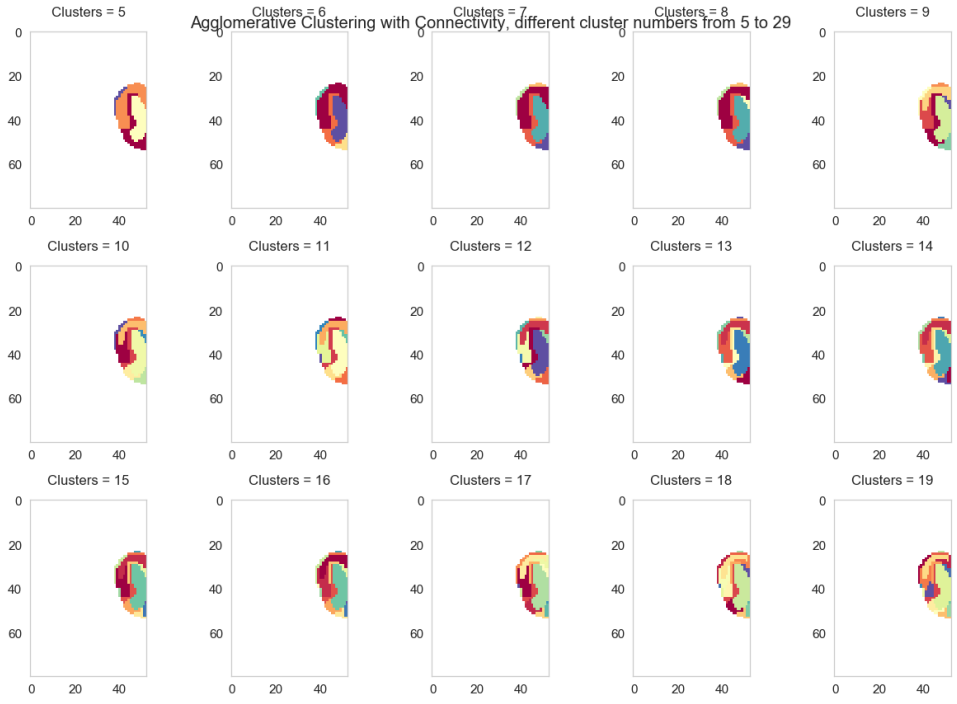
Agglomerative Clustering with Connectivity, different cluster numbers from 5 to 29
Clusters = 5
Clusters = 6
Clusters = 7
Clusters = 8
Clusters = 9
Clusters = 10
Clusters = 11
Clusters = 12
Clusters = 13
Clusters = 14
Clusters = 15
Clusters = 16
Clusters = 17
Clusters = 18
Clusters = 19